THE UNIVERSITY OF ALBERTA

SECONDARY SEDIMENTATION STUDY

by

© Larry D. Annis

A THESIS

SUBMITTED TO THE FACULTY OF GRADUATE STUDIES AND RESEARCH

IN PARTIAL FULFILMENT OF THE REQUIREMENTS FOR THE DEGREE

OF MASTER OF SCIENCE

DEPARTMENT OF CIVIL ENGINEERING

EDMONTON, ALBERTA

SPRING, 1977

DEDICATION

To Marilyn for patience

and understanding

ABSTRACT

The five secondary sedimentation tanks at the City of Edmonton Gold Bar Waste Water Treatment Plant are frequently subjected to large prolonged hydraulic loads. A comprehensive examination of the internal tank flow patterns and characteristics for a wide range of geometric and hydraulic variables was conducted. When the principles of open channel theory are combined with a velocity meter and stream profiles, a mechanism for monitoring the hydraulic loads to each tank was developed. Internal flow patterns in the prototype tanks were examined with a technique involving fluorescent dye and fluorometric measuring equipment.

Similitude theory incorporating the Froude number was used to develop a model sedimentation tank for laboratory analysis. Model flow patterns were derived for a broad range of hydraulic loads and geometric configurations. Prototype and model flow characteristics, integrated with sedimentation and density current theories, enable the prediction of optimal, practical hydraulic loading limits.

ACKNOWLEDGMENTS

This writer wishes to acknowledge the resource and financial contributions furnished by the City of Edmonton Department of Water and Sanitation. Most important are the many and varied contributions of the management team, the operations staff, the maintenance staff, and the laboratory staff at the City of Edmonton Gold Bar Waste Water Treatment Plant. Appreciation must be given to the staff at the University of Alberta, Thomas Blench Hydraulics Laboratory whose efforts were so vital to the model study. For guidance and direction, special appreciation must go to members of the academic staff in the hydraulics and environmental divisions of the University of Alberta Civil Engineering Department.

Without the cooperation, assistance, and patience of these many people, this study would not have been possible.

TABLE OF CONTENTS

LIST OF TABLES

LIST OF FIGURES

NOTATION

The following notations are used throughout this treatise:

A	cross sectional area
b_o	vertical dimension of the rectangular baffle opening
C	summation of the instrument measured fluorescence concentration and the proportional fluorescence correction
C_b	fluorescence background correction
C_c	proportional fluorescence correction
C_d	fluorescence dosed correction
C_i, C_j, C_k	fluorescence inflection points on the time-concentration curve (ordinate)
C_o	initial concentration of fluorescence dye in the injector
C_r	maximum concentration ratio, ordinate value when Equation 3.13 is valid
C_s	summation of fluorescence background correction and fluorescence dosed correction
C_t	instrument measured concentration of fluorescent dye
C_u	theoretical fluorescence concentration index
E	entrainment factor in stratified media

NOTATION

F	hydraulic Froude number
F_1	fluorometer dial reading
g	gravitational constant 32.2 ft/sec^2
$KMnO_4$	chemical symbol for potassium permanganate
L	any characteristic length in a hydraulic regime
MST	Mountain Standard Time
n	any numerical subscript
N.T.S.	not to scale
P	volume of a sedimentation tank cell
P_o	volume of the fluorescence dye injector
Q	rate of volumetric flow to a single cell of a sedimentation tank
Q_o	rate of volumetric flow to a sedimentation tank
Q_r	rate of volumetric flow in a tank return
Q_w	rate of volumetric flow over the tank effluent weirs
R_i	gradient Richardson number
S	specific gravity of a tank media
S_f	dimensionless geometric scale factor
S_r	fraction of removed suspended solids
S_1, S_2	defined specific gravities in successive stratified layers of a media
T	time
T_d	theoretical detention time index

T_f	actual detention time between the injection and sampling stations in a fluorometric test
T_i, T_j, T_k	fluorescence inflection points on the time-concentration curve (abscissa)
T_r	maximum time ratio, abscissa value when Equation 3.13 is valid
V	any defined component of velocity
$\overline{V}$	any defined mean component of velocity
V_a	a measured stream velocity occurring at depth Y_a
V_b	a measured stream velocity occurring at depth Y_b
V_L	maximum velocity in the lower laminar zone
V_s	average settling velocity of a sludge blanket
V_u	maximum velocity in the upper laminar zone
V_z	any velocity component along the Z axis
V_1, V_2	defined velocities in successive stratified layers of a media
X	longitudinal X axis in a Cartesian coordinate system
X_s	longitudinal distance along the X axis which an average particle requires to settle in the lower laminar zone
Y	vertical Y axis in a Cartesian coordinate system
y_a, Y_a	a vertical stream depth equal to 80% of y_o

NOTATION

$y_b Y_b$	a vertical stream depth equal to 20% of y_o
Y_L	depth of the lower laminar zone
y_o, Y_o	vertical distance from a channel or tank floor to the free liquid surface
Y_t	depth of the turbulent zone
Y_u	depth of the upper laminar zone
Y_1, Y_2	defined vertical depths in successive stratified layers of media
Z	latitudinal Z axis in a Cartesian coordinate system
ρ	media mass density

UNITS OF MEASURE

The following units of measure are used throughout this treatise:

cfs	cubic feet per second
cm	centimeters
cm/sec	centimeters per second
°C	degrees Celsius
ft	feet
ft/ft	feet per feet
ft/sec	feet per second
ft/sec^2	feet per second second
gm	grams
gm/l	grams per liter
in.	inches
µgm/l	micrograms per liter
ml	milliliters
ml/min	milliliters per minute
µm	millimicrons
migd.	million Imperial gallons per day
min.	minutes
MTS	Mountain Standard Time
N.T.S.	Not to Scale
U.S gpm	United States gallons per minute
U.S.gpd/ft	United States gallons per day per foot

[1] INTRODUCTION

The initial phase of the City of Edmonton Waste Water Treatment Plant was constructed in 1956 at a site on the south bank of the North Saskatchewan River and 50th Street. In 1970, the plant was expanded to a primary and secondary design capacity of 109 migd. and 45 migd. respectively. Using an activated sludge process, effective secondary treatment has generally been provided to peak hydraulic flows not exceeding 60 migd. (1). According to 1975 census records, the plant provides service to a population of 451,635 (2) persons within the greater Edmonton area. In addition to domestic sources, waste water of varied composition from industrial sources is being treated. According to current records, waste water is conveyed to the plant by 532 miles of sanitary sewers and 533 miles of combined sanitary-storm sewers (3).

The total treatment process can be briefly described in the following consecutive steps:

(1) Initially, waste water enters the primary grit tank where a sedimentation process removes heavier settleable debris and inorganic grit.

(2) Floating debris is removed by a parallel arrangement of automatic bar screens and is wasted at a sanitary land fill site.

(3) A distribution channel system directs the waste water to the primary sedimentation tanks where bottom sludge and surface skimmings are removed. These materials are collected for the digestion process while weirs direct the effluent to the secondary treatment process. In this step there exists the option of discharging primary effluent directly to the North Saskatchewan River.

(4) The primary effluent enters the secondary process through a Venturi meter and is directed to the aeration tanks by a distribution channel system. The waste is mixed with an aerated, recirculated liquor and is injected with additional air in a parallel arrangement of five aerators.

(5) The aerated mixed liquor is directed to the secondary sedimentation tank where the final effluent is collected by V notch weirs for discharge to the river. Surface skimmings are recirculated to the primary system and the bottom sludge is divided between the digesters and the liquor return system described in step 4. According to operation policies, the flow returned to the aeration tanks ranges between 25% and 30% of the total secondary flow.

(6) Waste sludge is digested anaerobically in five tanks for approximately 25 days and is then pumped to open lagoons for indefinite storage.

This investigation will deal only with the secondary sedimentation process described in step five of the total treatment process. The principal parameters which influence the efficiency of secondary sedimentation are tank geometry, hydraulic loads, and characteristics of suspended solids. This investigation will rigorously deal with the first two parameters. The characteristics of suspended solids are complex and vary directly with the volume, composition, and nature of the waste material. This complex variable can only warrant a thorough investigation of its own - an investigation which could and should be linked with this treatise.

Five independent secondary sedimentation tanks provide continuous service at the City of Edmonton Waste Water Treatment Plant. According to the convention adopted in this investigation, the tanks will be numbered from one to five from west to east (tank number one is the most westerly tank). Field measurements confirm that the five tanks are geometrically identical except for the baffle openings and the cross channel floor elevations. The tanks are rectangular with a width of 80.00 ft and a length of 165.00 ft. Each tank contains five 15.60 ft wide, longitudinal internal cells. According to the same convention, the internal cells are also numbered from one to five from west to east. The north wall of each cell is situated

on the extreme end opposite the inlet opening. A typical plan view is shown in the schematic of Figure 1.01. The normal liquid depth is 12.24 ft at the inlet end and the floor slopes at 0.00758 ft/ft toward the north wall. At the inlet end a fixed plank baffle wall extends upward from a terminus at an elevation b_o above the floor to a second terminus slightly above the normal water surface. Details of the tank profile are shown in the schematic of Figure 1.02. A typical baffle wall detail is shown in the schematic of Figure 1.03. A sectional detail for the cross channels is shown in Figure 1.04 and will be discussed further in Chapter 2.

The photograph of Figure 1.05 shows the surface appearance of the tank when in normal operation. Three of the four effluent weirs are shown in the foreground while the upper beam sections of the tank subdividers, the skimming flights, and tank inlet are shown in the background. The baffle wall at the inlet, tank subdividers, and the sludge-skim flights are more clearly shown in the photograph of Figure 1.06 where the tank has been emptied for maintenance work. The flights are nominal 2 in. by 8 in. timber planks on a moving chain which is continuous over the full length of the tank. It is important to notice that the tank subdividers are not

monolithic walls, but are open frames of vertical columns and horizontal beams. Therefore lateral currents can and probably do occur across the tank width.

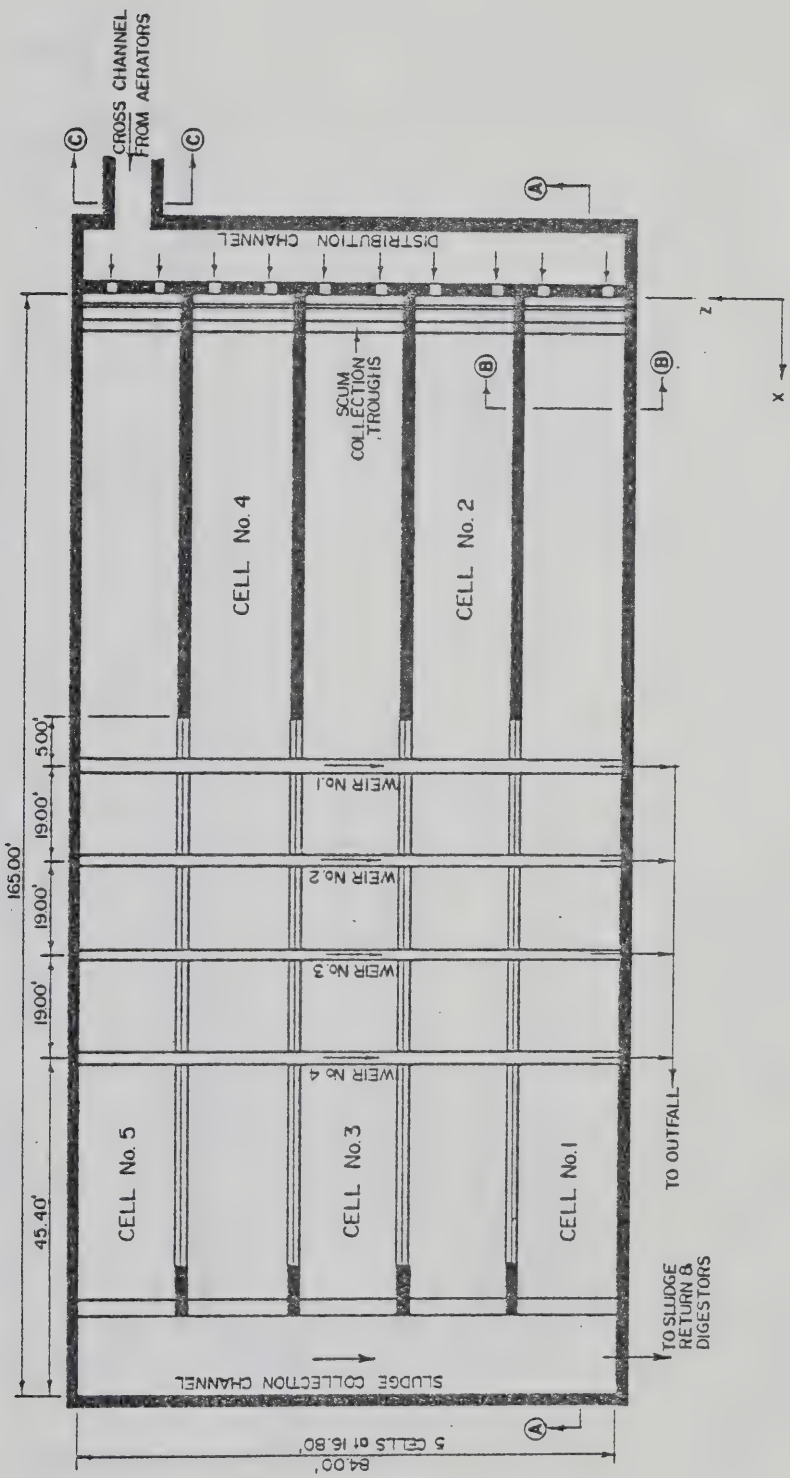

NOTES:
A. CHAINS & FLIGHTS ARE NOT SHOWN.
B. PLAN IS TYPICAL FOR EACH OF FIVE SEDIMENTATION TANKS.
C. PLAN IS NOT TO SCALE.

FIG. 1.01 TYPICAL PLAN OF SECONDARY SEDIMENTATION TANKS

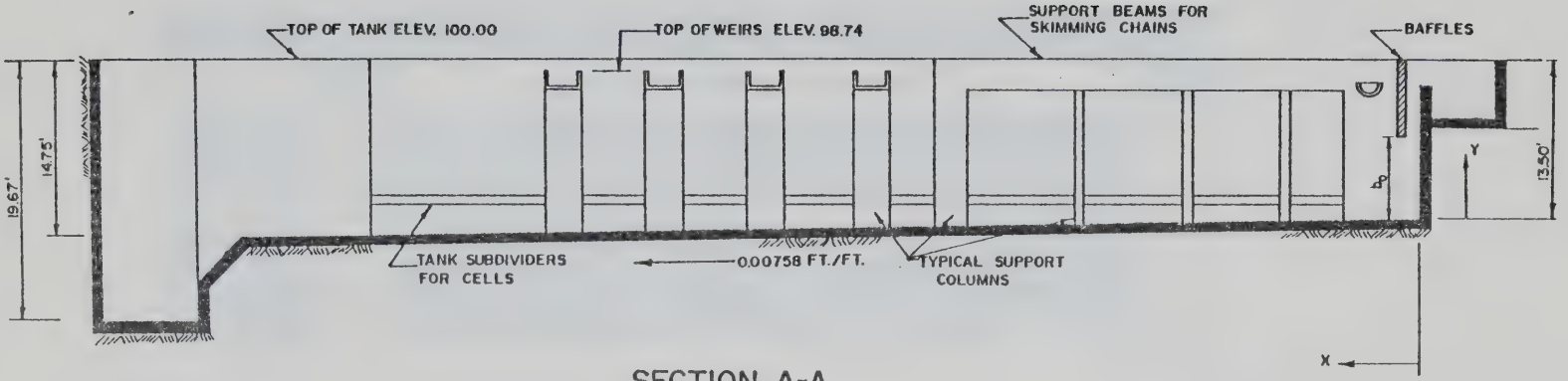

SECTION A-A

TANK PROFILE

N.T.S.

NOTE:

(A) CHAINS AND FLIGHTS ARE NOT SHOWN.

(B) ELEVATIONS ARE BASED ON AN ASSUMED DATUM.

SEDIMENTATION TANK NUMBER	bo (Ft.)
1	9.67
2	6.00
3	6.00
4	6.00
5	6.00

FIG. 1.02 TANK PROFILE

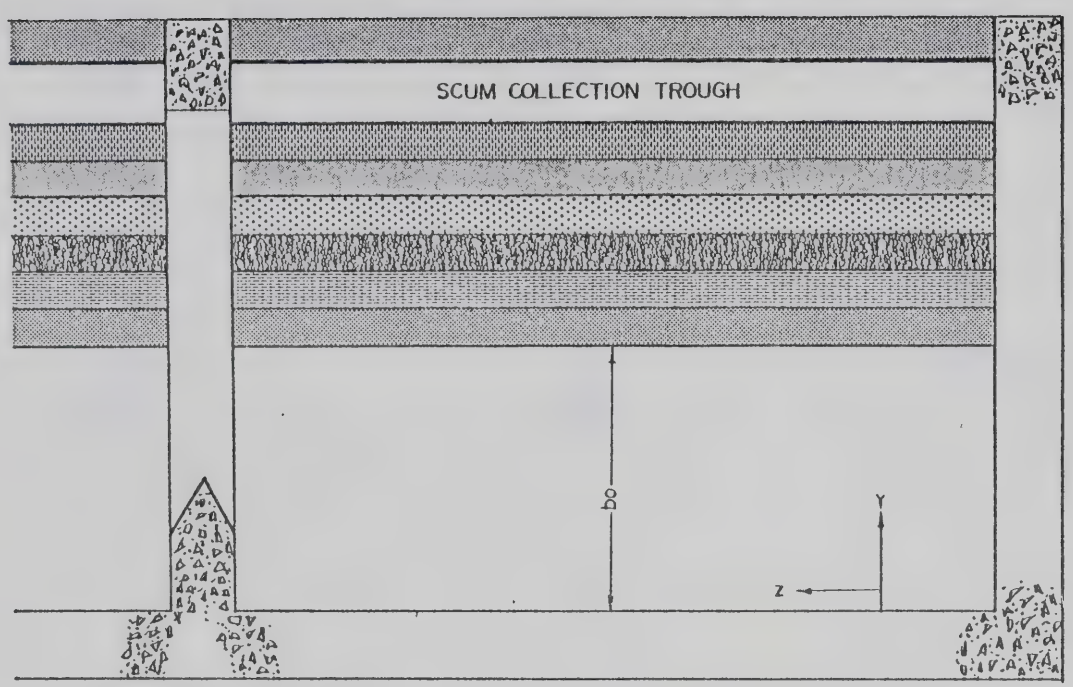

SECTION B-B
(NOT TO SCALE)

FIG. 1.03 CELL CROSS SECTION

SECTION C-C
(NOT TO SCALE)

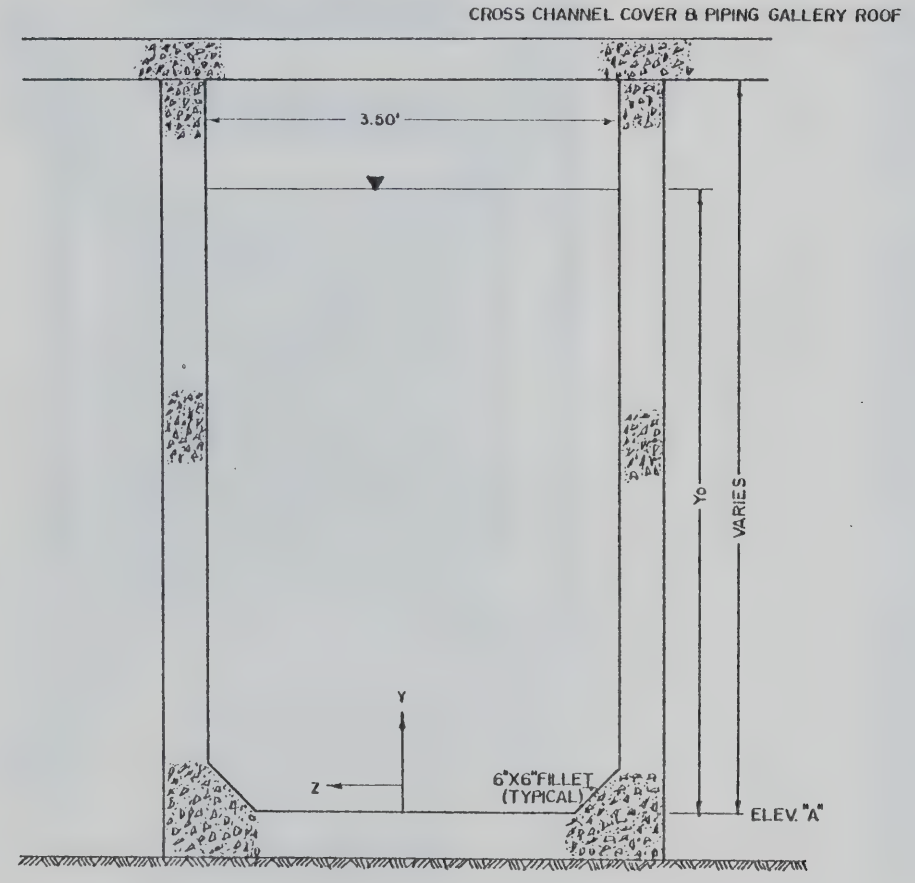

CROSS CHANNEL	ELEV. "A" (FT.)
1	94.20
2	94.33
3	94.24
4	94.09
5	94.11

FIG. 1.04 CROSS CHANNEL AT GAUGING STATION

Fig. 1.05 Prototype Sedimentation Tank in Normal Operation

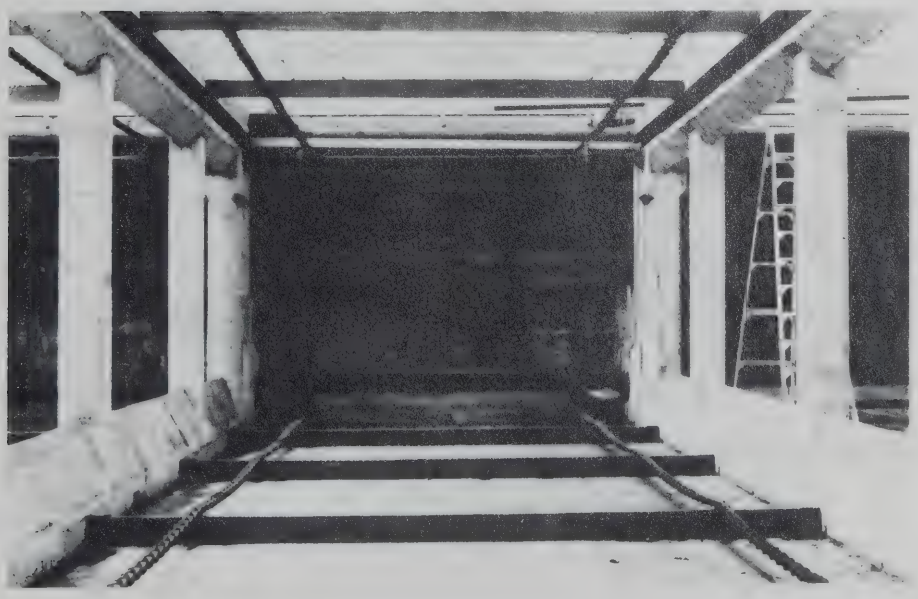

Fig. 1.06 Influent Opening and Cell Detail of Empty Prototype Sedimentation Tank

[2] HYDRAULIC FLOWS

It is necessary to determine the hydraulic loading on each of the five secondary sedimentation tanks before an accurate performance evaluation can be attempted. In this investigation a simple open channel stream analysis was made at an accessible control station. It was convenient to select the downstream end of each cross channel as the gauging station. The cross channels connect the aerators with the sedimentation tank and flow with a free surface over the top of the secondary piping gallery. The numbering convention for the cross channels will be the same as the tank convention.

Each of the cross channels is geometrically identical except for the floor elevation. The channel cross section at the gauging station is shown in the schematic of Figure 1.04. All cross channels are 28.20 ft long and none have any longitudinal floor slope. The concrete roof on the secondary piping gallery provided a firm datum for measurements. Handrailing adjacent to the gauging station provided a substantial falsework system for cumbersome velocity measuring equipment.

At each gauging station flow velocities were measured with a Cushing Model 611P velocity meter and a Model 81 magnetic sensor. The unit was calibrated

under controlled conditions at the University of Alberta Hydraulics Laboratory. Beginning at the floor of each cross channel, velocity and depth measurements were taken in six inch increments until the sensor elements were just below the liquid level. For each group of velocity readings a corresponding surface elevation with respect to an assumed datum was recorded. Initially, velocity measurements were taken on profiles in the channel center as well as on either side within four inches of the channel wall. This procedure was abandoned in favor of a single profile in the channel center when it was discovered that the side profiles had no significant effect on the determination of the mean velocity.

From each group of stream measurements, a generally shaped logarithmic velocity profile was developed. The velocity elevation above the channel floor is represented on the ordinate, while the velocity is represented on the abscissa of a Cartesian coordinate system. Completed velocity profiles are shown in Appendix 1. In a procedure suggested by Chow (4), the mean velocity, $\overline{V}$, is determined by averaging the respective velocities occurring at elevations equal to 20% and 80% of the total stream depth. This procedure is summarized in the schematic of Figure 2.01.

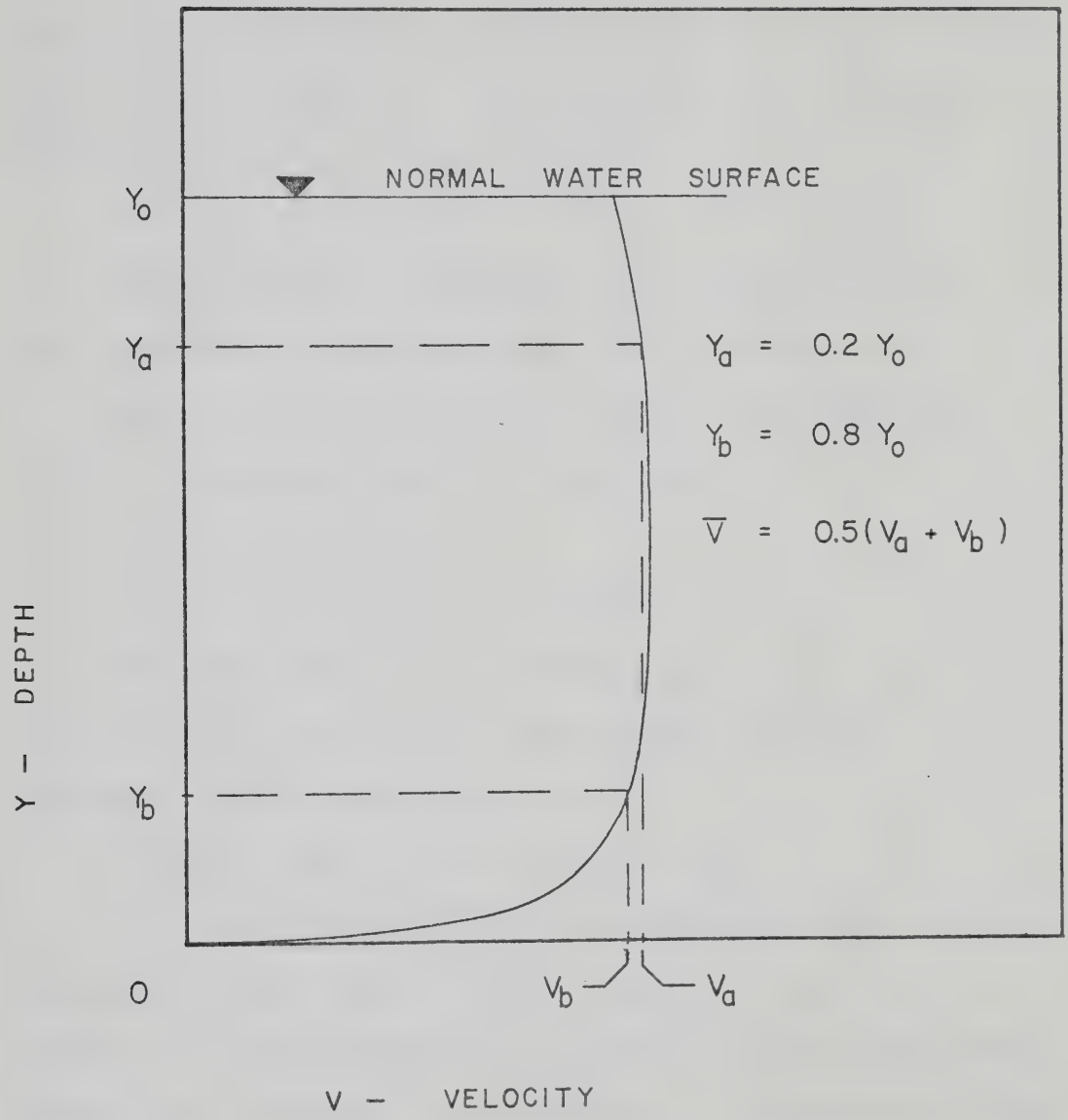

FIG. 2.01 TYPICAL VELOCITY PROFILE FOR CROSS CHANNELS

Since the geometrics of the five cross channels are identical, the cross sectional area can be defined by a common equation. From Figure 1.04, the cross sectional area can be represented by:

[2.01] $A = 3.50\ yo - 0.25$

Where yo and A represent the stream depth in feet and area in square feet, respectively.

Rates of volumetric flow Qo can be calculated by the continuity equation according to:

[2.02] $Qo = A\overline{V}$

Where $\overline{V}$ is the mean velocity.

When Equation 2.01 is multiplied by the mean velocity, the result is a manipulated form of Equation 2.02. This results in:

[2.03] $Qo = \overline{V}\ (3.50\ yo - 0.25)$

In Equation 2.03, $\overline{V}$ and Qo have the units of feet per second and cubic feet per second, respectively. Table 2.01 has summarized the stream depths and mean velocities assembled in Appendix 1. The corresponding rates of flow are shown in the right hand column of Table 2.01.

The values of yo and Qo appearing in Table 2.01 are plotted as the ordinate and abscissa, respectively, on arithmetic graph paper. On a large scale, five distinct linear relations having the general Cartesian form of $y = mx + b$ were derived. The graphical

Table 2.01. Summary of Cross Channel Hydraulic Parameters.

Cross Channel	yo* (ft)	$\overline{V}$* (ft/sec)	Qo** (CFS)
1	4.68	1.21	19.5
1	4.71	1.53	24.8
1	4.75	1.65	27.0
2	4.61	2.30	36.5
2	4.57	1.54	24.2
2	4.63	1.89	27.6
2	4.66	2.46	39.5
3	4.82	1.99	33.1
3	4.77	1.61	26.5
3	4.82	1.91	31.7
3	4.69	2.42	39.1
4	4.98	1.97	32.1
4	4.97	1.62	27.8
4	5.02	2.17	37.6
5	4.92	2.06	35.0
5	4.92	2.01	34.1
5	4.83	1.46	24.3

* Values of yo and $\overline{V}$ are derived in Appendix 1.

** Values of Qo are calculated from Equation 2.03.

representation has been deleted from this treatise, however they are shown mathematically for each cross channel as:

Cross Channel No. 1

[2.04] $Qo = 150.00\ yo - 682.50$ for $yo \geq 4.55$ ft

Cross Channel No. 2

[2.05] $Qo = 164.58\ yo - 727.44$ for $yo \geq 4.42$ ft

Cross Channel No. 3

[2.06] $Qo = 104.52\ yo - 471.44$ for $yo \geq 4.51$ ft

Cross Channel No. 4

[2.07] $Qo = 100.31\ yo - 467.46$ for $yo \geq 4.66$ ft

Cross Channel No. 5

[2.08] $Qo = 123.21\ yo - 571.71$ for $yo \geq 4.64$ ft.

Here the positive number represents the depth-flow slope and the negative number represents the product of the slope and depth intercept. The depth intercept is defined as that depth where the flow becomes zero. The limits provided for yo in each equation represent the actual magnitudes of the depth intercepts. These were in fact confirmed when the tank levels were lowered to a point where water just began breaking over the bottom of the V-notch in the effluent weirs.

When the magnitude of the slope is examined in the previous cross channel equations it is clear that a near submerged condition exists in the system. This is the effect of a 2.00 ft head difference between the

water surfaces of the primary grit tanks and the secondary effluent weirs. Under normal operating conditions there exists a fluctuating range in yo of approximately six inches. Thus it is essential that extreme caution and precision be used when field measuring yo. With due care, the cross channel equations agree reasonably well with the output from the plant Venturi meters. The curves in Appendix 2 indicate a percentage error ranging from 6.4% to 13.5% for the two methods. Flows from the cross channel equations are characteristically greater than the Venturi meter flows.

For practical reasons, this study will consider only the flows to the individual cells rather than the entire tank. Numerous efforts were made to precisely monitor flows through the small influent openings in each cell using a theory similar to the one used in the cross channel study. Due to adverse distribution channel geometry and turbulent eddy currents, the precise approach was abandoned in favor of flow estimating. In this investigation it will be assumed that the total tank flow is equally distributed amongst the five cells within the tank. Hence the cell flow, Q, is estimated to be 20% of the tank flow measured at the cross channel gauging station. Mathematically this will be:

$$[2.09] \qquad Q = 0.20\ Qo$$

[3] FLUOROMETRIC EXAMINATION

The preceding chapter has provided a reasonably accurate mechanism for measuring the hydraulic load to each of the five secondary sedimentation tanks. The investigation will now examine the flow characteristics within the individual tanks. Various methods of flow study were attempted, including the velocity meter and buoys of various shapes and densities - all of which provided data of little value. Useful results were obtained with fluorescent dye and a fluorometric analyzer.

Because each sedimentation tank is subdivided into five equal cells with longitudinal streamlines normal to the effluent weirs, it was assumed that lateral currents are insignificant and can be ignored. This assumption implies a two dimensional flow regime such that:

[3.01] $V_z = 0$

Longitudinal currents (X component of velocity) can be readily studied in the prototype cell with fluorometric methods. Fluorometric methods of studying the vertical currents (Y component of velocity) in the prototype cells must be discarded in favor of modeling methods.

Known concentrations of Du Pont Rhodamine B fluorescent dye were injected in the distribution

channel stream of each tank with a constant flow injector. Dye was injected at a point sufficiently downstream to ensure flow to only the first cell of each tank. The injector and a time clock were started simultaneously. During the execution of each dye test, a Sirco, Model MK-VS7 automatic sampler collected samples at one of three stations. The sampling points were approximately two feet below the normal water surface and were situated either adjacent to the first weir, the fourth weir, or the northerly end wall. An automatic timing frequency ranging between three and four minutes collected samples of sufficient representation. Samples were collected generally over a two and one half hour period in order to accurately define the cell flow pattern.

Immediately following the sample collection, a fluorometric analysis was made with a G.K. Turner, Model III, Fluorometer. Primary and secondary filter lenses having wave lengths of 548 millimicrons and 590 millimicrons, respectively, were used. The unit was equipped with four light source apertures in the ratio of 1:3:10:30. Normal samples of secondary effluent required only the use of the 3, 10, and 30 apertures. Samples were handled manually and individually in small quartz glass tubes.

Since the fluorometer provides fluorescence dial readings on a dimensionless scale in unit increments between one and one hundred, it was necessary to develop a group of calibration curves. A series of known dilutions using distilled water and Rhodamine B dye were used as the calibrant for each aperture - the zero end points of which were samples of pure distilled water. As shown in Appendix 3, the calibration curves are arithmetically linear. From simple graphical analysis the curves can be mathematically represented as:

Aperture No. 3

$$[3.02] \quad C_t = 0.2083\ F_1$$

Aperture No. 10

$$[3.03] \quad C_t = 0.0729\ F_1$$

Aperture No. 30

$$[3.04] \quad C_t = 0.0370\ F_1.$$

The dimensionless fluorometric dial reading is represented by F_1 and the concentration of fluorescence dye in micrograms per liter is represented by C_t.

Fluorescence concentration C_t is a function of temperature and the quantity of settleable solids. According to Butts (5) fluorescence concentrations in water are inversely proportional to temperature changes by an exponential function. Butts also indicates the degree of fluorescence change in the vicinity of 20° Celsius is small when temperature changes are small.

Since the temperature of samples was maintained between 16 and 20° Celsius, corrections were considered unnecessary in this study.

Conversely, settleable solids have a large influence on fluorescence and can not be ignored. When a fluorescent dye is injected into a solution laden with suspended solids, a dye adsorption reaction on individual solids particles can be expected. As the suspended solids settle to the bottom of the sedimentation tank, the concentration of dye in the effluent will become less in an amount much less than the normal dilution process. If one is only concerned with the dilution process, then the fluorescence of the collected sample must include an upward correction.

The correction factor is readily developed by fluorometrically analysing mixed liquor and final effluent samples where the quantities of suspended solids are known. First, a background correction is developed from an undosed sample and secondly, a correction is developed from a dosed sample. In both cases samples of unsettled mixed liquor and settled final effluent are used. The summation of the two corrections will be the total correction for settled solids. In this investigation the correction will be derived from a graphical analysis of fluorescence concentration and the fraction of removed suspended solids. Because the adsorption process is complex

and beyond the scope of this thesis, the correction will be estimated by assuming that fluorescence is inversely proportional to the amount of removed suspended solids. Hence a simple linear slope-intercept derivation will be used.

From Table 3.01, the dimensionless fraction of suspended solids removed S_r is 0.9955 (i.e. 1.0000 - 15.0000/3344.0000) for both background and dosed samples of final effluent. In Figure 3.01, fluorescence values of 1.09 µgm/l and 4.01 µgm/l (from Table 3.01) are plotted respectively, as ordinates against a common abscissa value of S_r = 0.9955. When the fraction of removed suspended solids is zero, as would occur in unsettled mixed liquor, the corresponding fluorescence value will occur as the Y intercept. Also in Figure 3.01, fluorescence values of 5.42 µgm/l and 6.04 µgm/l (from Table 3.01) are plotted respectively, as ordinates against a common abscissa value of S_r = 0.0000. By the slope-intercept method the fluorescence background correction C_b in micrograms per liter can be shown as:

$$[3.05] \qquad C_b = -4.35\ S_r + 5.42$$

In a similar manner, the fluorescence correction for the dosed sample C_d in micrograms per liter is:

$$[3.06] \qquad C_d = -2.40\ S_r + 6.04$$

Thus it is mathematically shown that the concentration of background and dosed fluorescence diminishes as

settleable solids are removed. It is desirable to preclude the effects of natural background fluorescence and consider only the effects of dosed fluorescence. It is reasonable then to assign a negative sign to the quantity defined by C_b and sum equations 3.05 and 3.06. This manipulation leads to:

[3.07] $$C_s = 1.95\ S_r + 0.62$$

Equation 3.07 defines the intermediate region between lines C_b and C_d in Figure 3.01. This summation of background and dosed corrections is represented by C_s in micrograms per liter.

Clearly, equation 3.07 is valid only for the initial injector dye concentration of C_o = 2.5 µgm/l. A more general form can be derived if it is assumed that the magnitude of the correction is directly proportional to any initial fluorescence concentration C_o in the dye injector such that:

[3.08] $$\frac{C_s}{C_o} = \frac{C_c}{C_t}$$

The measured concentration of fluorescence at any time T in the prototype tank is represented by C_t in micrograms per liter. The proportional concentration correction of C_s is represented by C_c in micrograms per liter. Hence for a fluorometric dye test using small initial concentrations of Rhodamine B dye in mixed liquor, equations 3.07 and 3.08 can be combined to take the form:

[3.09] $$C_c = 0.78\ S_r + 0.25\ C_t$$

Table 3.01 Average Fluorescence and Suspended Solids Measurements for Correction Factors.

Sample		Description
Fluorescence (µgm/l)	Suspended Solids (mg/l)	
1.09	15	Background - Final Effluent
5.42	3344	Background - Mixed Liquor
4.01	15	Dosed* - Final Effluent
6.04	3344	Dosed* - Mixed Liquor

* The dosed sample represents a 2.5 µgm/l solution of Rhodamine B dye.

The typical fraction of removed suspended solids S_r is 0.9955 (i.e. 1.000 - 15.0000/3344.0000) which accurately represents the secondary process in normal operation. These measurements were taken from secondary sedimentation tank No. 1 on March 22, 1976 and are graphically analysed in Figure 3.01.

In each dye test the fraction of removed solids is readily evaluated by standard laboratory methods and is assumed constant throughout the test period. The final corrected concentration of fluorescence C is the summation of any measured value C_t at time T and the quantity represented by C_c in equation 3.09.

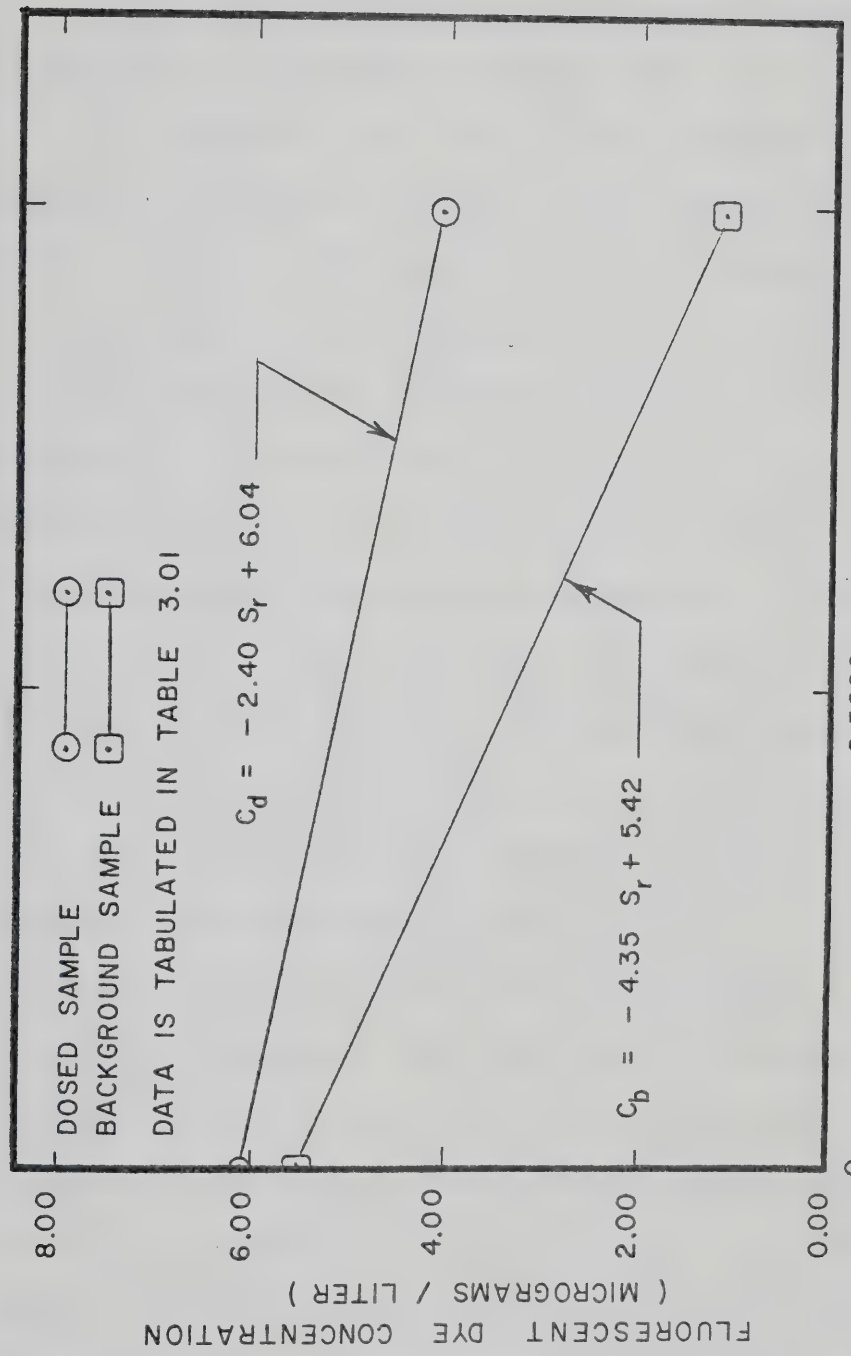

FIG. 3.01 FLUORESCENCE CORRECTION FOR SETTLEABLE SOLIDS

Mathematically, this will be:

$$[3.10] \qquad C = C_t + C_c$$

The results of eight independent dye tests are assembled in the time-concentration curves of Appendix 4. In the assembly, the lower curve represents the field measured concentration C_t and the upper curve represents the corrected concentration for the percentage of removed solids according to equation 3.10. For the purpose of theory development, the ideal time-concentration schematic of Figure 3.02 is a representation of the Appendix 4 curves. In the schematic the lower plateau region between the ordinate and point I indicates the time period T_i for the first detectable particles of fluorescent dye to reach the sampling station. The portion of curve between points I and J represents the time (T_j-T_i) for the control volume to attain the maximum concentration of dye. This is clearly a function of the velocity and the strength of the dye initially injected. The time period represented by (T_k-T_j) is significant only in that as this magnitude becomes large, point J is more accurately defined. When the injection of dye is stopped the control volume begins washing out and the concentration begins diminishing to the original state. This behaviour occurs to the left of point K. The most significant portion of the time-concentration curve in this study

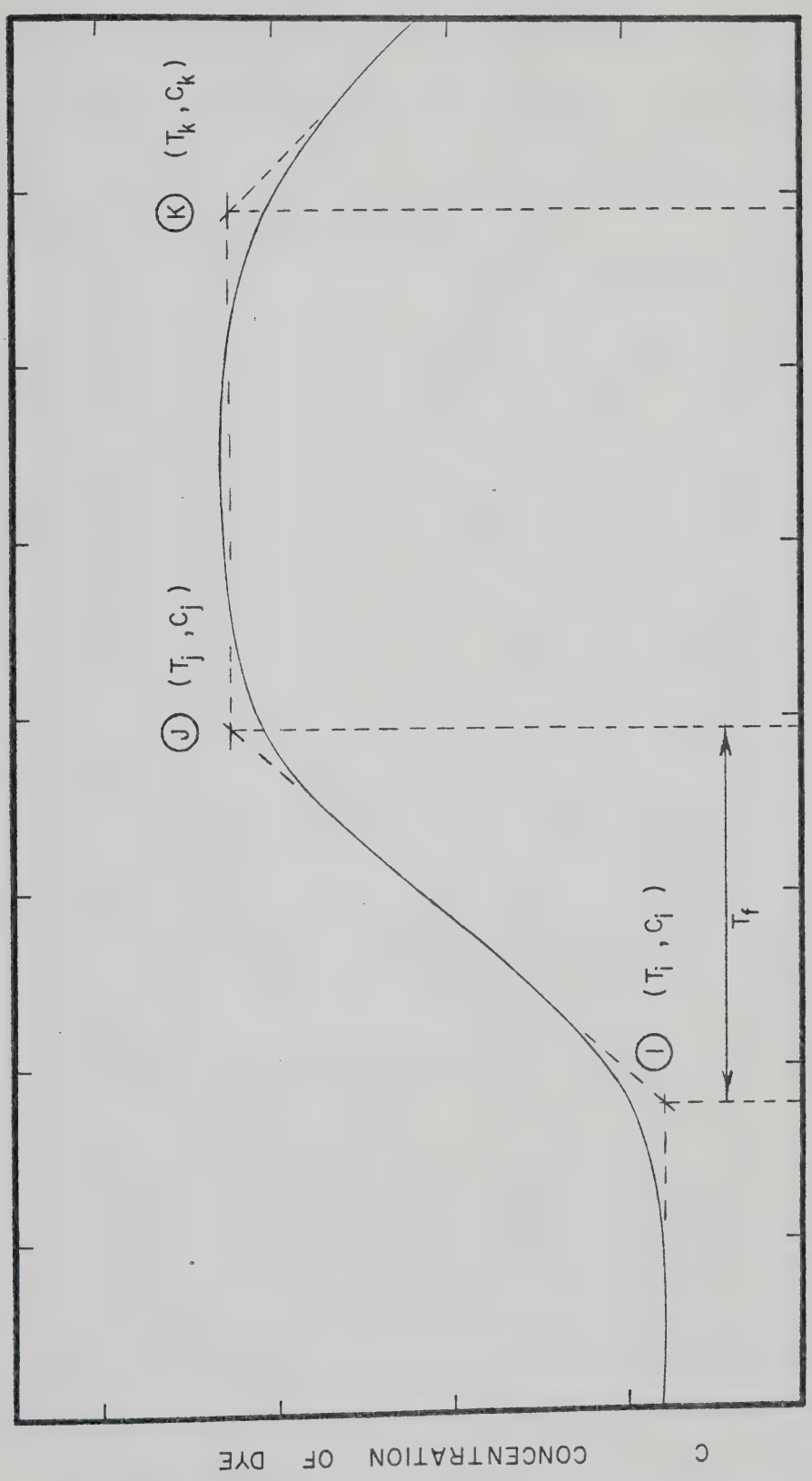

FIG. 3.02 TIME – CONCENTRATION CURVE SCHEMATIC

occurs between points I and J. This period (T_j-T_i) represents the detention time of dye particles between the injection station and sampling station and will be identified simply as T_f.

The ideal curve in Figure 3.02 has illustrated a pattern which can be observed in the curves of Appendix 4. In all cases the lower plateau regions are well defined, however, the upper plateau regions are erratic and must be estimated by visual observation. The erratic trends can generally be attributed to two conditions. First, flow variations during the test execution cause an inverse variation in the dye concentration. In reference to the typical flow record shown in Figure 3.03, it is important that all testing be performed during the periods of fairly constant flow beginning at either 11:00 AM, 6:00 PM, or 5:00 AM on any day. In this investigation all testing was started at the beginning of the flow plateaus marked by the two morning times.

Secondly and less frequently, instantaneous changes in secondary sewage composition caused an erratic trend in the time-concentration curve. Often sudden, short-lived waves of suspended solids particles were observed at the sampling station. These waves were especially conspicuous during periods of high flow. Because the fluorometer is sensitive to abnormal fluorescence levels

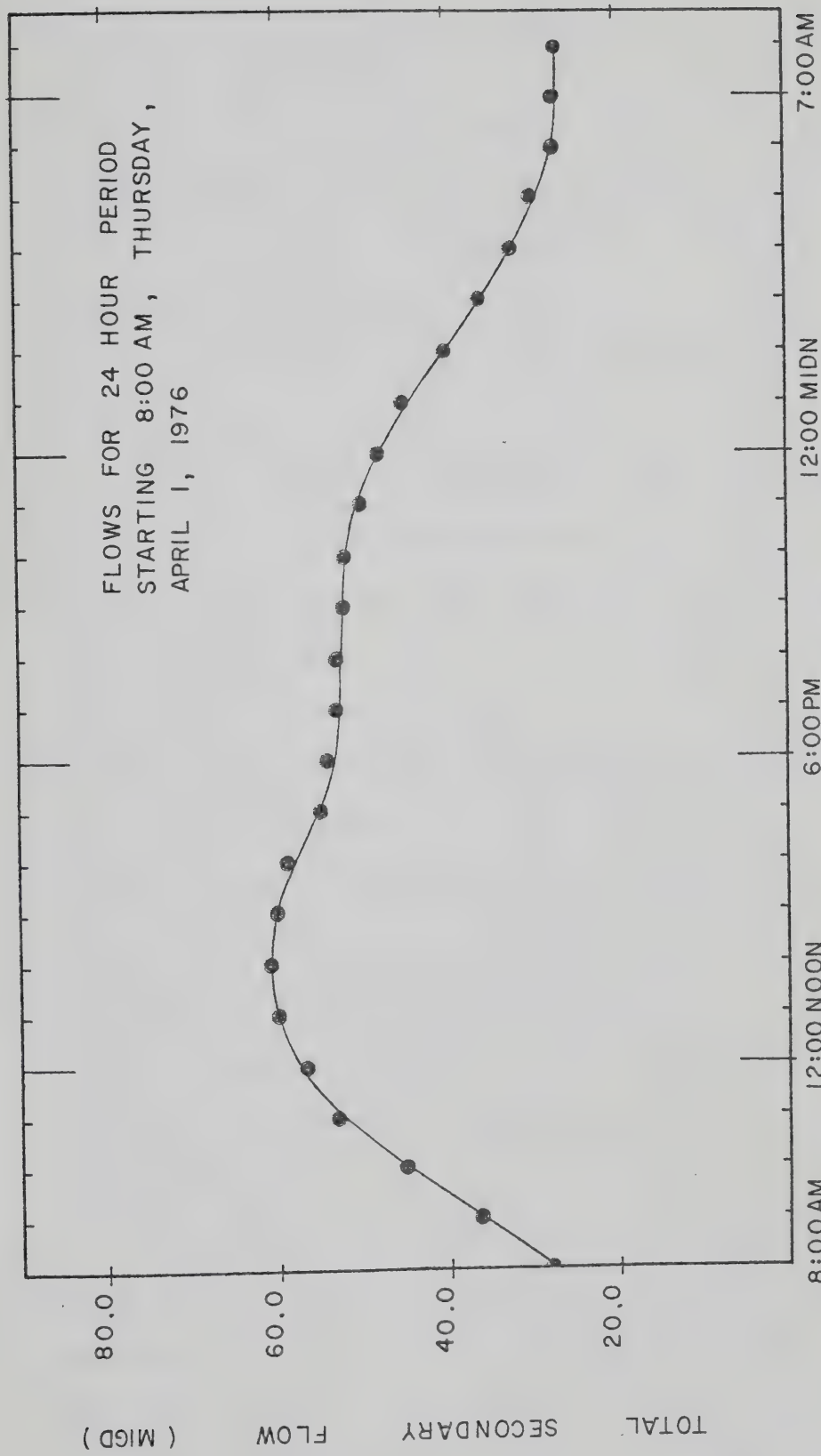

FIG. 3.03 TYPICAL SECONDARY SEWAGE FLOW

generated by these waves, erratic readings were obtained. This characteristic is especially notable in tests 7 and 8, where samples were taken adjacent to the northerly walls of the prototype tank. With good judgment, the high fluorescence readings were accurately edited from the test data. Table 3.02 summarizes the detention times and cell flows derived from the eight dye tests in Appendix 4.

A more important approach to the fluorometric examination is the dimensionless analysis of the time-concentration curve. The complexities of varying cell flows and dye injection rates can be mathematically eliminated, if dimensionless ratios for time and concentration are used. Time and concentration terms can be made dimensionless ratios by dividing each with an index term. These ratios can then be plotted on a Cartesian coordinate system for common comparisons. The abscissa and ordinate are represented as T/T_d and C/C_u, respectively, where T and C are actual measured quantities in a dye test. Denominators T_d and C_u are the index terms.

The dimensionless theory was applied to sedimentation processes in a treatise by Camp (6), in a section dealing with short-circuiting and stability. Using the Camp theory, this study will define the time index T_d as the detention time for fluid particles in the control

Table 3.02 Summary of Prototype Dye Tests

Test Number & Sampling Criteria	Cell Flow Q (CFS)	Dye Detention Time T_f (Min)	Maximum Time Ratio T_r	Maximum Concentration Ratio C_r
1 b	5.4	35	0.82	1.21
2 a	2.4	62	0.65	1.21
3 a	6.0	99	2.52	1.00
4 b	1.5	67	0.48	2.25
5 c	6.8	47	2.06	0.98
6 d	6.2	64	1.98	0.88
7 f	5.2	45	1.74	0.85
8 e	5.1	62	1.32	1.06

Sampling Criteria:

(a) Tank No. 1, Weir No. 1, b_o = 6.00 ft

(b) Tank No. 3, Weir No. 1, b_o = 9.67

(c) Tank No. 1, Weir No. 4, b_o = 6.00

(d) Tank No. 3, Weir No. 4, b_o = 9.67

(e) Tank No. 1, North End, b_o = 9.67

(f) Tank No. 3, North End, b_o = 6.00

This summary is developed from the parameters in Appendices 4 and 5.

volume according to:

$$[3.11] \qquad T_d = \frac{P}{Q}$$

The cell volume and rate of flow are represented by P and Q, respectively. The dye concentration index C_u is defined as the concentration of dye which is instantaneously dispersed in the control volume of the cell. If it is assumed that the dye is totally conserved in the control volume, then C_u can be mathematically defined as:

$$[3.12] \qquad C_u = \frac{P_o C_o}{P}$$

The initial volume and concentration of dye in the injector is represented by P_o and C_o, respectively.

Figure 3.04, a reprint with modifications from Camp in "Sedimentation and Settling Tank Design," (6) illustrates six typical dispersion curves for tanks. According to Camp, curve A is developed from the "ideal dispersion tank" and is approximated by the equation shown in Figure 3.04. By definition this tank has an instantaneous and uniform distribution of suspended particles. Curve F (actually a straight line) represents the "ideal settling basin" where T/T_d is constant at unity and C/C_u can approach infinity. When T/T_d is unity, the velocities of all stream lines within the tank are uniform and constant. Situated between hypothetical curves A and F are intermediate

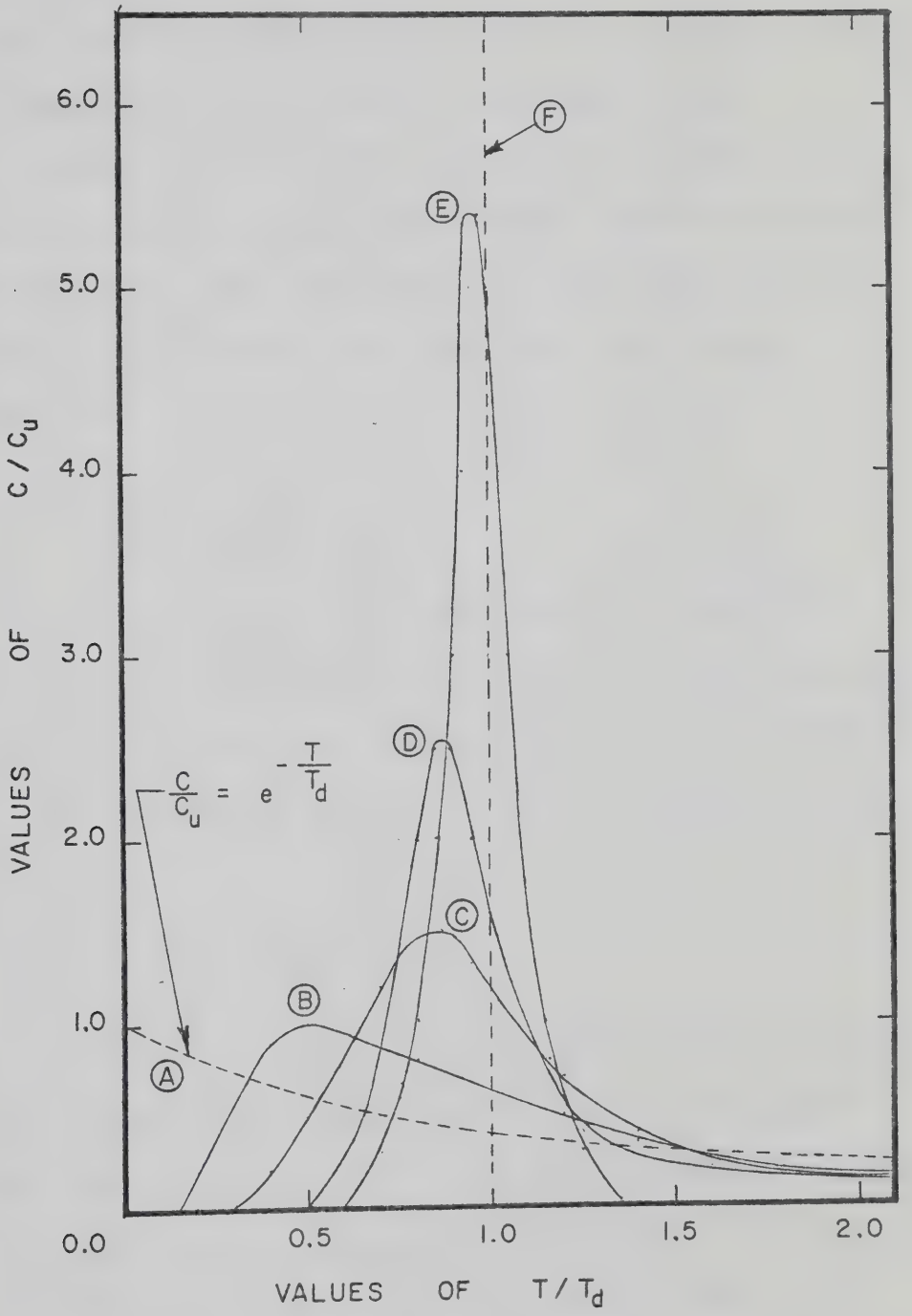

FIG. 3.04 TYPICAL DISPERSION CURVES FOR TANKS — REPRINTED WITH MODIFICATIONS FROM T. R. CAMP (6)

curves B, C, D, and E. Curves B, C, and D are derived from operating prototype tanks of various configurations. Curve E depicts a model tank in the Camp study.

According to the Camp study, dimensionless time-concentration curves generally assume a Gaussian shape. The indicator of tank performance is the magnitude of T/T_d when C/C_u reaches a maximum value according to the differential:

$$[3.13] \qquad \frac{d\ (T/T_d)}{d\ (C/C_u)} = 0$$

It will be assumed that the center of gravity on the abscissa of the slightly less than perfect Gaussian curve occurs at the point where C/C_u reaches a maximum value. By definition in this study, when differential equation 3.13 is valid then:

$$[3.14] \qquad T_r = \frac{T}{T_d}$$

It is apparent that as T_r assumes values less than one, the actual travel time T of a particle is less than the detention time T_d. Thus flow stream lines are not reaching certain regions within the control volume, short-circuiting occurs, and dead spaces exist. Conversely, as T_r assumes values greater than one, the actual travel time of a particle exceeds the detention time and flow stream lines are recirculating.

Also by definition, when differential equation 3.13 is valid, the following will apply:

$$[3.15] \quad C_r = \frac{C}{C_u}$$

If C_r assumes values less than one, then the actual particle concentration C is less than the ultimate concentration C_u. Thus the flow stream lines are directing the solution to other regions in the control volume and a favorable condition of particle dispersion exists. When C_r assumes values greater than one, the actual particle concentration exceeds the ultimate concentration. Thus flow stream lines are not causing sufficient dilution, short-circuiting occurs, and dead spaces exist.

The ideal sedimentation process will occur when T_r and C_r are equal to one. This condition would provide a control volume precisely large enough to accommodate all particles with no recirculation and small enough to preclude short-circuiting and dead spaces. Since sewage flows and composition are variables, the ideal process can be considered purely hypothetical and will not be pursued further in this study.

It can now be said of Figure 3.04 that the sedimentation performance improves as T_r approaches and exceeds one and as C_r approaches and becomes less than one. Mathematically these limits are shown as:

[3.16] $T_r \geq 1.00$

[3.17] $C_r \leq 1.00$

The dimensionless theory has been applied to the fluorometric tests for the prototype sedimentation tanks in this study. The developed curves appear in Appendix 5. Dye tests 1, 2, 4, 7 and 8 have resulted in distinct Gaussian shaped curves. The remaining curves have merely a Gaussian trend which possibly would have been more distinct had the test period been longer. The values of T_r and C_r have been estimated and are summarized in the two right hand columns of Table 3.02. Dye flows are constant in all tests.

The theories for the time-concentration curves and the dimensionless time-concentration curves are applied to actual field data collected from the first cells of sedimentation tanks one and three. A qualitative review of Table 3.02 with respect to equations 3.16 and 3.17 is covered in the following discussion:

Test No. 1 (Tank No. 3, Weir No. 1)

The test indicates short-circuiting between the baffle and the weir. Dead spaces will exist in the remote regions of the cell. There is a negative deviation of approximately 20% for both T_r and C_r. The flow of 5.4 cfs is considered a normal load and can be expected during most daytime hours.

Test No. 2 (Tank No. 1, Weir No. 1)

The test indicates short-circuiting between the baffle and the weir with dead spaces in the remote regions of the cell. Negative deviations of 35% and 20% exist for T_r and C_r, respectively. Although typical for the early morning hours, the flow of 2.4 cfs is small and short-lived.

Test No. 3 (Tank No. 1, Weir No. 1)

The test with a large midday flow of 6.0 cfs indicates a highly efficient process. A positive deviation of 152% occurs for T_r while C_r assumes the ideal unit value. Flow stream lines appear to be directing the dye to the remote regions at some elevation well below the first effluent weir. The test tends to confirm the presence of the lower positive current and the upper negative current discussed in Chapter 4. The large magnitude of T_f = 99 min also reinforces this pattern. In large flows, large values of jet stream momentum logically account for the emergence of dye particles at points downstream from the first weir.

Test No. 4 (Tank No. 3, Weir No. 1)

The results of this test with the low flow of 1.5 cfs are consistent with the second test. Short-circuiting occurs between the baffle and the first weir

while dead spaces occur in the remote regions of the cell. A negative deviation of 52% and 152% exist for T_r and C_r, respectively.

Test No. 5 (Tank No. 1, Weir No. 4)

Positive deviations of 106% and 2% for T_r and C_r respectively, indicate optimum performance in this test. The large flow of 6.8 cfs appears to disperse the dye particles throughout the cell in a manner similar to the flow of the third test. The dye detention time of T_f = 47 min indicates a generally direct path between the baffle and the fourth weir. This test also reinforces the concept of a lower positive current and an upper negative current.

Test No. 6 (Tank No. 3, Weir No. 4)

Positive deviations of 98% and 12% occurring for T_r and C_r, respectively, indicate an optimal process in this test. The flow of 6.2 cfs is a heavy flow which frequently occurs. The dye detention time T_f = 64 min continues to confirm the presence of a lower positive current which is similar to the third and fifth tests.

Test No. 7 (Tank No. 3, North End)

Samples were collected adjacent to the northerly end of the cell where a large vertical roller appears to

exist. Positive deviations of 74% and 15% occur for T_r and C_r, respectively, with an intermediate flow of 5.2 cfs. The detention time T_f = 45 min, similar to the time in the fifth test, implies that a lower current zone exists.

Test No. 8 (Tank No. 1, North End)

This test, with an intermediate flow of 5.1 cfs, is similar in every way to the seventh test. A positive deviation of 32% occurs for T_r and a small negative deviation of 6% occurs for C_r. A detention time of T_f = 62 min tends to confirm the existence of a lower positive current.

On the basis of eight dye tests the following patterns appear to exist:

(1) Short-circuiting and dead spaces are minimal as the flows approach the larger magnitudes of 6.0 to 6.5 cfs. The present tank is hydraulically efficient for flows of this order. It is predictable that flows in excess of 6.5 cfs will result in values of T_r less than unity, a condition of hydraulic overloading.

(2) Short-circuiting and dead spaces dominate the sedimentation process at low flows. This trend merely confirms the presence of a hydraulic safety factor for the peak flow periods and can not be considered a critical problem.

These trends will be investigated further under controlled laboratory conditions in the model study of Chapter 4.

In conjunction with the fluorometric study, Table 3.03 provides a tabulation of the settling velocities of solid particles entering the secondary sedimentation process. Samples of mixed liquor, taken at the cross-channel gauging station, were placed in a 6.00 cm diameter, 1000 ml graduated cylinder. In conformance with the discussion by Metcalf and Eddy (7), the time rate of vertical displacement V_s of the sludge blanket (zone settling region) was measured with a stop watch. Since the sludge removal chains are in continuous operation in each cell, the compression zone of settling is not considered. The settling velocities from four independent tests are shown in Table 3.03. When discussing tank performance in Chapters 4 and 5, the average settling velocity of $V_s = 6.68\ (10^{-2})$ cm/sec [$2.19\ 10^{-3}$) ft/sec] will be used.

Table 3.03 Average Settling Velocities for Suspended Solids in Secondary Mixed Liquor.

Test No.	Measured Settling Velocity V_s	
	$X(10^{-2})$ (cm/sec)	$X(10^{-3})$ (ft/sec)
1	4.05	1.33
2	9.54	3.13
3	3.90	1.28
4	9.24	3.03
Average	6.68	2.19

[4] MODEL STUDY

Flow patterns in the prototype sedimentation tank were examined in closer detail with a laboratory model. In all portions of the sedimentation tank a free water surface exists with very low velocities. This condition is analogous to open channel hydraulics where only the ratio of dynamic forces to inertial forces is significant. The ratio of dynamic forces to gravitational forces is represented by the Froude number F and is shown mathematically as:

$$[4.01] \qquad F = \frac{\overline{V}}{[gL]^{1/2}}$$

The mean velocity in the system is represented by $\overline{V}$, g is the gravitational constant (32.2 ft/sec^2), and L is a vertical or horizontal characteristic length. Streeter (8) has used dimensional analysis with the Buckingham Pi Theorem to derive equation 4.01.

From the basic definition of the Froude number, it can be said that the ratio of dynamic forces to gravitational forces is the same for a prototype and its model counterpart. Mathematically this will be:

$$[4.02] \qquad F_p = F_m$$

The subscripts p and m represent prototype and model Froude numbers, respectively. Equations 4.01 and 4.02 can be manipulated to form:

$$[4.03] \quad \frac{\overline{V}_p}{[gL_p]^{1/2}} = \frac{\overline{V}_m}{[gL_m]^{1/2}}$$

It is necessary to design a model having geometric dimensions which completely coincide with prototype dimensions. Consequently, a constant geometric scale factor S_f can be defined as:

$$[4.04] \quad S_f = \frac{L_p}{L_m}$$

Equation 4.04 can be substituted into Equation 4.03 and simplified. This manipulation leads to:

$$[4.05] \quad \frac{\overline{V}_p}{\overline{V}_m} = S_f^{1/2}$$

The characteristic lengths in Equation 4.04 can be squared and cubed for an area parameter A and a volume parameter P, respectively. The result of this operation is:

$$[4.06] \quad \frac{A_p}{A_m} = S_f^2$$

$$[4.07] \quad \frac{P_p}{P_m} = S_f^3$$

When the hydraulic continuity equation, $Q = A\overline{V}$, is substituted in Equation 4.05 for the velocity and combined with Equation 4.06, a volumetric rate of flow ratio is derived: This will be:

[4.08] $$\frac{Q_p}{Q_m} = S_f^{5/2}$$

Velocity is the time rate of displacement of the form:

[4.09] $$\overline{V} = \frac{L}{T}$$

Time is represented by T. Equation 4.09 can be combined with Equation 4.04 and simplified. This simplification will be:

[4.10] $$\frac{T_p}{T_m} = S_f^{1/2}$$

It is desirable to construct a model with as large a scale as possible for purposeful research and small enough for laboratory accommodations. Thus practical dictations call for a scale factor of twenty ($S_f = 20.0$). The previously developed equations for length, area, volume, velocity, discharge, and time can be summarized in the following fashion:

[4.11] $$\frac{L_p}{L_m} = 20 \qquad \text{(Length)}$$

[4.12] $$\frac{A_p}{A_m} = (20)^2 \qquad \text{(Area)}$$

[4.13] $$\frac{P_p}{P_m} = (20)^3 \qquad \text{(Volume)}$$

[4.14] $$\frac{\bar{V}_p}{\bar{V}_m} = (20)^{1/2} \qquad \text{(Velocity)}$$

[4.15] $$\frac{Q_p}{Q_m} = (20)^{5/2} \qquad \text{(Discharge)}$$

[4.16] $$\frac{T_p}{T_m} = (20)^{1/2} \qquad \text{(Time)}$$

Using the coordinate convention of the prototype, the ordinate and abscissa of the model will coincide with the influent wall and the floor, respectively. The latitudinal axis will be represented by Z.

Only one cell of the prototype tank was scaled to model proportions. The 1:20 reduction developed a model tank having an effective length of 8.25 ft, a width of 0.80 ft and an average liquid depth of 0.70 ft. The tank was constructed of clear acrylic plexiglass plate having a 1/2 in. wall thickness and was framed in rolled aluminum stock. The model was designed to be geometrically coincident with the prototype with two exceptions. Firstly, a horizontal floor was used in lieu of a sloping floor. It was not practical to scale a floor slope with a magnitude of 0.00753 ft/ft. Secondly, the sludge chains and flights were deleted from the model tank. The economics and physical complexities of a small scale moving chain outweighed any useful gain.

The model was designed as a self-contained unit where all water was discharged and recirculated to a central reservoir. The reservoir consisted of a standard forty-five-gallon steel drum with one end removed and an epoxy paint rust control liner. A Monarch Model 454 submersible pump was installed in the reservoir. Hydraulic loading was controlled with a throttling valve and a flow meter in the pump discharge line. Initially, a 5/8 in. Neptune-Trident water meter was used for control. Later the meter was replaced with a more efficient and accurate Fischer and Porter rotometer rated for a maximum flow of 2.7 ± 2% U.S. gallons per minute.

The piping design provided effluent weirs and a return line in the model tank for recycle to the reservoir. Flows in the return line, Q_r, were maintained within the range of 20% to 30% of the total model flow Q, by a throttling valve and time-volumetric calibration. Apart from the four effluent weirs normally occurring in the prototype, two additional weirs were installed in the model. The effluent weirs were fabricated from 1 1/2 in. copper tubing longitudinally machine cut on either side at the spring line. The upper semicircular sections were removed entirely and the remaining edges were sharpened for the benefit of good weir hydraulics. Each of the weirs were fitted

to machined, eccentric cam fittings on either side of the tank. These gasket sealed fittings provided fine vertical adjustments for each weir. The flows across the weirs, Q_w, were redirected to the reservoir by means of a common external collector manifold and flexible tubing connectors. Flow rates for each weir were further controlled by means of a throttling clamp bar across the flexible connectors.

The fixed baffle wall at the influent end of the prototype tank was simulated in the model by an aluminum plate designed as a sluice gate. For greater versatility in the efflux opening b_o, a threaded adjustment was installed on the model baffle. Water depths in the tank were measured with a pointer gauge equipped with a 0.001 ft vernier. The same assembly served as a holder for a standard laboratory syringe. This apparatus enabled the injection of fine, minute dye streams into the main stream of the model for any value of X, Y, or Z. A conceptual plan of the sedimentation tank model is shown in Figure 4.01. The photographs of Figures 4.02 and 4.03 illustrate actual details of the model.

Water was used as the fluid media in the model study and as expected was a source of two principal obstacles in the analysis. Firstly and least significantly, surface tension caused unbalanced flows over the

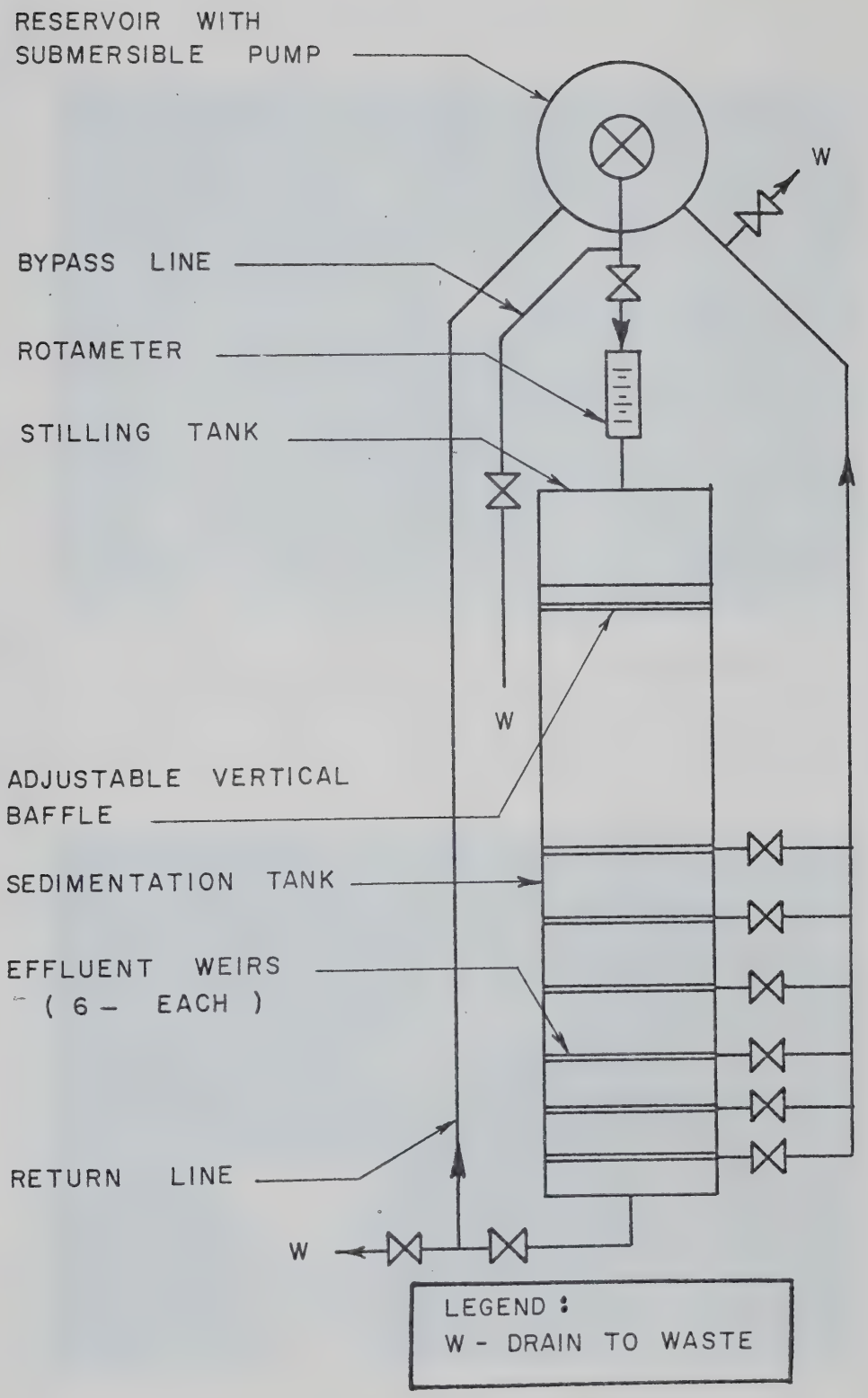

FIG. 4.01 SCHEMATIC OF SEDIMENTATION TANK MODEL

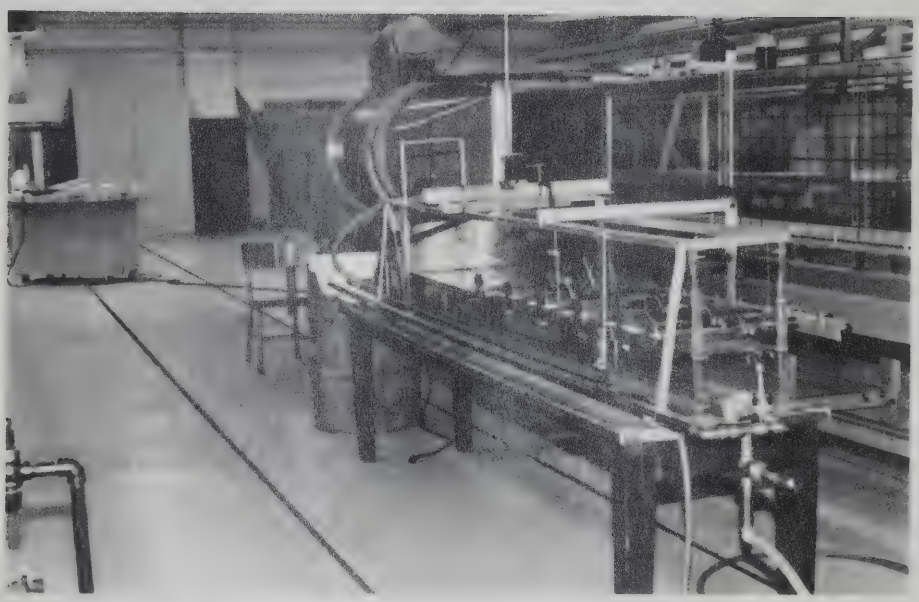

Fig. 4.02 Effluent End of Sedimentation Tank Model

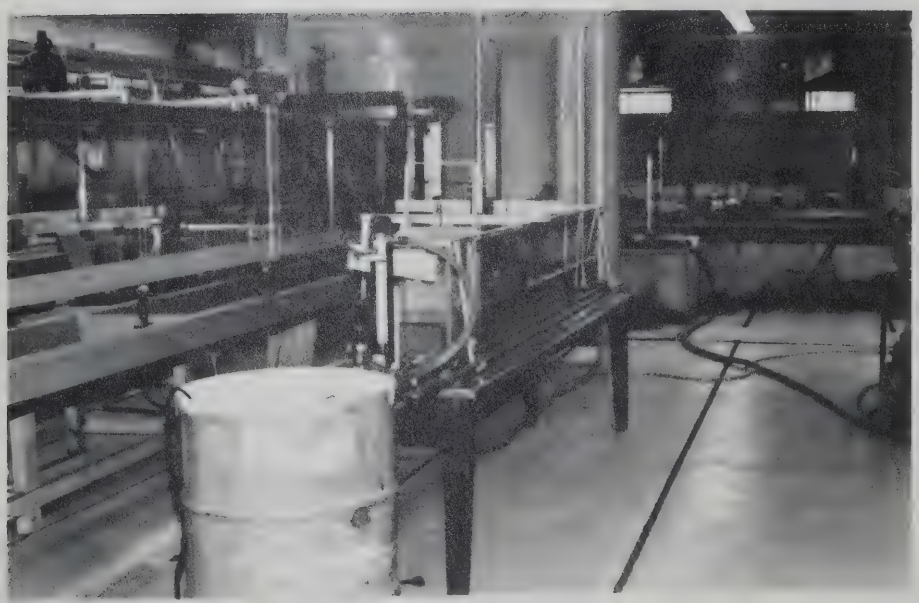

Fig. 4.03 Influent End of Sedimentation Tank Model

edges of the effluent weirs. Initially, injections of "Calgon" detergent relieved the condition, however, this method was abandoned when found to be in conflict with the solution to the density current obstacle. Finally, the solution for surface tension interference was found to be in the precise leveling of all weirs and the fine adjustment of the external bar clamp. Although flows in each weir were equalized with precision, it was necessary to operate them in a submerged condition. Latitudinal (Z direction) movements of dye streams on the surface were insignificant, hence flows along the length of the model weir were considered uniform. Except for exceedingly heavy flows, the prototype weirs are seldom operated under submerged conditions.

Secondly and more critically, density currents caused interference in the model operation. Since the water was continuously recirculated in the closed system, adverse temperatures induced a specific gravity differential and abnormal flow patterns developed. Water was stored in the reservoir and tank at an ambient temperature of approximately 19 to 20 degrees Celsius (°C.) in the laboratory. During each test, heat generated by the submersible pump caused the reservoir temperature to rise to about 25°C. Since the specific gravity is inversely proportional to temperature,

positive currents[1] are formed in the upper zone and negative currents[1] are formed in the lower zone of the tank. When specific gravity differentials induced by floc particles are considered for a normally operating prototype, it is apparent that these model flow patterns are unreasonable.

The density current dilemma was overcome by heating water within the model tank to a temperature of about 30°C. City tap water having a temperature of 18°C was pumped from the reservoir to the tank and all water was wasted rather than recirculated. Consequently, a distinct positive current with a temperature ranging between 18°C and 25°C occurred in the lower zone of the tank while a distinct negative current with a temperature ranging between 25°C and 30°C occurred in the upper zone. The two zones were clearly separated by a turbulent zone. Uncontrollable heat exchanges caused the specific gravity differential to be short lived, thus only one velocity profile was obtained from each test.

More useful is a comparison of the media specific gravities in the prototype and model. With respect to

---

[1] In a Cartesian coordinate system a positive current is defined as one with the velocity component in the positive X direction and a negative current is defined as one with the velocity component in the negative X direction.

the temperature ranges of the model media in the preceding paragraph, Table 4.01 has been reprinted from the Handbook of Chemistry and Physics (9). In the third column of Table 4.01 it is seen that the specific gravity of water has a maximum deviation of -0.155% at 18°C. and +0.140% at 30°C. with respect to the equilibrium temperature of 25°C. When the typical model test is operating under normal conditions, 50% of the maximum specific gravity deviation can be considered the average deviation. Thus in a normal model test, it can be said that the specific gravity of the water media has an average deviation of ±0.074%. The exact values appear in the right hand column of Table 4.01.

The specific gravity distribution for prototype media is shown graphically in Figure 4.04. A hydrometer was used to measure the specific gravity of the influent and final effluent in the prototype tank. Since a continuous operating chain prevents any sludge accumulation in the prototype cell, it is assumed that the specific gravity due to suspended solids varies inversely and linearly with the depth. When the fraction of removed suspended solids is of the order of 98% and the prototype depth does not exceed 12.0 ft, the specific gravity S is related to the depth Y according to:

$$[4.17] \quad Y = -12371.1 \quad S + 12396.5$$

$$\text{for } 0.0 \geq Y \leq 12.0$$

Table 4.01 Relative Density of Water - Reprinted from Handbook of Chemistry and Physics (9)

Water Temperature (Deg.C.)	Specific Gravity	Percentage Differential Based on Specific Gravity at 25°C. (%)	Average Differential (%)
18	0.99862	-0.155	-0.078
25	0.99707	0.000	0.000
30	0.99567	+0.140	+0.070

Equation 4.17 is used to calculate the specific gravities at the top, bottom, and intermediate levels of the prototype cell. These values and the average deviations are tabulated in Table 4.02. To summarize, the average specific gravity of the prototype media varies by ±0.05% and the average specific gravity of the model media varies by ±0.07%. When this comparison is considered, it must be remembered that the prototype media is laden with varying quantities of suspended solids and has a mean temperature of 20°C. while the model media has no suspended solids and has a mean temperature of 25°C. Thus specific gravity differentials are the inherent weaknesses of model studies of this kind.

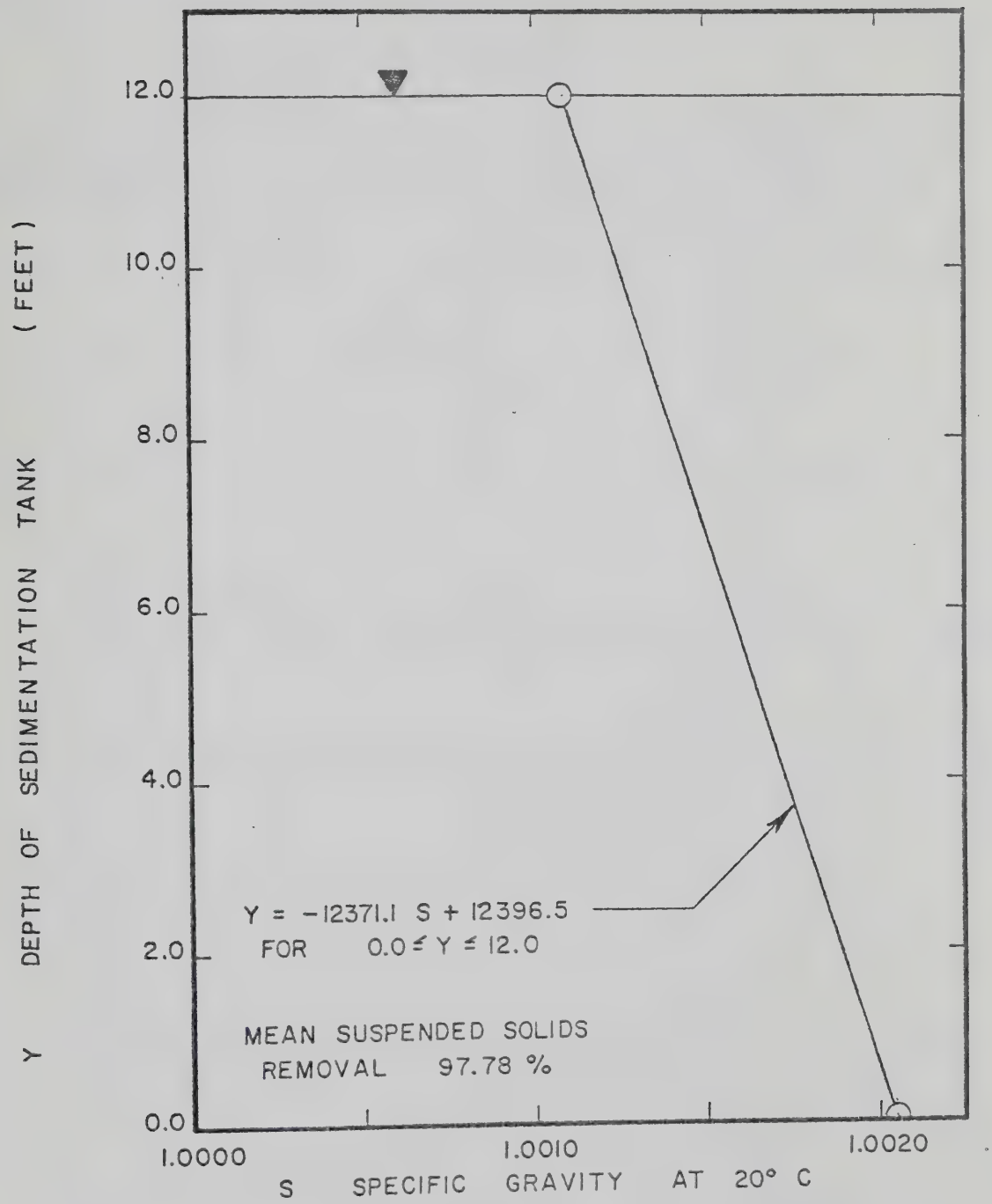

FIG. 4.04 MEAN SPECIFIC GRAVITY AS A FUNCTION OF DEPTH IN THE SECONDARY SEDIMENTATION TANK

Table 4.02 Relative Density of Water in Prototype Tank - Calculated from Equation 4.17

Prototype Water Depth Y (ft)	Specific Gravity S	Percentage Differential Based on Specific Gravity at Y = 6 ft (%)
0	1.00205	+0.048
6	1.00157	0.000
12	1.00108	-0.049

More accurate model parameters could certainly have been developed if more sophisticated density control equipment had been available. Yet, it is difficult to economically justify more sophisticated equipment when the prototype parameters are never constant. Clearly, Figure 4.04 can be considered an approximation of prototype specific gravity behavior. Specific gravity is a function of temperature, chemical composition, suspended solids composition, and biological activity. These functions are continuously changing on short and long term bases.

Apart from limitations caused by poorly controlled specific gravity differentials, the model study continues to be a valuable guide for predicting flow patterns and trends in the prototype cell. Numerous methods of model analysis were attempted and most provided results of little value. Qualitatively, a successful analysis

was made by using small grains of potassium permanganate ($KMnO_4$) crystals. Quantitatively, velocity profiles with numerical values were developed from dye movements within the tank.

When density currents within the tank are carefully manipulated, positive laminar currents occur in the lower region and negative laminar currents appear in the upper region. A turbulent zone at mid-depth separated the upper and lower currents. This zone was composed of erratic localized velocities with large and small magnitudes in all directions of X, Y, and Z. At the influent end adjacent to the baffle, the upper negative current turned down and became entrained in the lower current in a manner similar to a submerged hydraulic jump. At the end adjacent to the return line, the lower positive current turned up and assumed the negative direction. In both cases when the upper and lower currents become entrained with one another, there was a critical condition of turbulence.

The turbulent zone depth Y_t, a function of flow, is small at low flows. As flows reach intermediate proportions, Y_t only slightly increases. When flows are further increased to abnormally large magnitudes, the value of Y_t increases until the total depth is consumed in turbulence. For low and intermediate flows, the water surface is nearly quiescent. In the $KMnO_4$

test, molecular diffusion of floating dye particles dominated any displacement due to the X, Y, and Z components of velocity. The exceptions to this pattern are the higher velocity regions at each end of the tank and adjacent to either side of the effluent weirs.

By strategically placing grains of $KMnO_4$, the described flow patterns are readily observed. The size and density of the crystals provided a slow settling velocity which left a distinct, lingering purple trail. Figure 4.05 is developed from the $KMnO_4$ study. The insert of Figure 4.05 and Figure 4.06 show a typical velocity profile where the maximum velocities in the upper and lower laminar zones are represented by V_u and V_l, respectively. Depths of the upper and lower laminar zones are denoted by Y_u and Y_l, respectively.

Quantitative velocity profiles were obtained from the model study by injecting small amounts of dye in the main stream. Undiluted amounts of red food coloring were injected with a syringe and a long hypodermic needle mounted on the pointer gauge. When minute traces of dye were injected, the specific gravity differentials between the dye and media were insignificant. This procedure caused the movement of distinct red dye nodules at the same velocity and parallel to the media streamlines. The velocity of the nodules was measured

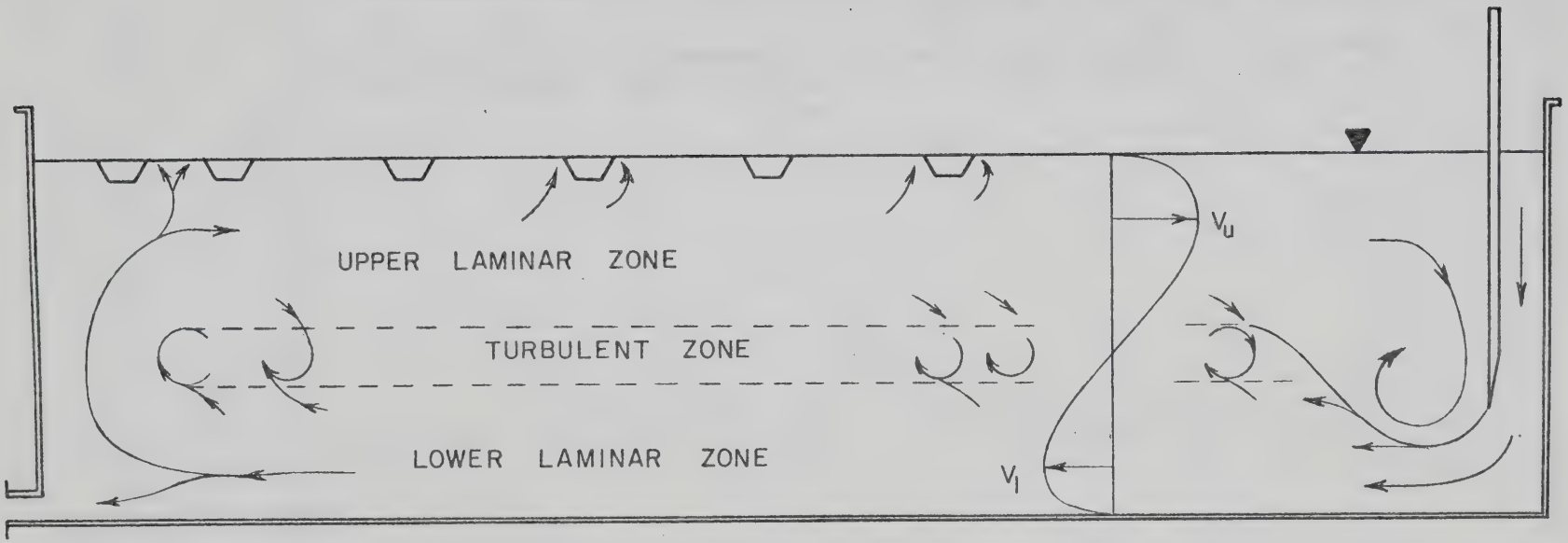

PROFILE SCHEMATIC MODEL TANK (N.T.S.)

FIG. 4.05 TYPICAL FLOW PATTERN FROM POTASSIUM PERMANGANATE TEST

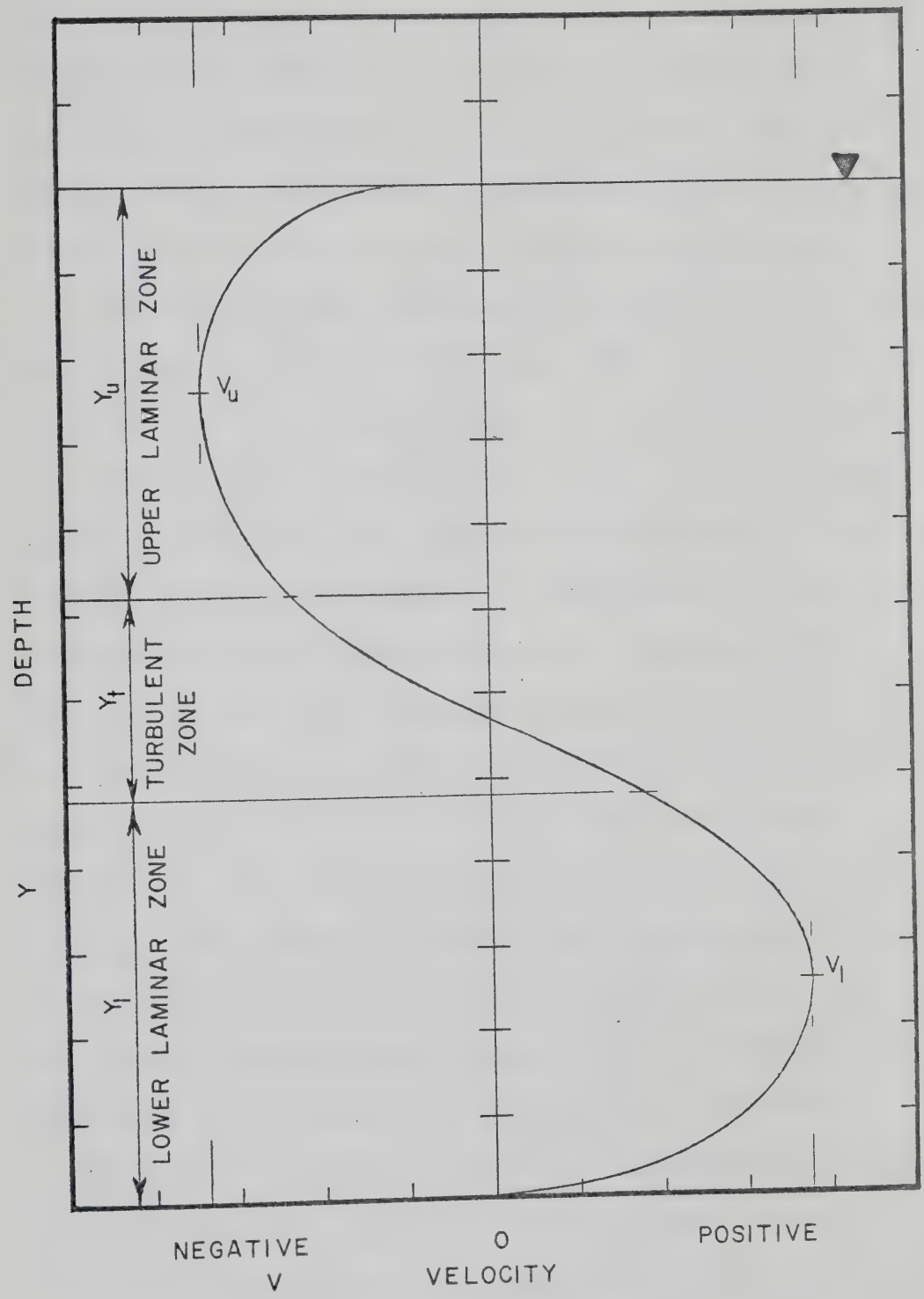

FIG. 4.06 CHARACTERISTIC VELOCITY PROFILE WITHIN THE MODEL TANK

with a stop watch as they moved across a linear grid installed on either side of the tank. As long as measurements were restricted to the upper and lower laminar zones at low and intermediate flows, accurate values of velocity along the X-axis were obtained.

Dye injections were made at several stations along the X axis, however the optimum model station was found to be X = 2.00 ft. Injections at this station eliminated the effects of slightly higher velocities from weir constrictions and from turbulence generated by the end rollers. Again, the molecular dispersion of dye particles on the surface and floor dominated any dispersion patterns normally generated by fluid motion. A variety of flowing weir combinations was used in the model study. Flows were equally balanced between a combination of either four, five, or six weirs. In all testing, the amount of return flow leaving the bottom of the tank was maintained within the range of 20% to 30% of the total influent model flow Q. Efflux openings, b_o, at the model baffle ranged between 0.100 ft and 0.561 ft. There was no apparent effect on flow patterns for any value of b_o at model stations $X \geq 0.90$ ft regardless the magnitude of the total flow. As the magnitude of b_o was decreased to 0.100 ft, the efflux velocity became greater and more turbulent. This resulted in greater amounts of floor scour adjacent to

the baffle and an increasing envelope of turbulence at the juncture of the upper and lower currents. Conversely, as b_o was increased the efflux velocity became smaller and the envelope length was decreased.

When model dye tests are confined to model station X = 2.00 ft, the following summary is applicable:

(1) Model flow patterns are only a function of influent flow Q.

(2) The location of flowing effluent weirs in the model has a negligible effect on the flow patterns. At any time at least four weirs should be operating with balanced flows.

(3) The rate of return flow was maintained within the range of 20% to 30% of the total model influent flow Q. However, larger and smaller percentages did not significantly influence the patterns at X = 2.00 ft.

(4) The magnitude of b_o at the model baffle opening does not significantly influence patterns at X = 2.00 ft. When $X \leq 0.90$ ft there was a strong influence.

Intrinsic with this summary, Table 4.03 provides a tabulation of parameters from ten model dye tests. The fifth and sixth columns record measured velocities, V_u

Table 4.03 Summary of Model Parameters from Dye Tests

Test No.	(1) Influent flow Q $X(10^{-3})$ (CFS)	(2) Return flow Q_r $X(10^{-3})$ (CFS)	(3) Weir flow Q_w $X(10^{-3})$ (CFS)	(4) Total Tank Depth Y (FT)	(5) Lower Zone Velocity V_l $X(10^{-2})$ (FT/SEC)	(6) Upper Zone Velocity V_u $X(10^{-2})$ (FT/SEC)	(7) Lower Zone Depth Y_l (FT)	(8) Turbulent Zone Depth Y_t* (FT)
1	4.519	0.924	3.595	0.670	2.88	-2.51	0.20	0.30
2	4.519	0.924	3.595	0.670	3.06	-1.72	0.18	0.25
3	3.915	0.727	3.188	0.659	2.10	-1.67	0.23	0.10
4	3.915	0.727	3.188	0.659	1.99	-1.89	0.25	0.25
5	3.915	0.727	3.188	0.659	2.37	-1.54	0.21	0.15
6	3.321	0.831	2.490	0.655	1.64	-0.52	0.25	0.10
7	4.919	1.185	3.734	0.657	3.08	-2.75	0.20	0.45
8	4.919	1.185	3.734	0.657	2.35	-0.61	0.26	0.50
9	3.631	0.949	2.682	0.659	3.49	-1.99	0.13	0.10
10	3.631	0.949	2.682	0.659	3.00	-0.78	0.15	0.15

* Due to the erratic nature of turbulence, the upper and lower boundaries of the turbulent zone are not precisely defined. The magnitude of Y_t can only be estimated by visual observation.

and V_1, which conform to the characteristic velocity profile shown in Figure 4.06. It is seen that the maximum lower velocity is positive and the maximum upper velocity is negative.

If a continuous state is assumed, the depth of the lower laminar zone Y_1 can be determined from the hydraulic continuity equation. Although the fluid media is continually passing from the lower laminar zone to the turbulent zone by virtue of entrainment, it is reasonable to assume that the same entrainment process causes an equal and opposite transfer back to the lower zone. On this basis, the depth of the lower zone is represented by a manipulated form of the continuity equation according to:

[4.18] $$Y_1 = \frac{1.25\ Q}{V_1}$$

The numerical term, constant for all tests, is the reciprocal of the width of the tank. The corresponding values of Y_1 appear in the seventh column of Table 4.03.

It is noteworthy that the absolute magnitudes of the negative measurements V_u are significantly smaller than the corresponding magnitudes of V_1 in the lower zone. The smaller magnitudes depict the quantity of fluid media extracted from the circuit by the effluent weirs and the return line. This intermittent extraction will require the use of spatially varied flow theory for the evaluation of Y_u rather than continuous flow theory.

Although important in the total process, activity in the upper zone has secondary importance with respect to lower and turbulent zone activity.

The eighth column of Table 4.03 provides a record of the turbulent zone depth Y_t. The very nature of turbulence and entrainment causes great difficulty in locating definitive boundaries in a turbulent regime. At best Y_t can only be estimated by visually observing dye patterns in the tank profile. The values of the eighth column in Table 4.03, although mere approximations, are establishing a clear trend. The magnitude of Y_t is a function of the model flow Q such that as Q increases so also does Y_t. The turbulent zone exists in some degree for all flows, even those which correspond to the low early morning prototype flows. The model study established that Y_t tends to never be smaller than 0.100 ft. As the model flow Q becomes very large, Y_t approaches the maximum value of depth Y.

The model parameters of Table 4.03 are scaled to prototype proportions by Equations 4.11, 4.14, and 4.15. Table 4.04 provides a tabulation of these transformed model parameters.

Even though unpredictable localized velocities in the turbulent zone are frequently smaller than those in the laminar zones, turbulent velocities do attain high magnitudes for all components of X, Y, and Z. This

Table 4.04 Summary of Calculated Prototype Parameters

Test No.	(1) Influent flow Q (CFS)	(2) Return flow Q_r (CFS)	(3) Weir flow Q_w (CFS)	(4) Total Tank Depth Y (FT)	(5) Lower Zone Velocity V_l (FT/SEC)	(6) Upper Zone Velocity V_u (FT/SEC)	(7) Lower Zone Depth Y_l (FT)	(8) Turbulent Zone Depth Y_t* (FT)
1	8.08	1.65	6.43	13.4	0.13	-0.11	4.0	6.00
2	8.08	1.65	6.43	13.4	0.14	-0.08	3.6	5.00
3	7.00	1.30	5.70	13.2	0.09	-0.07	4.6	2.00
4	7.00	1.30	5.70	13.2	0.09	-0.08	5.0	5.00
5	7.00	1.30	5.70	13.2	0.11	-0.07	4.2	3.00
6	5.94	1.49	4.45	13.1	0.07	-0.02	5.0	2.00
7	8.80	2.12	6.68	13.1	0.14	-0.12	4.0	9.00
8	8.80	2.12	6.68	13.1	0.11	-0.03	5.2	10.00
9	6.50	1.70	4.80	13.2	0.16	-0.09	2.6	2.00
10	6.50	1.70	4.80	13.2	0.13	-0.03	3.0	3.00

* Due to the erratic nature of turbulence, the upper and lower boundaries of the turbulent zone are not precisely defined. The magnitude of Y_t can only be estimated by visual observation in model studies.

Prototype parameters are calculated from Table 4.03 with equations 4.11, 4.14, and 4.15.

unpredictable nature is not conducive to efficient settling of low density floc particles. Consequently, this thesis will define the turbulent zone as an undesirable barrier which must be kept at a practical minimum in the sedimentation process. Table 4.03 indicates Y_t begins increasing for a model flow Q of 3.321 (10^{-3}) cfs (Test No. 6). This flow can be rounded to 3.3 (10^{-3}) cfs and will constitute an inflection point for Y_t. Scaled to prototype proportions, the depth of the turbulent zone will be 2.00 ft and the flow Q will be 5.9 cfs in a single cell. This is equivalent to a tank flow of 29.5 cfs (15.9 migd.) and to a secondary flow, with five sedimentation tanks, of 147.5 cfs (79.4 migd.). Prototype flows of this magnitude produce lower laminar zone depths Y_1 of the approximate order of 5.00 ft.

The settling velocities, assembled in the latter part of Chapter 3, can be used to determine longitudinal requirements for prototype settling. Velocities V_1 and V_s can be considered velocity vectors in the positive X direction and negative Y direction, respectively. If the velocity vectors are related in direct proportion to the displacements, the required cell length in the X direction can be determined. This proportion is mathematically shown to be:

$$[4.19] \qquad X_s = \frac{Y_1}{2} \frac{V_1}{V_s}$$

In this equation, X_s represents the longitudinal displacement in the lower laminar zone of the cell which the average particle requires to reach the floor. Although the settling distance is equal to the total depth of the laminar zone, the mean distance must be considered. Thus, in Equation 4.19, 0.5 Y_1 must be used rather than 1.0 Y_1.

Table 3.03 has defined the average settling velocity V_s as 2.19 (10^{-3}) ft/sec and Table 4.04 indicates the desirable lower laminar zone depth Y_1 is 5.00 ft. Also from the latter table the representative maximum velocity V_1 in the lower zone can be approximated as 0.10 ft/sec. When these values are substituted in Equation 4.19, X_s becomes 114 ft. The prototype cell is 165.0 ft long of which 18.0 ft is rendered ineffective by the turbulent roller adjacent to the baffle. This provides a net effective length of approximately 147 ft for the settling process. Generally the prototype cells are adequate for intermediate hydraulic loads when the suspended solids have good settling characteristics.

[5] STRATIFICATION

According to a discussion by Schlichting (10), Prandtl is known to have developed a dimensionless stratification parameter identified as the gradient Richardson Number R_i (L.F. Richardson used energy methods to predict stratification patterns). This is mathematically shown as:

[5.01]

$$R_i = \frac{\frac{-g}{\rho}\frac{d\rho}{dY}}{\left(\frac{dV}{dy}\right)^2}$$

The media density is defined by ρ and y denotes the depth measured upward from the bottom of a stratified layer in a Cartesian coordinate system. The differentials in the numerator and denominator signify density and velocity gradients, respectively.

Schlichting (10), has said of equation 5.01:

> "When the density decreases upwards, the arrangement is stable, and it becomes unstable when the density variation is reversed."

Thus the regime is stable when R_i is greater than zero and unstable when R_i is less than zero. When a regime has a completely homogeneous media, the density gradient becomes zero and R_i becomes zero. In this study it is reasonable to assume that the density and velocity gradients are linear functions. The assumption regarding the former parameter is merely a reiteration of Figure 4.04. Equation 5.01 can be rewritten in the following manner:

[5.02]

$$R_i = \frac{\frac{-g}{\rho_2}\left(\frac{\rho_2-\rho_1}{y_2-y_1}\right)}{\left(\frac{V_2-V_1}{y_2-y_1}\right)^2}$$

Numerical subscripts n and $n+_1$ (i.e. 1 and 2) refer to parameters for different values of y while X and Z are held constant such that $Y_{n+_1} > Y_n$.

It is noteworthy that when Equation 5.02 is simplified and placed under the square root radical, it becomes equivalent to the densimetric Froude number. The densimetric Froude number concept, often used by present day hydraulic researchers, will not be used in this treatise. The selection of the gradient Richardson number enables the full use of both positive and negative numbers for mathematically describing regime conditions.

Equation 5.02 will be a more useful form when it is algebraically simplified and the specific gravity term S is substituted for the density term. The gradient Richardson number equation will then assume the form:

[5.03]

$$R_i = \frac{-g(S_2-S_1)(y_2-y_1)}{S_2(V_2-V_1)^2}$$

Any fluid media layer of high specific gravity will seek an equilibrium position below a media layer of low specific gravity whether in a static or dynamic state. Research by Ellison and Turner (11) has shown the existence of turbulent entrainment in the boundary zone between fluids of different specific gravities. They

have further concluded that the amount of turbulent entrainment, E, is a function of the gradient Richardson number of the form:

$$[5.04] \qquad E = E(R_i)$$

By means of extensive hydraulic testing, Ellison and Turner (11) have shown that equation 5.04, when graphically illustrated, assumes a general exponential form. The graphical illustration has been reprinted for this study and appears in Figure 5.01. When a homogeneous specific gravity condition exists, R_i is zero and Figure 5.01 indicates that E becomes 0.074. When R_i assumes the critical value of 0.83, then entrainment ceases to exist and E becomes zero. Thus for a stable regime with small, positive values of R_i, entrainment between two stratified fluid layers will occur in varying degrees. When an unstable regime occurs with negative values of R_i, uniformity is overcome by the erratic vertical movement of fluid particles seeking a stable position of equilibrium.

Regime stability in the prototype cell will be examined over the full depth. In this examination parameters of a general order of magnitude will be considered, since all parameters cover an average range and are not precise numbers. Representative depths and velocities will be selected for the lower and upper zones which are not subjected to irregularities

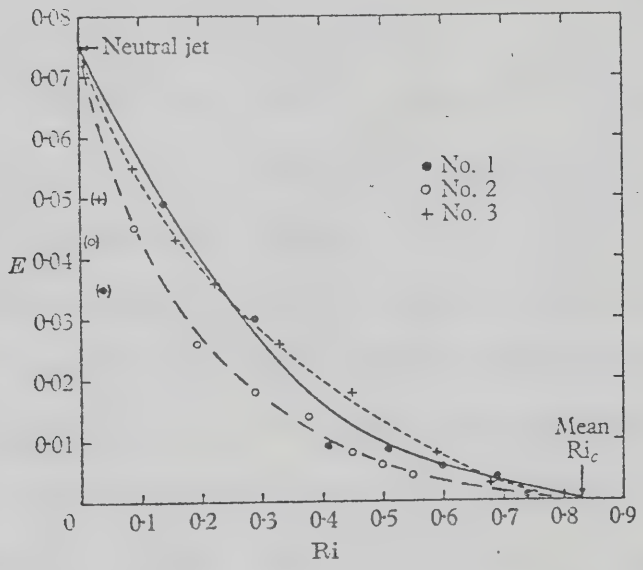

FIGURE 2. Entrainment, E, as a function of Richardson number, Ri, for three experiments on surface jets. The value of $E(0)$ has been taken from published results on neutral jets, and Ri_c obtained from a more extensive series of measurements of the depth of the final layer.

FIG. 5.01 ENTRAINMENT (E) AS A FUNCTION OF THE GRADIENT RICHARDSON NUMBER (R_i) FROM ELLISON AND TURNER (11)

from the surface, floor, or turbulent zone. Hence the conditions occurring at elevations equal to 20% and 80% of the normal depth Y will be considered. From prototype measurements, the normal depth is constant at 12.0 ft, thus elevations for Y_1 and Y_2 will be 2.4 ft and 9.6 ft, respectively.

The values of Y_1 and Y_2 can be substituted into Equation 4.17 and the specific gravities can be estimated. The specific gravity values for S_1 and S_2 will be 1.00186 and 1.00128, respectively. Velocities at Y_1 and Y_2 are estimated to be equal to the maximum velocities V_l and V_u in the laminar zones. A brief review of Table 4.04 indicates the general order of magnitude for V_1 and V_2 will be +0.10 ft/sec and -0.07 ft/sec, respectively. Using the convention of Equation 5.03, numerical terms are summarized as:

$S_1 = 1.00186$	$S_2 = 1.00128$
$V_1 = +0.10$ ft/sec	$V_2 = -0.07$ ft/sec
$Y_1 = 2.4$ ft	$Y_1 = 9.6$ ft

When these values are substituted in Equation 5.03, the gradient Richardson number is found to be +4.65. Clearly, the calculated value of R_i far exceeds the previously defined critical value and entrainment due to specific gravity differentials does not exist. The regime is definitely in a stable condition.

To reiterate, calculations with Equation 5.03 have been made with general order of magnitude numbers. The result is a very conservative positive gradient Richardson number. More generally, the nature of the secondary process will provide specific gravity differentials which virtually never exceed 0.2%. Under no condition can the depth differential exceed 12.0 ft. The only remaining variable is the velocity differential which is a function of hydraulic flow. Although this latter differential will have a wide variation range, it is hardly likely that a magnitude will ever be encountered which will cause R_i to be less than the critical value.

[6] CONCLUSIONS

Intrinsic to this treatise is the assumption that the suspended floc particles have ideal settling characteristics in the secondary sedimentation process. No attempt has been made to analyse the many complex variables which influence those ideal settling characteristics, clearly a broad area of research alone. Often the secondary facilities generate a suspended floc which is far from ideal. This leads to sludge bulking or nitrogen gas binding and consequently a total upset of the sedimentation process. These two occurrences destroy normal specific gravity characteristics and the concept of density currents and entrainment stability in this work is invalidated.

For the less than ideal conditions this writer has visually observed the surface emergence of floc particles usually in the vicinity of the first and second weir. The media assumes a brown colored gelatinous scum and inordinate quantities of floc particles are carried over the weirs. When ideal floc occurs, the media has a slightly gray turbid color, the scum is grey, and few floc particles pass over the weir. During prolonged periods of low and intermediate flows ideal floc conditions do in fact exist. As the City collection system is expanded each year, prolonged heavy flows are more frequently encountered. Consequently the design

capacity of the sedimentation process is exceeded and the performance is upset.

Let it be assumed that abnormally heavy hydraulic loads do not occur and that floc settling characteristics are optimal. The conclusions of this study can be assembled in the following manner:

(1) In the model study a high degree of velocity scour was observed on the floor in the vicinity of the baffle. This is caused by the downward movement of hydraulic momentum and a sudden change of direction. The scouring condition is compounded by the turbulent roller generated at the juncture of lower positive current and the upper negative current. The condition persists over a wide range of hydraulic flows and generally expires when the distance from the model entrance X is equal to or greater than 0.90 ft. Evidence of the turbulent roller during high flow periods has been observed when the approximate distance from the prototype entrance X is equal to or less than 20.0 ft. The adverse scouring velocity can be minimized by increasing the baffle efflux b_o in both the model and prototype. It is recommended that the prototype baffles be shortened in a manner that they extend 3.0 ft below the normal water surface. This modification will maximize the opening b_o and will

protect the scum collection troughs against undue surface current interference.

(2) The fluorometric examination has provided evidence that a positive current in a lower zone transports dye particles along the floor from the baffle to the northerly wall. The same particles are carried to the effluent weirs by means of a negative current in the upper zone. This concept is supported by the large detention time valve T_f which fluorescent dye particles require for travelling between the injection point and the first weir. The magnitude of T_f is gauged against a similar time derived from the velocity in the lower laminar zone in the model study. When density currents are carefully manipulated, this same upper-lower current concept can be observed in the model study. These currents result in a vertical turbulent roller adjacent to the northerly wall. It is recommended that if an additional effluent weir is installed in the prototype, the upturn roller should be avoided by locating the weir not less than 20.0 ft from the northerly wall.

(3) The model study has indicated the presence of an intermediate turbulent zone which is generated by shear stress between the positive lower current and the negative upper current. The unpredictable

turbulent zone provides both high and low magnitudes of velocity in small localized regions for all hydraulic loads. In an efficient sedimentation process it is desirable to keep turbulent zones to an absolute minimum. In the model study the turbulent zone depth Y_t tends to remain constant at 0.100 ft for low and intermediate flows. As the model flow approaches and exceeds 3.5 (10^{-3}) cfs, the depth of the turbulent zone begins increasing from the constant value until the entire depth is consumed. Transformed to prototype proportions, this critical point flow is approximately 5.9 cfs. When the suspended floc has ideal settling characteristics, it is recommended that the hydraulic load to any prototype cell in the secondary system not exceed 5.9 cfs (3.2 migd.). This loading is equivalent to 29.5 cfs (15.9 migd.) for a single sedimentation tank composed of five cells and 147.5 cfs (79.4 migd.) for the entire secondary facility composed of five sedimentation tanks. In a single prototype tank there exists 672 ft of effective effluent weir. If the tank flow of 29.5 cfs is considered, the effective weir loading is 28423 U.S. gpd/ft. Although large this loading is consistent with the range 20,000 to 30,000 U.S. gpd/ft prescribed by

Metcalf and Eddy (7). Due to frequently poor floc characteristics the weir loading should perhaps be in the lower end of the range at 20,000 U.S. gpd/ft. This would result in a maximum prototype tank flow of 20.8 cfs (11.2 migd.) and a secondary facility flow of 104.0 cfs (56.0 migd.).

(4) When prototype flows are maintained within the range established by plant operating procedures, there is conservative regime stability with respect to entrainment generated by specific gravity differentials. This is confirmed by the gradient Richardson number. The exception clearly is a system upset by less than ideal floc conditions.

There is evidence that the first weir is situated too near the influent baffle for an efficient process when floc settling is poor. This characteristic is particularly noticeable when waves of suspended solids emerge at the surface of the prototype in the region between the baffle and the first weir during peak flow periods. On occasion small values of T_f appeared in the fluorometric test when samples were collected at the first weir. It does appear that the efficiency of the process would be improved if the first weir were removed from service and replaced with a new weir within the previously recommended limits of the northerly wall. The first weir should be completely

effective if excessive hydraulic loads are minimized and good floc characteristics are maintained.

Important in this treatise is a statement regarding further study in the treatment process. Primarily, an in-depth examination of all process mechanisms in the secondary aerators could and should be linked with this paper. Flow patterns, air consumption requirements, and rates of return liquor flow should be examined for an optimal combination with hydraulic loading.

It would be desirable to examine the reasons for excessive accumulations of scum and foam in the secondary sedimentation process. These conditions appear to be developing from prolonged heavy hydraulic loads and changes in the general composition of the media. Due to flow recycling, the scum condition appears to be transferred to the primary and digestion processes.

BIBLIOGRAPHY

(1) COUTTS, R.R., "Edmonton Water and Sanitation Waste Treatment - 1973 Annual Report", City of Edmonton Waste Water Treatment Plant.

(2) SCOTT, L.C., "1975 Civic Census", City of Edmonton Election Office, June 20, 1975.

(3) KLASSEN, Wayne, Personal Communication, City of Edmonton Water and Sanitation Department, June 14, 1976.

(4) CHOW, Ven Te, Open Channel Hydraulics, McGraw-Hill Book Company, New York, New York, 1959, Page 27.

(5) BUTTS, Thomas A., "Fluorometric Calibration Curves", Journal of the Sanitary Engineering Division, Proceedings of the American Society of Civil Engineers, Volume 95, No. SA 4, August 1969, Page 705.

(6) CAMP, Thomas R., "Sedimentation and the Design of Settling Tanks", Transactions of the American Society of Civil Engineers, Volume 111, Paper No. 2285, 1946, Page 895.

(7) METCALF and EDDY, Inc., Wastewater Engineering Collection, Treatment, and Disposal, McGraw-Hill Book Company, New York, New York, 1972, Pages 290, 530.

(8) STREETER, Victor L., Fluid Mechanics, 3rd edition, McGraw-Hill Book Company, New York, New York, 1962, Page 155.

(9) WEAST, Robert C., Chief Editor, et al. Handbook of Chemistry and Physics, 48th College edition, Chemical Rubber Company, Cleveland, Ohio, Page F-5.

(10) SCHLICHTING, Hermann, Boundary-Layer Theory, 6th edition, Translated by J. Kestin, McGraw-Hill Book Company, New York, New York, 1968, Page 491.

(11) ELLISON, T.H. and J.S. TURNER, "Turbulent Entrainment in Stratified Flows", Journal of Fluid Mechanics, Volume 6, Cambridge at the University Press, London, England, 1959, Page 423.

APPENDICES

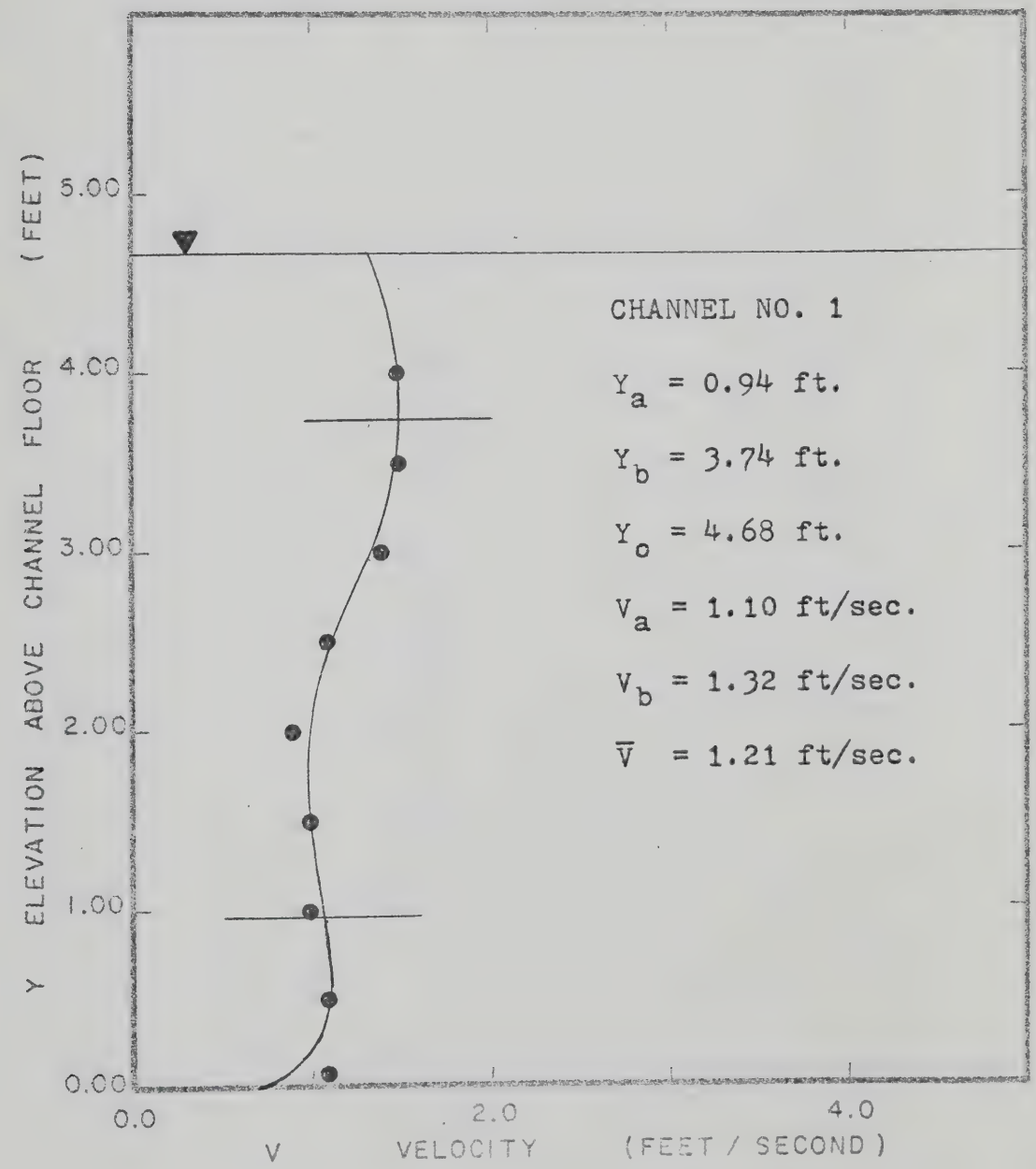

FIG, 1.01A CROSS CHANNEL VELOCITY PROFILE

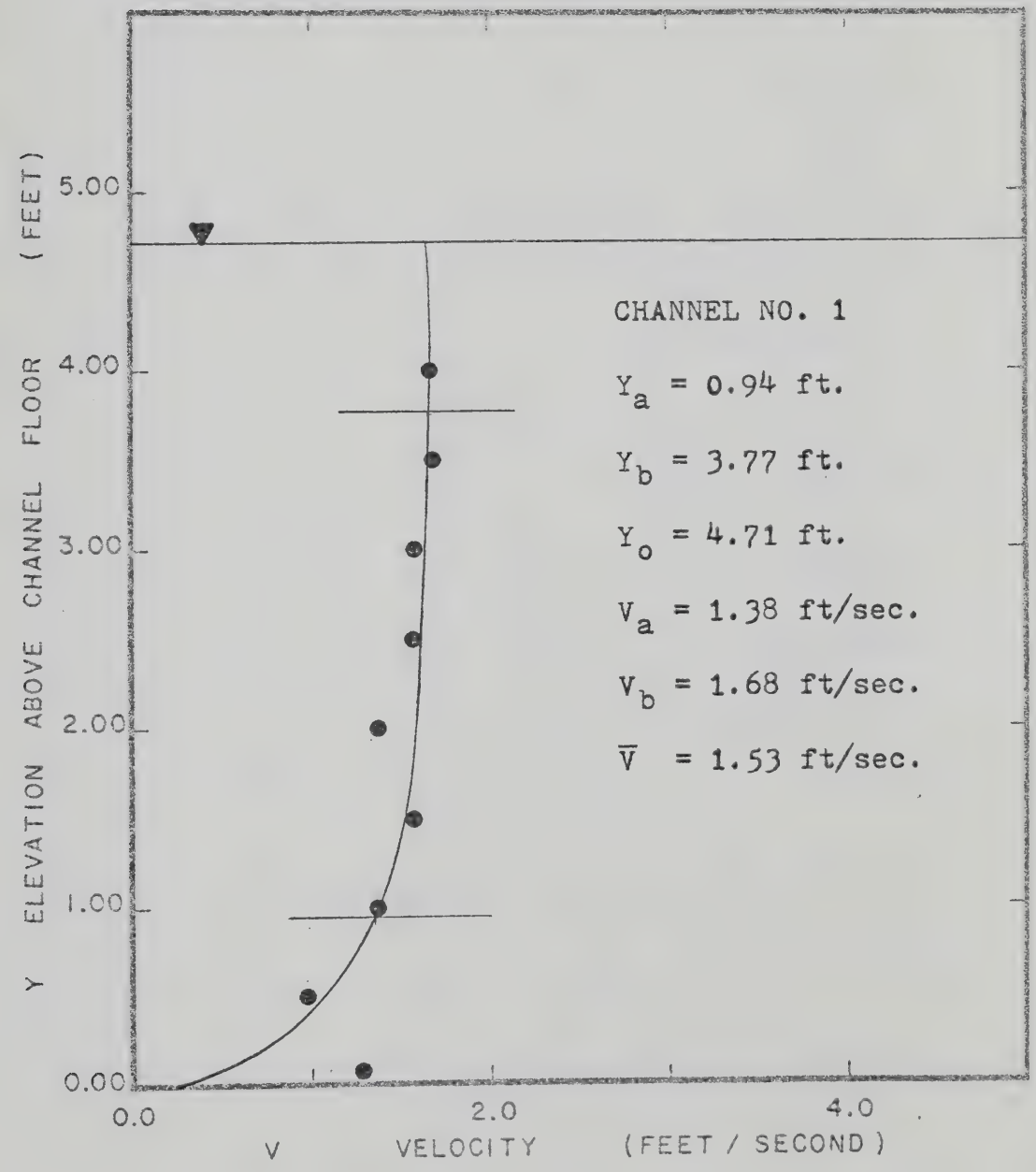

FIG, 1.02A CROSS CHANNEL VELOCITY PROFILE

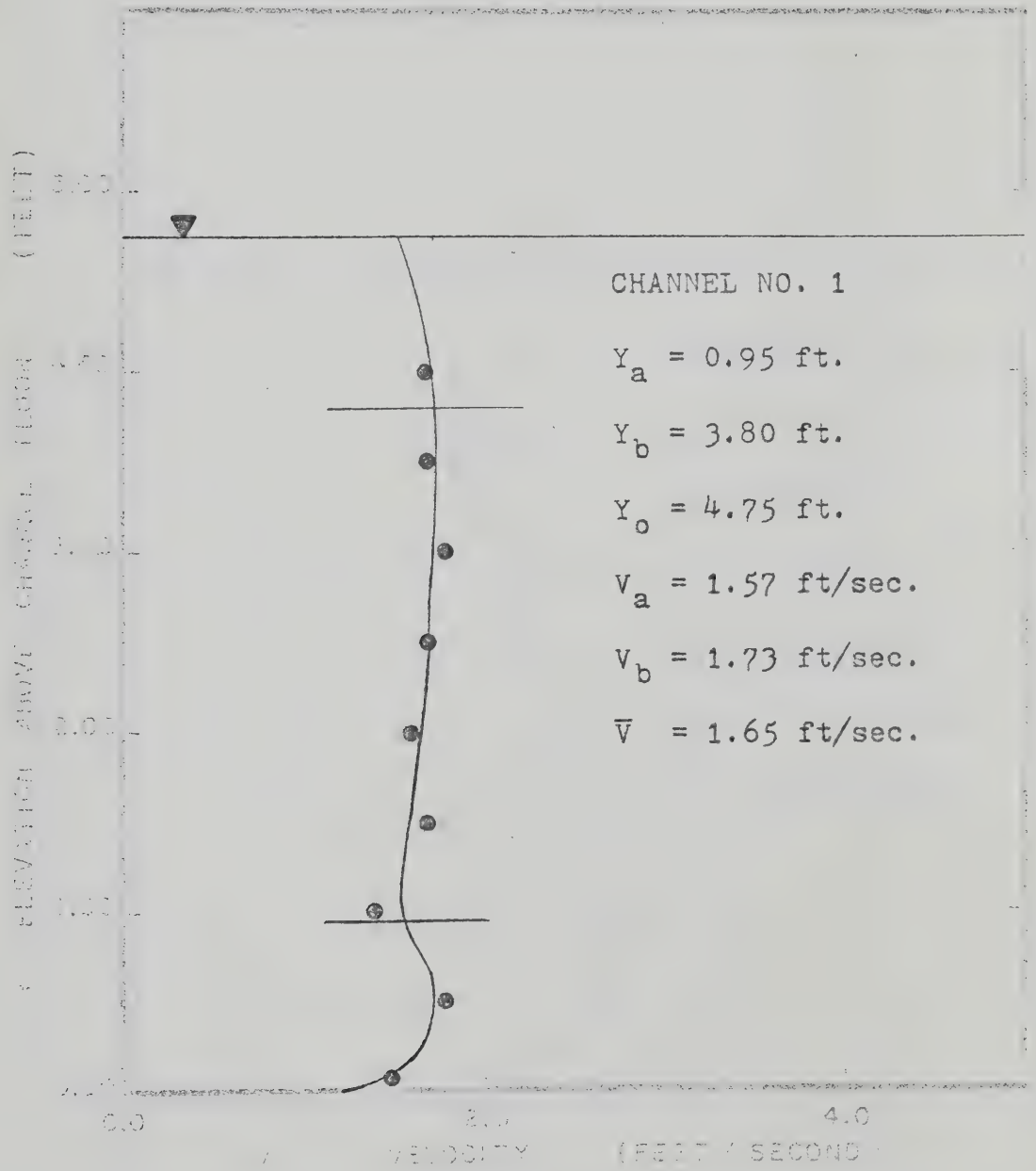
CHANNEL NO. 1
Y_a = 0.95 ft.
Y_b = 3.80 ft.
Y_o = 4.75 ft.
V_a = 1.57 ft/sec.
V_b = 1.73 ft/sec.
$\bar{V}$ = 1.65 ft/sec.
4.0

FIG. 1.03 A

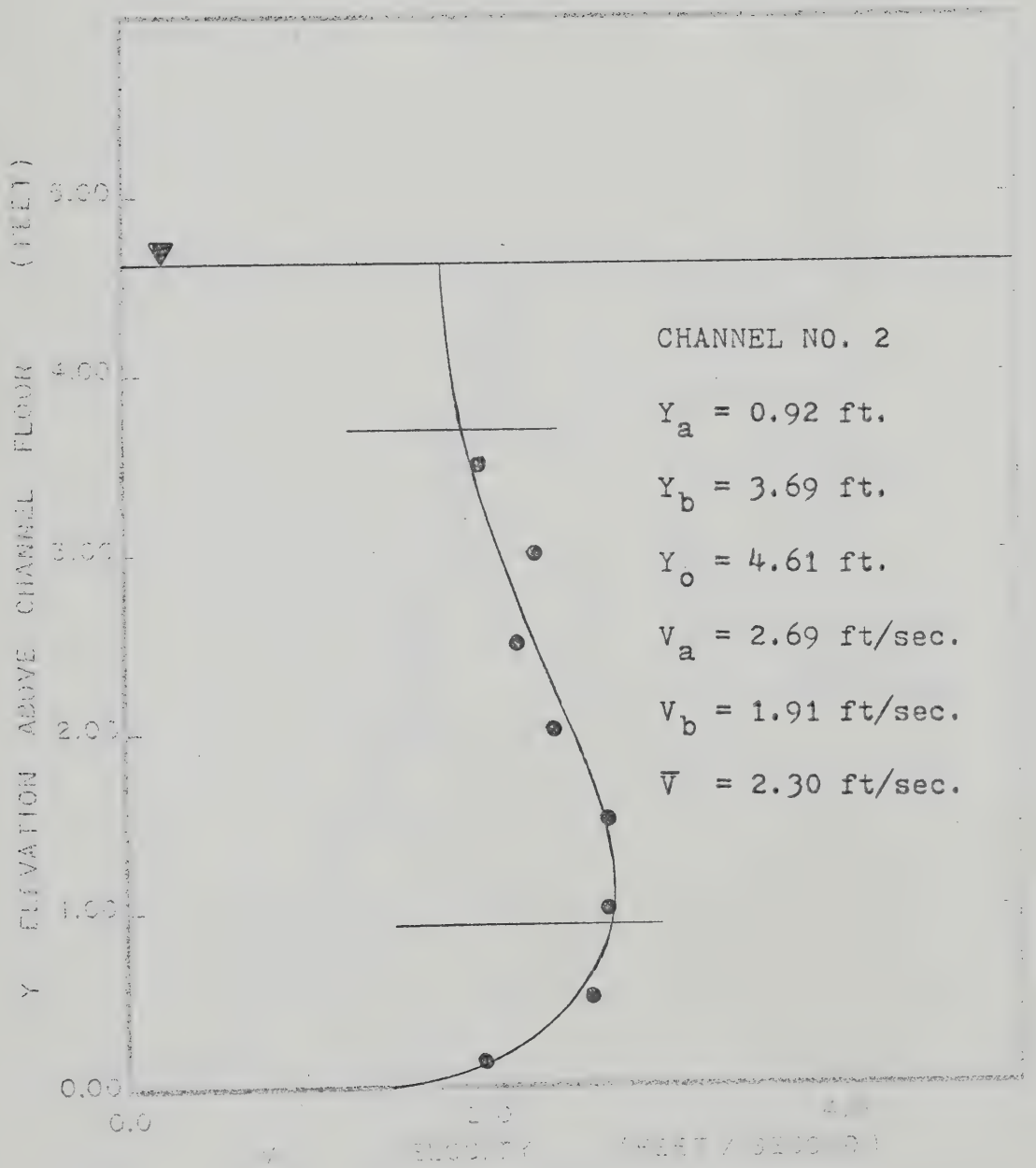
CHANNEL NO. 2
Y_a = 0.92 ft.
Y_b = 3.69 ft.
Y_o = 4.61 ft.
V_a = 2.69 ft/sec.
V_b = 1.91 ft/sec.
$\bar{V}$ = 2.30 ft/sec.
Y ELEVATION ABOVE CHANNEL FLOOR (FEET)
0.00
1.00
2.00
4.00
0.0

FIG. 1.04A

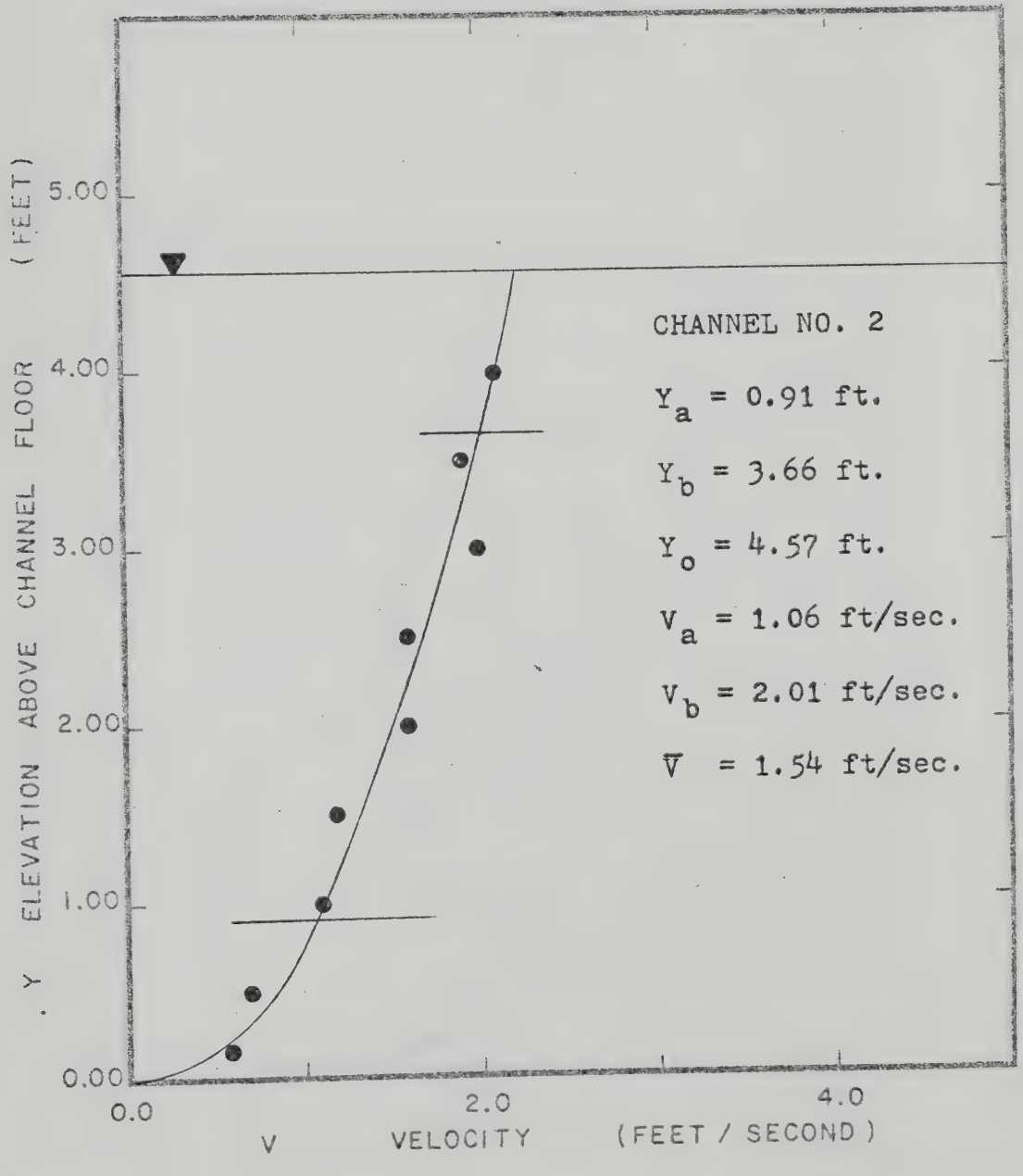

FIG, 1.05A CROSS CHANNEL VELOCITY PROFILE

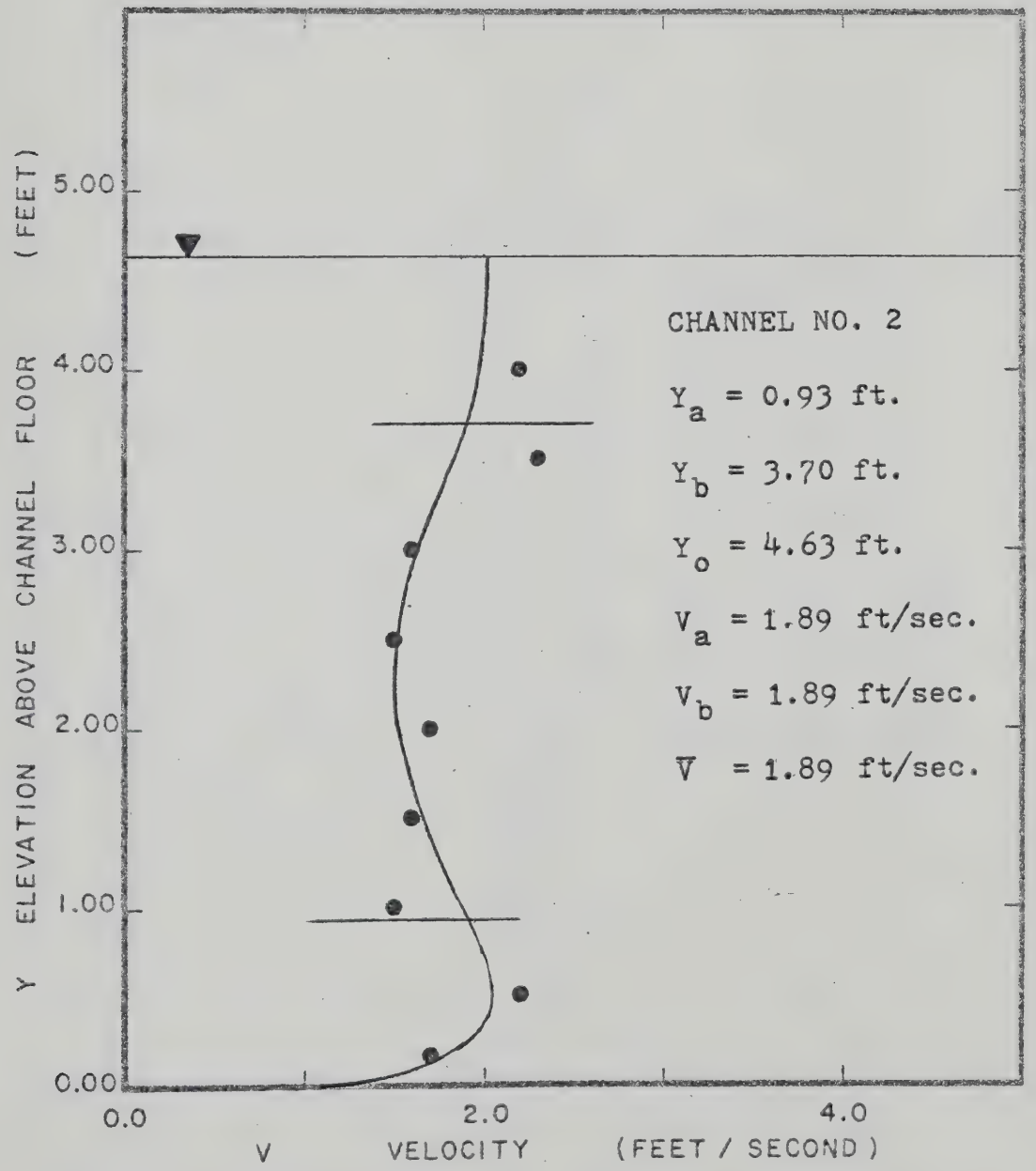

FIG, 1.06A CROSS CHANNEL VELOCITY PROFILE

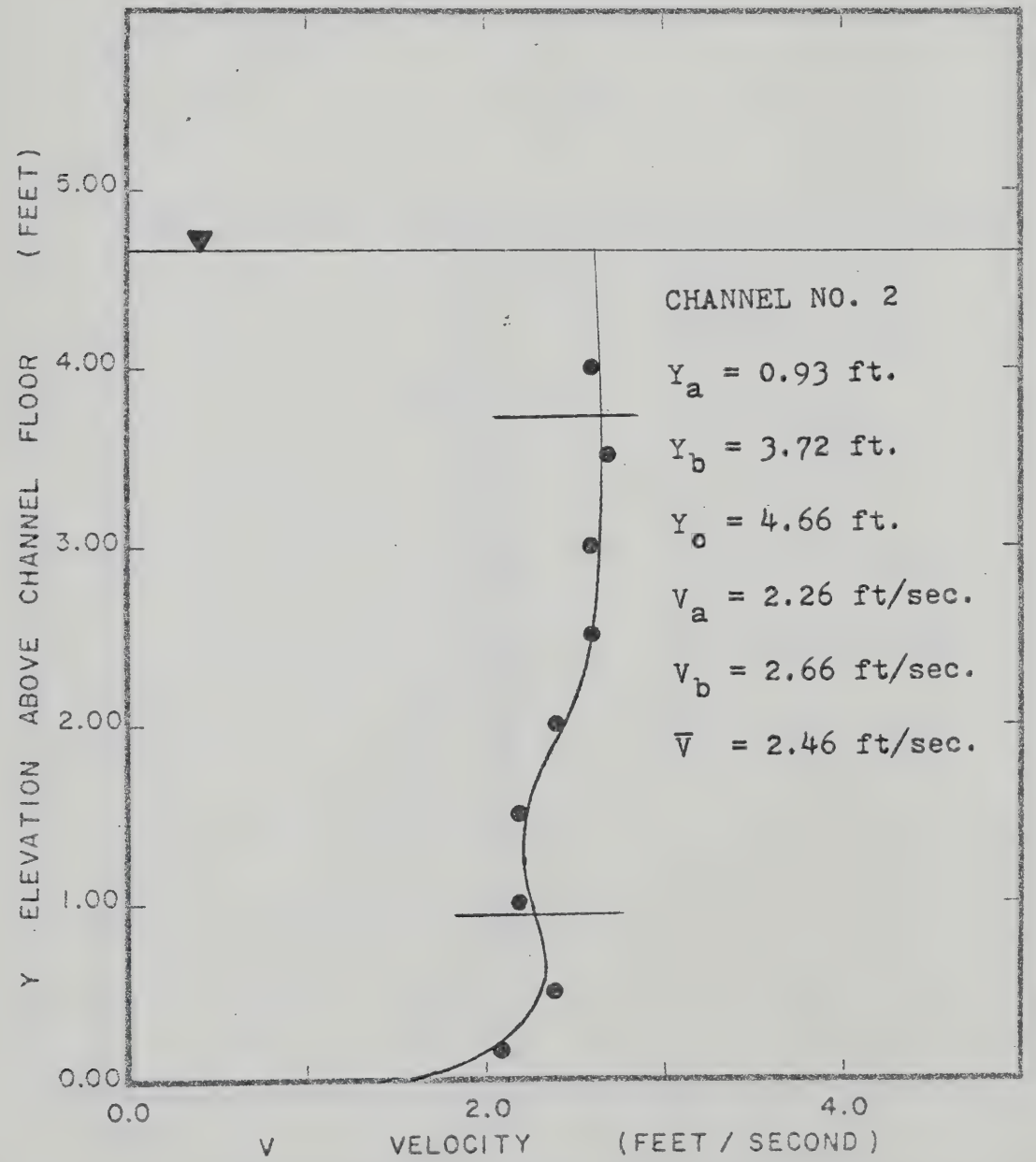

FIG, 1.07A CROSS CHANNEL VELOCITY PROFILE

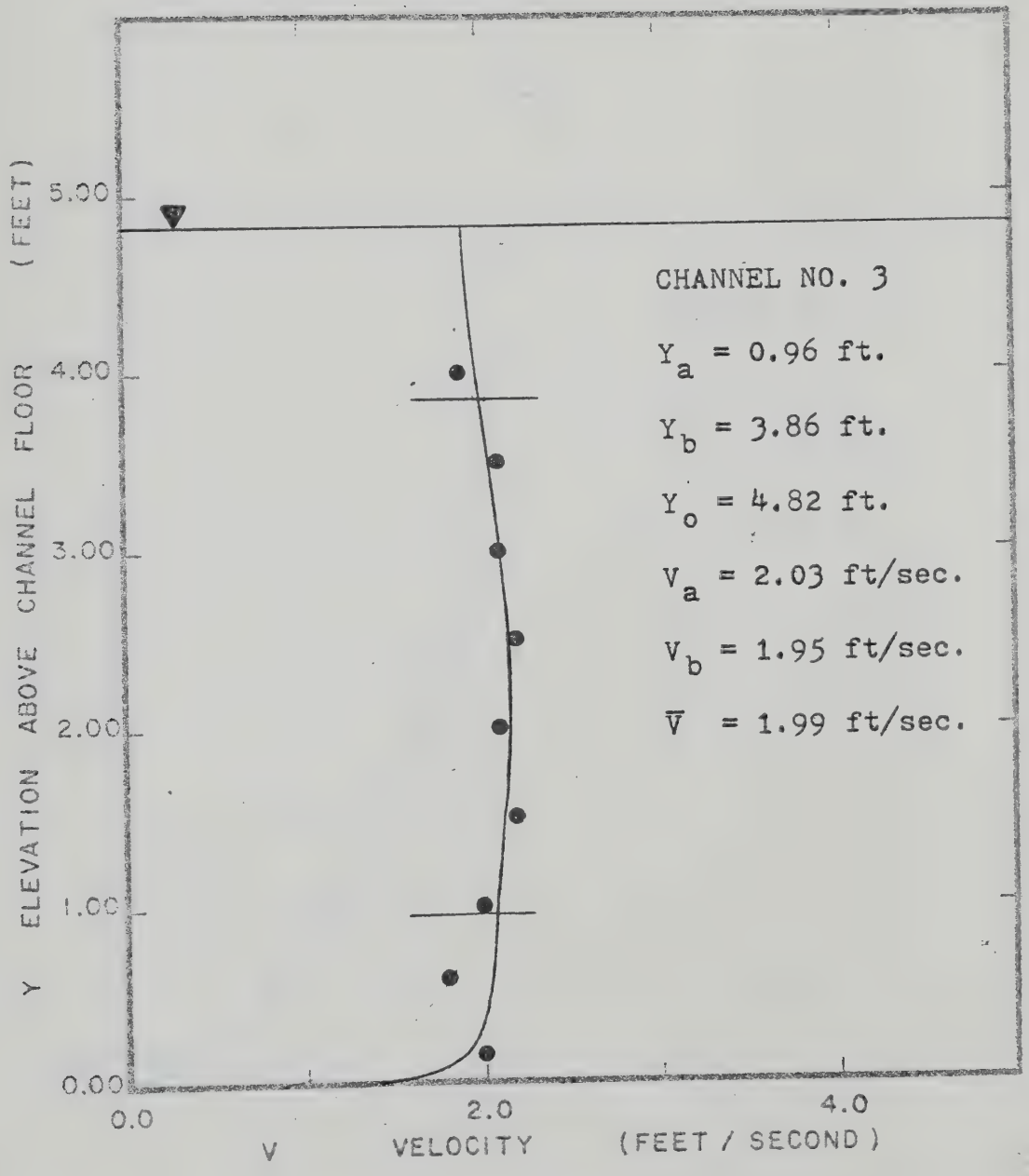

FIG, 1.08A CROSS CHANNEL VELOCITY PROFILE

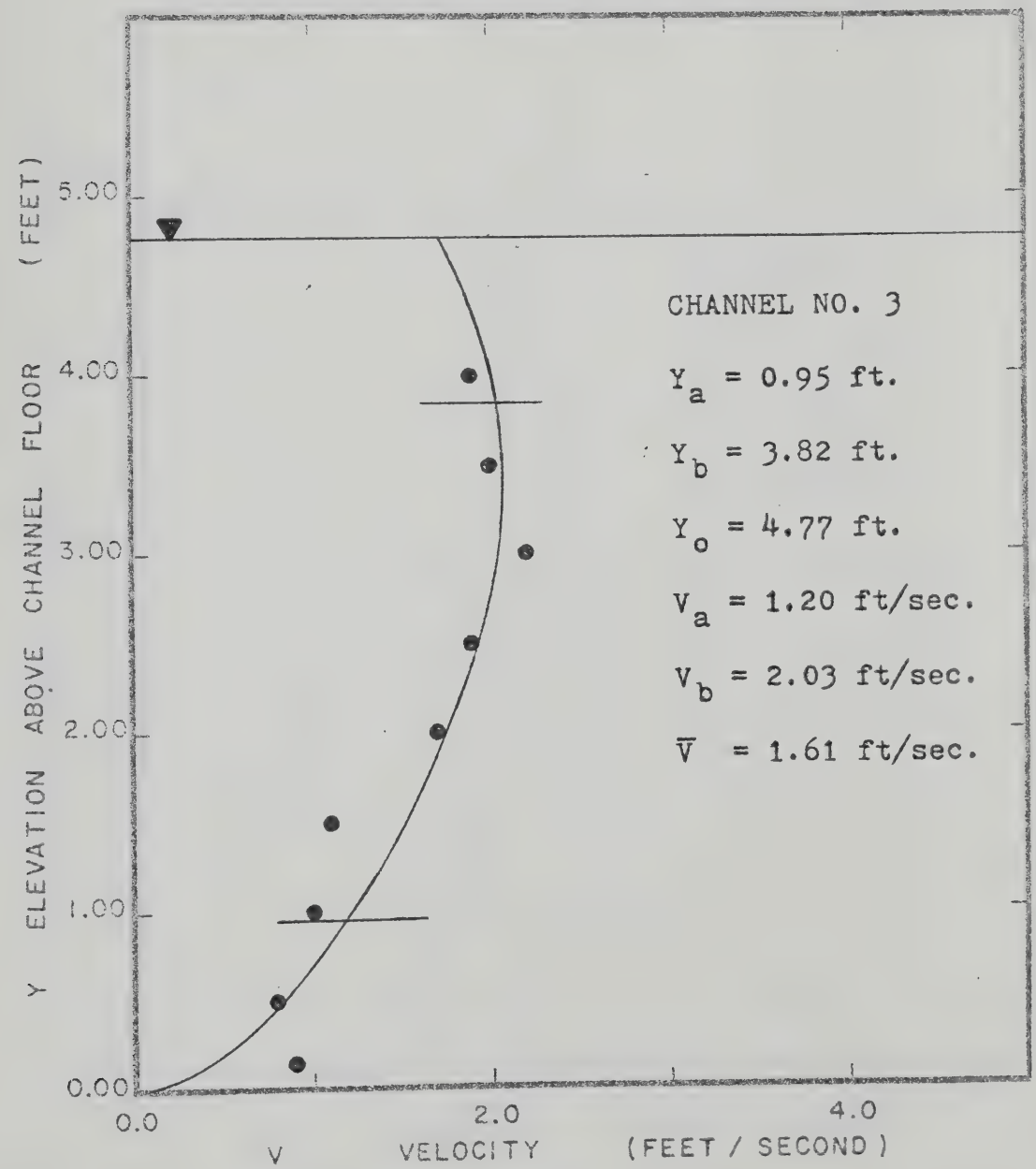

FIG, 1.09A CROSS CHANNEL VELOCITY PROFILE

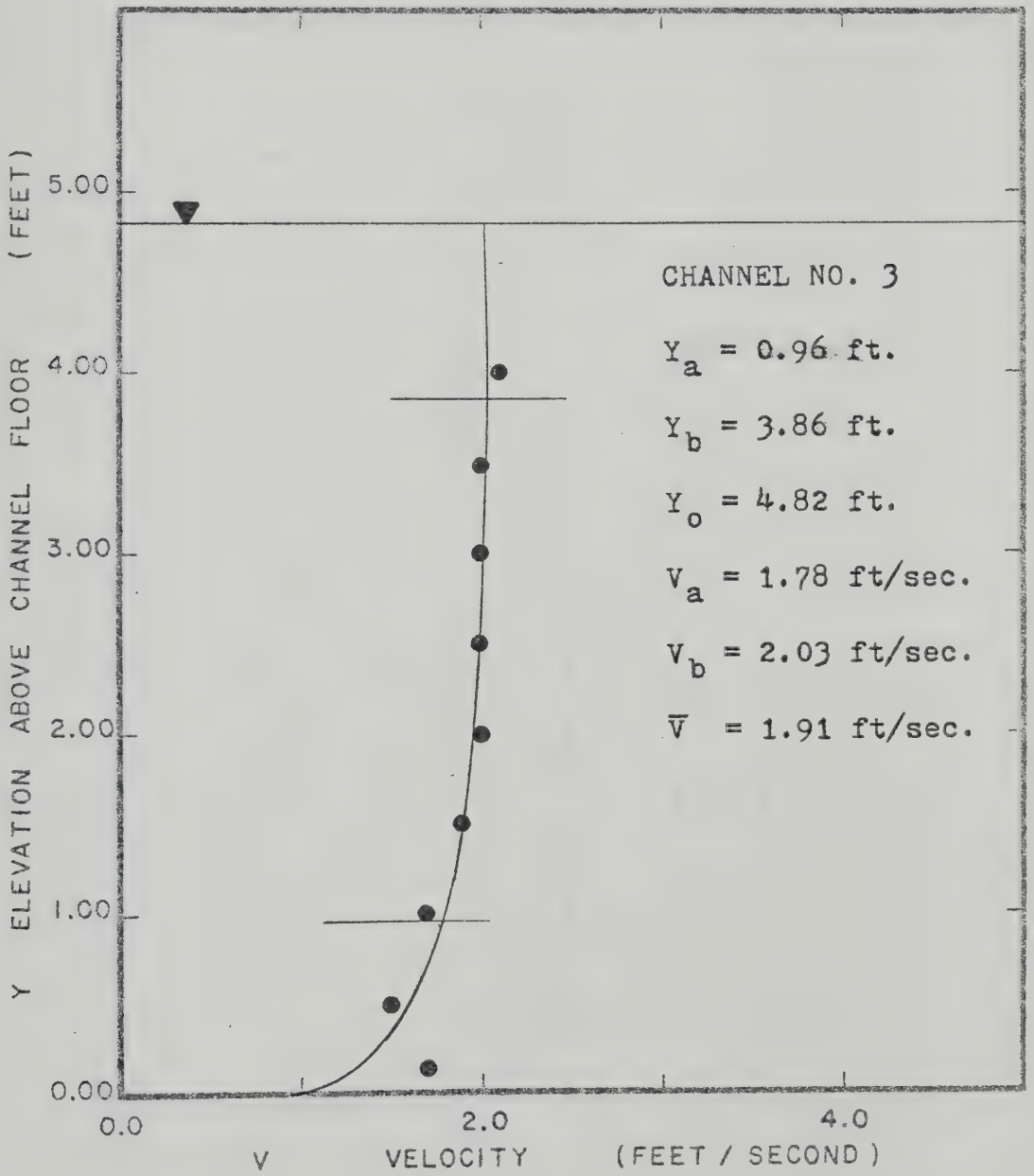

FIG, 1.10A CROSS CHANNEL VELOCITY PROFILE

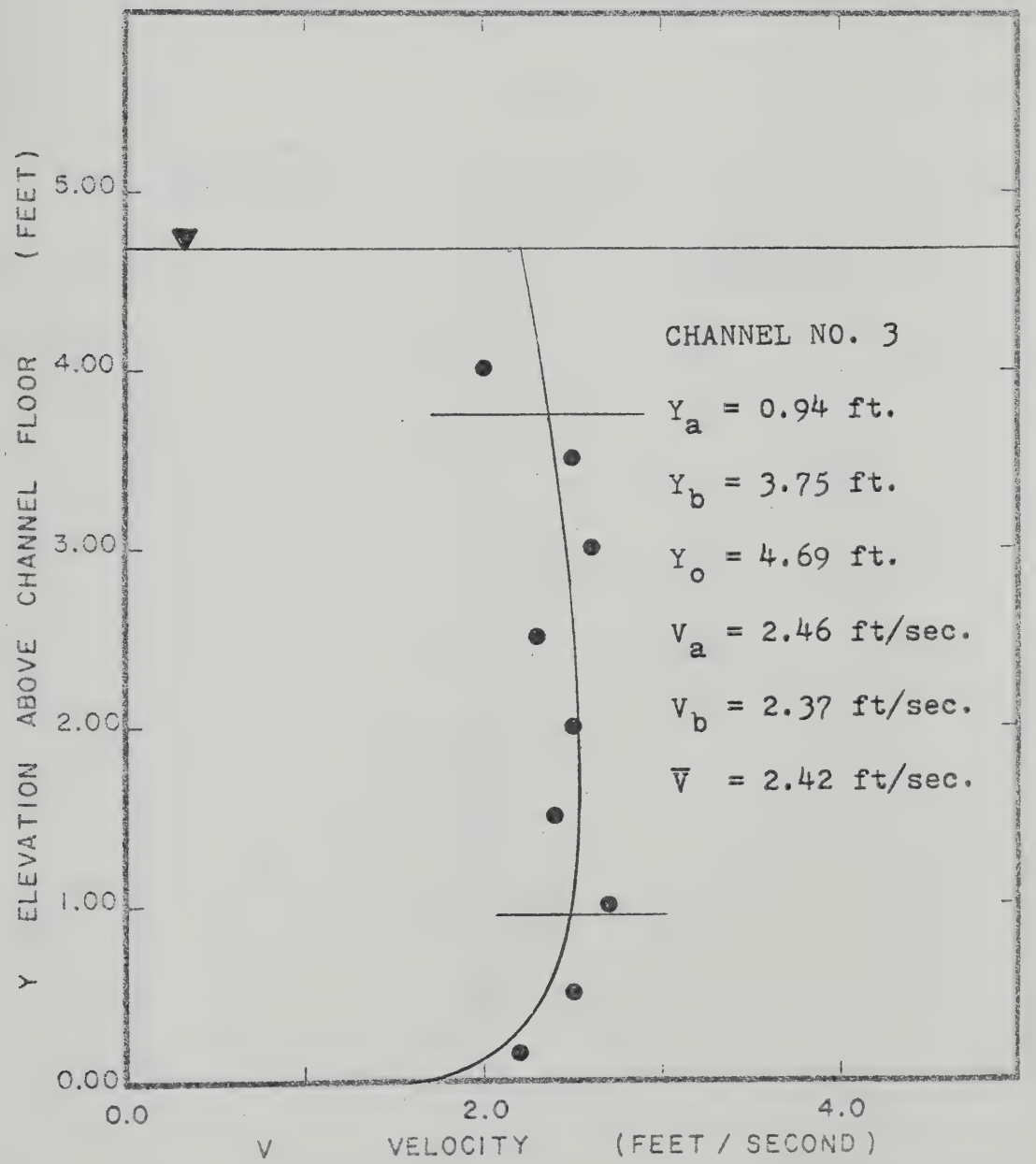

FIG, I.11A CROSS CHANNEL VELOCITY PROFILE

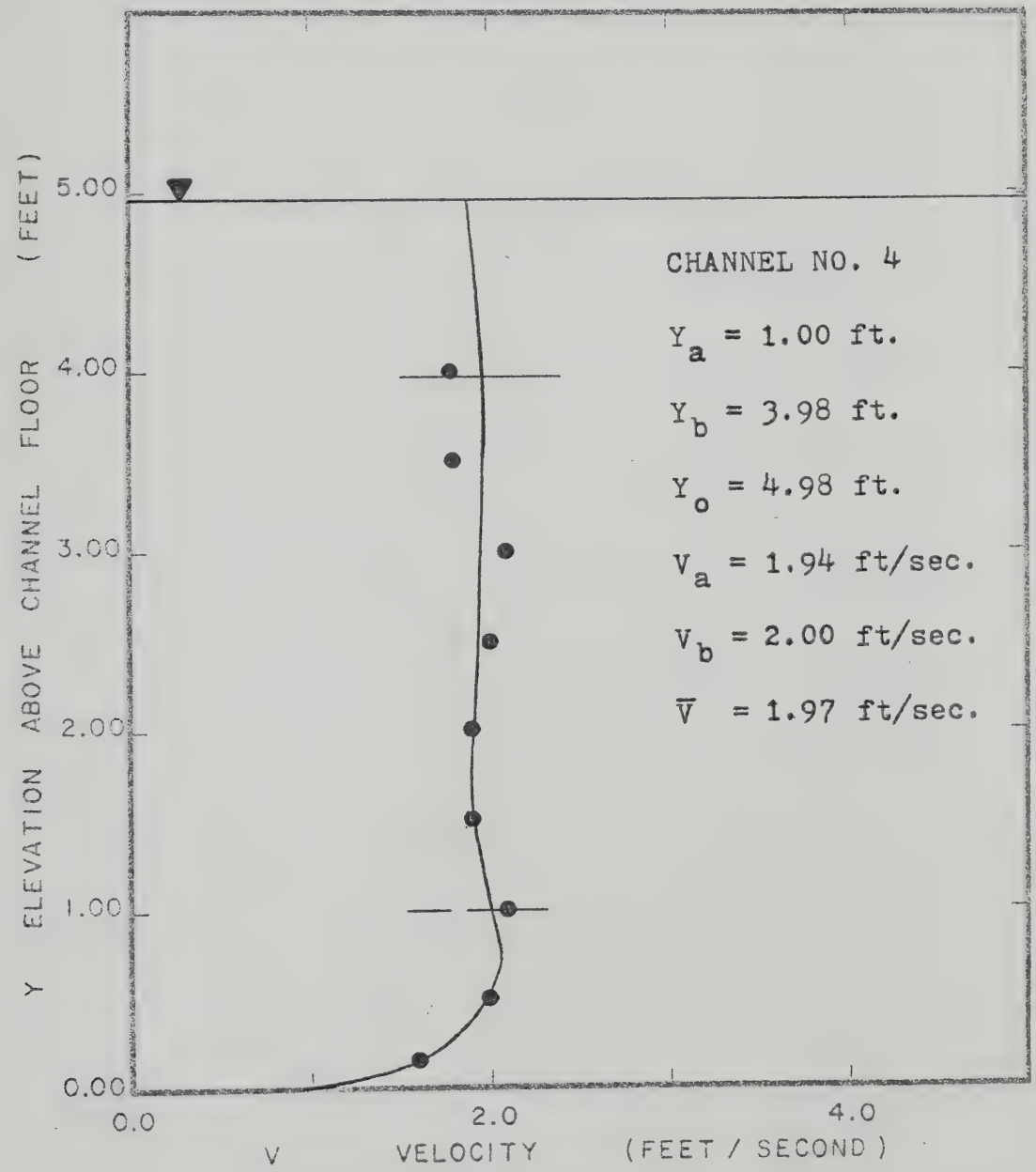

FIG, 1.12 A CROSS CHANNEL VELOCITY PROFILE

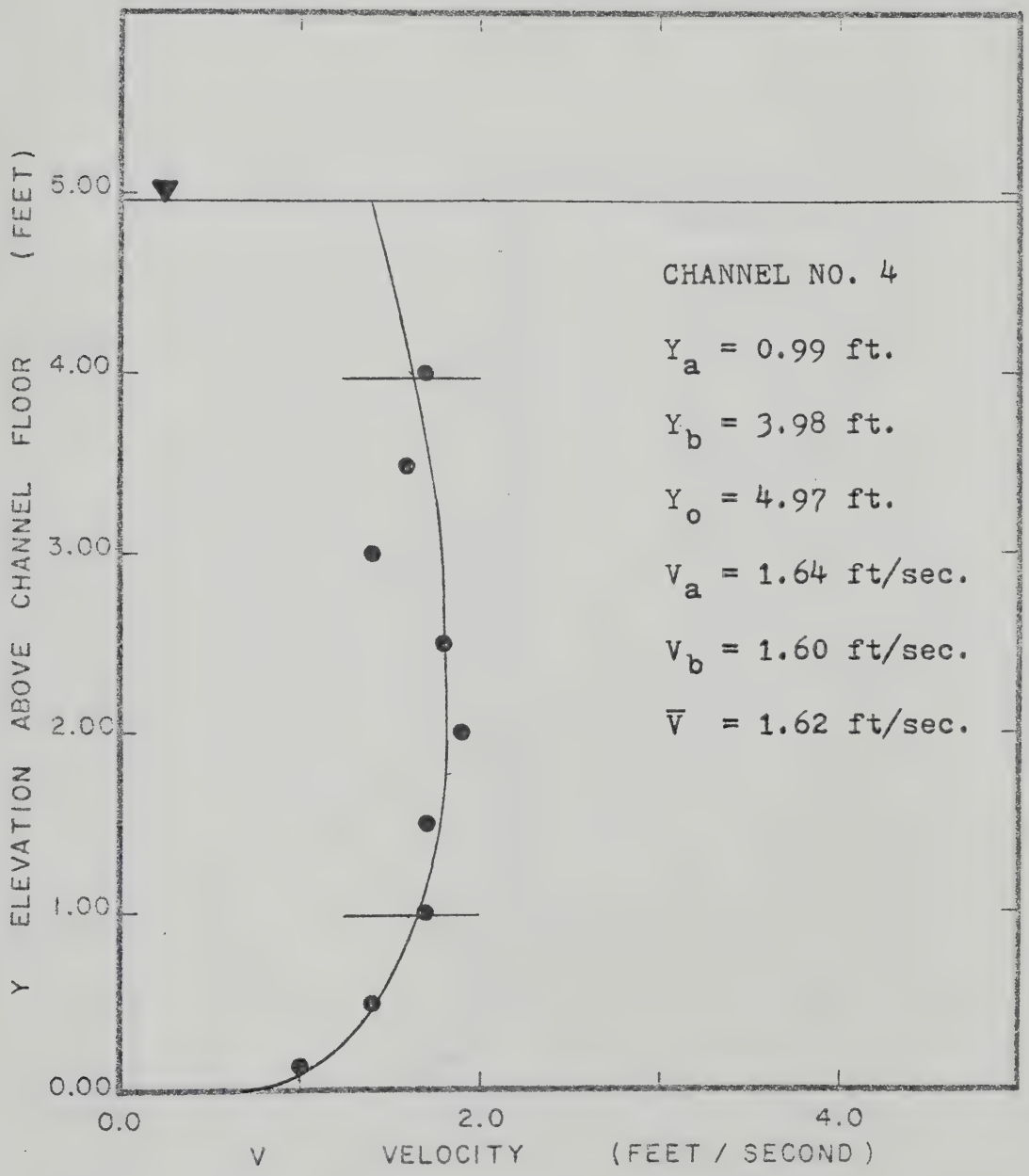

FIG, 1.13A CROSS CHANNEL VELOCITY PROFILE

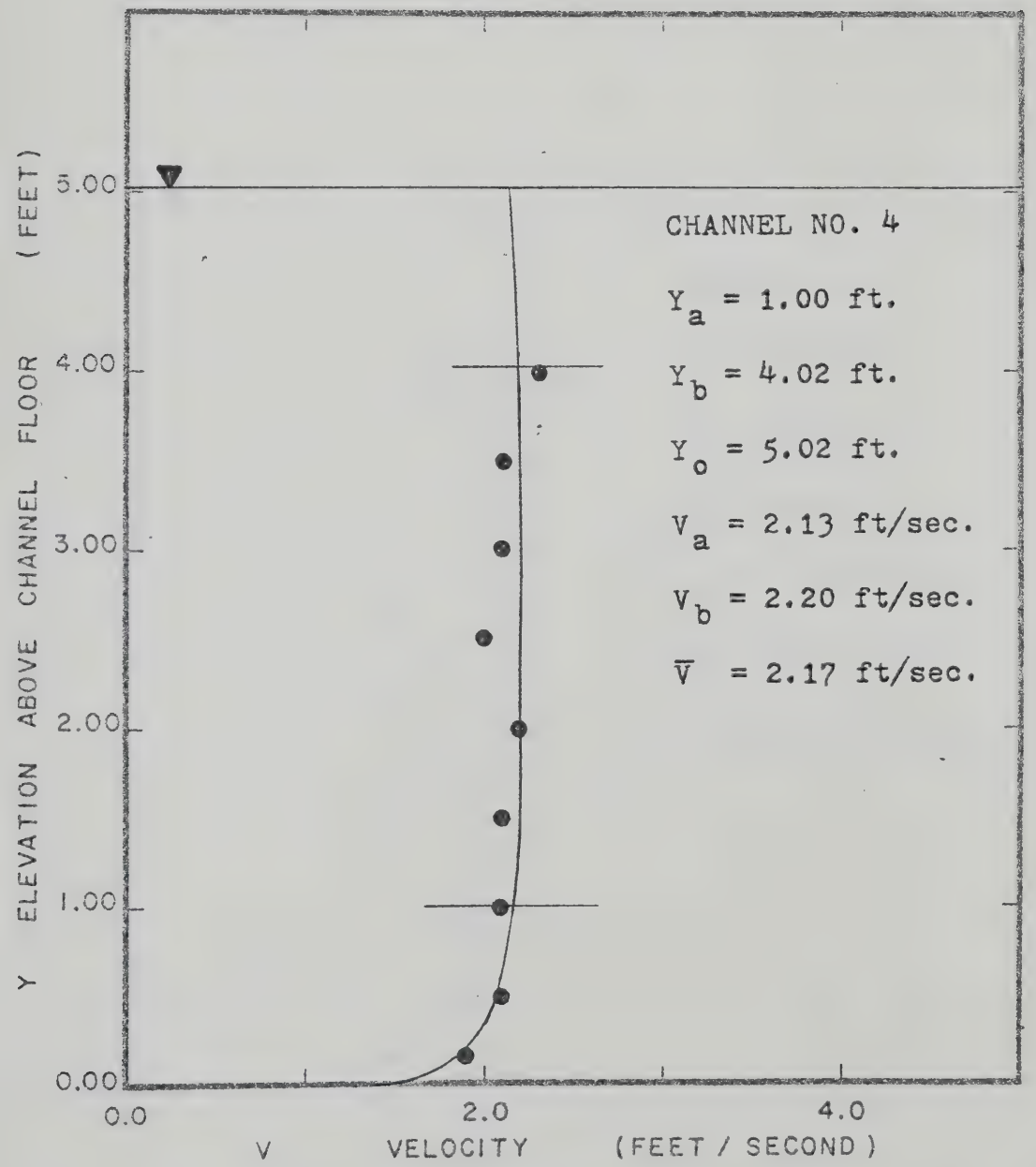

FIG, 1.14 A CROSS CHANNEL VELOCITY PROFILE

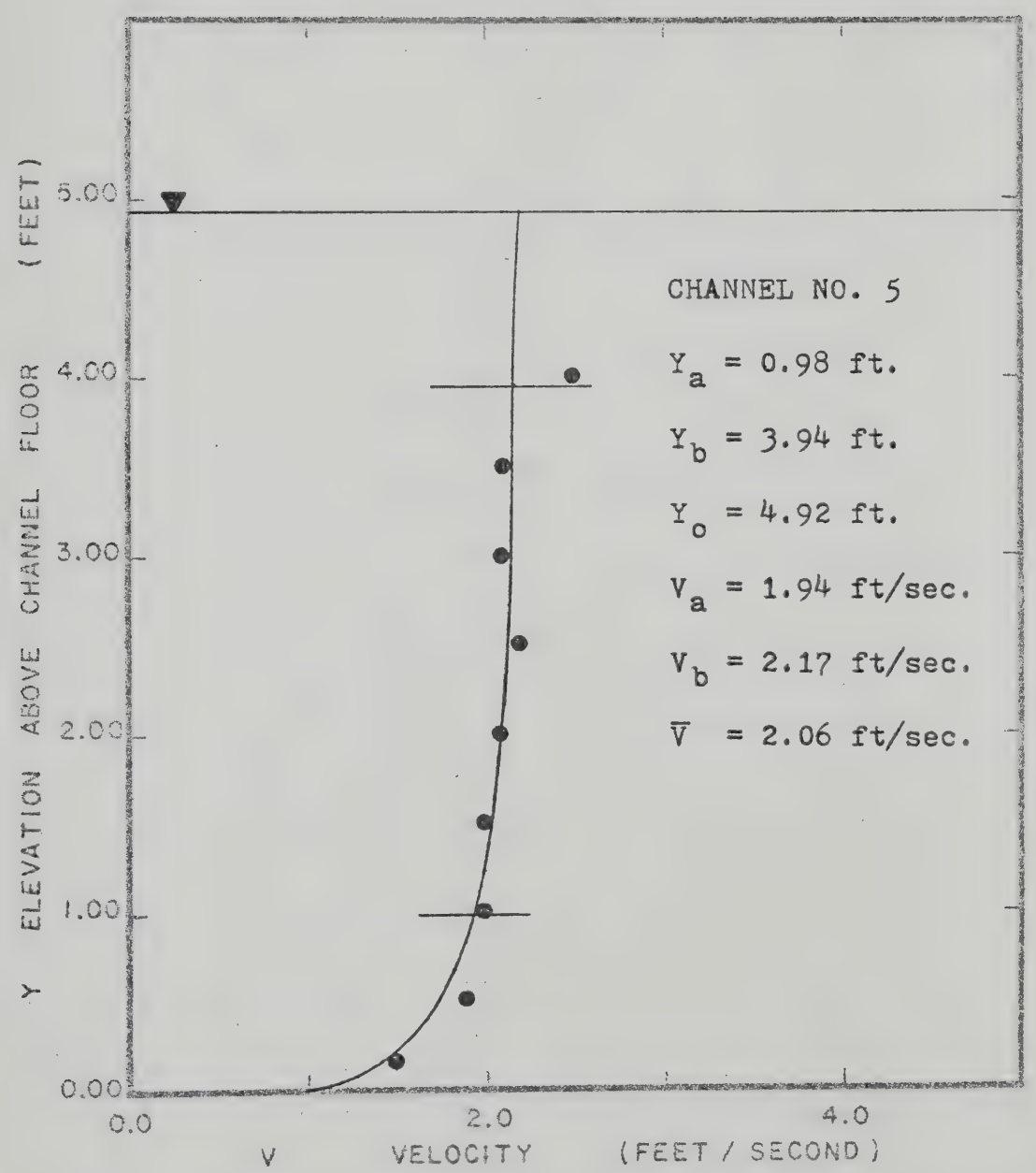

FIG. 1.15 A CROSS CHANNEL VELOCITY PROFILE

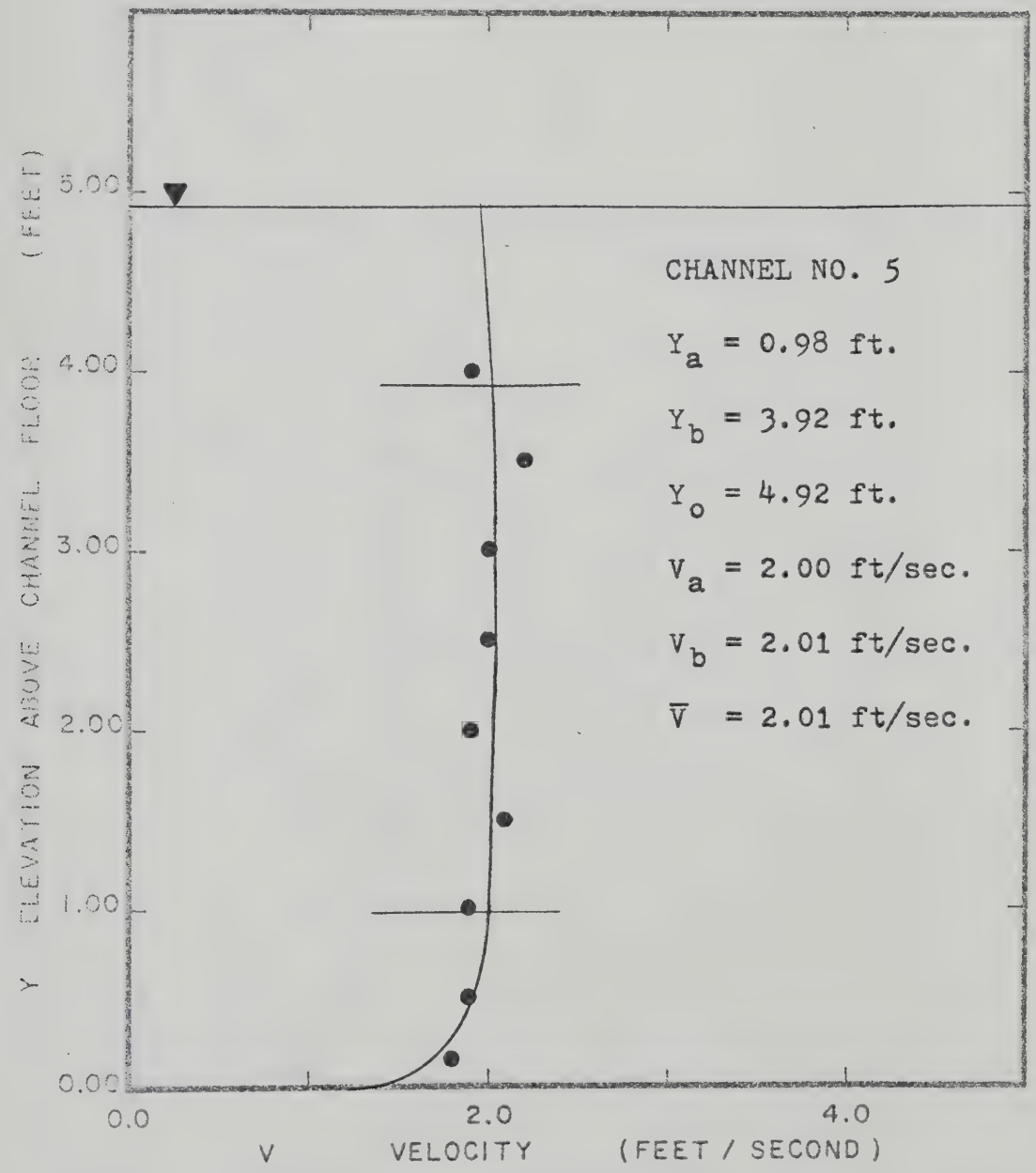

FIG. 1.16 A CROSS CHANNEL VELOCITY PROFILE

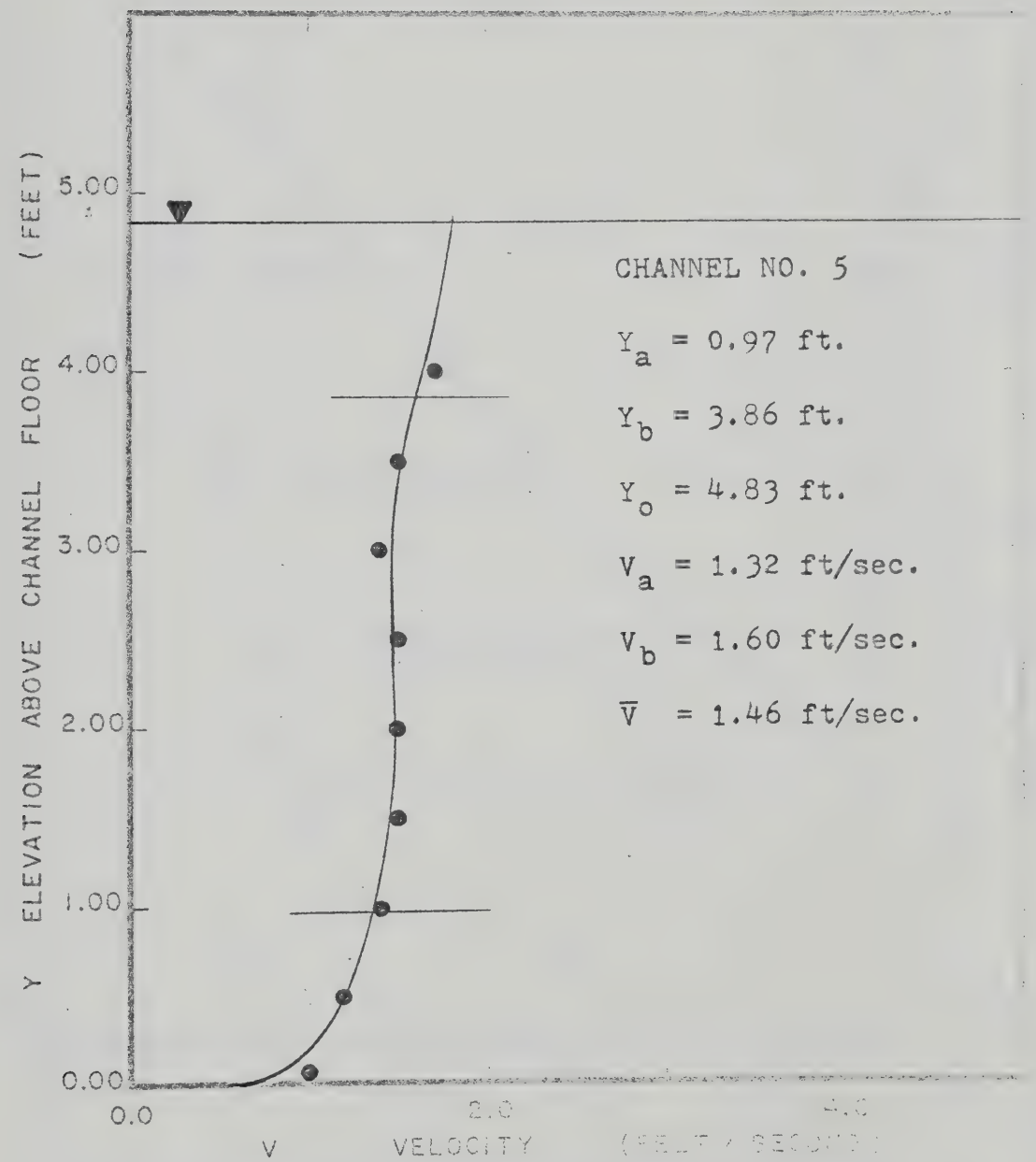

FIG, I.17A CROSS CHANNEL VELOCITY PROFILE

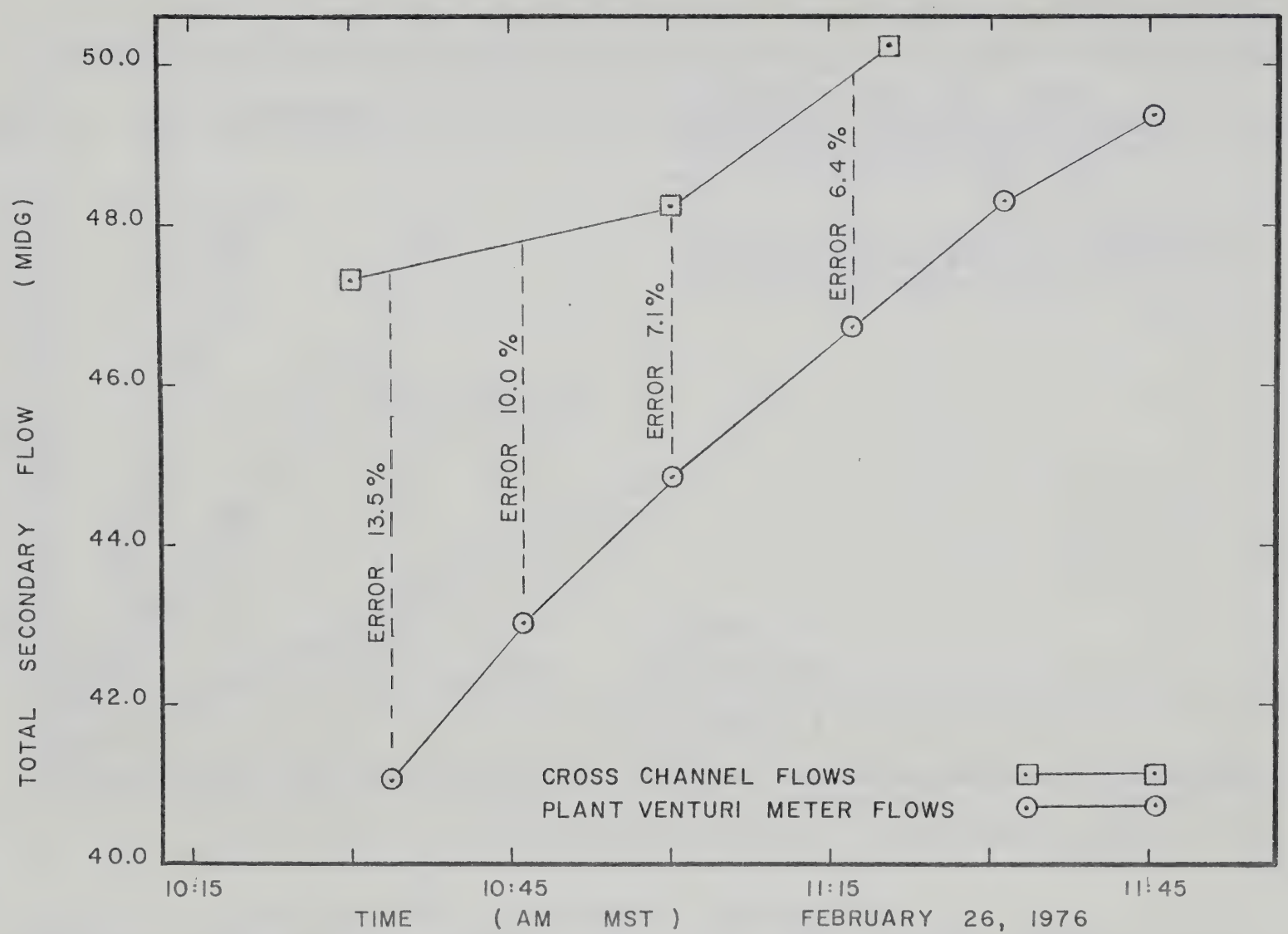

FIG. 2.01 A HYDRAULIC FLOWS FROM CROSS CHANNEL & PLANT VENTURI METER METHODS

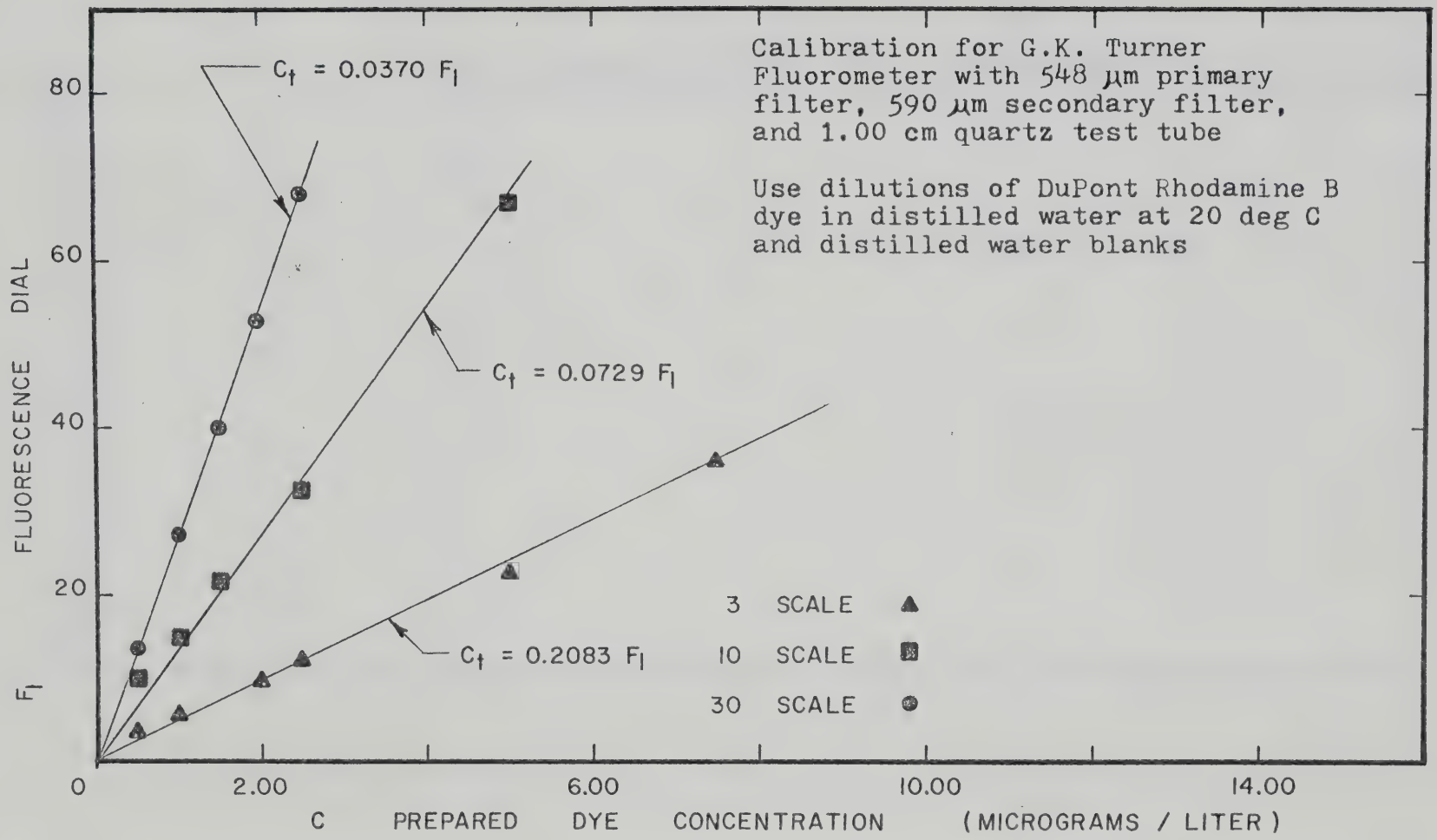

FIG. 3.01 A CALIBRATION FOR G. K. TURNER FLUOROMETER

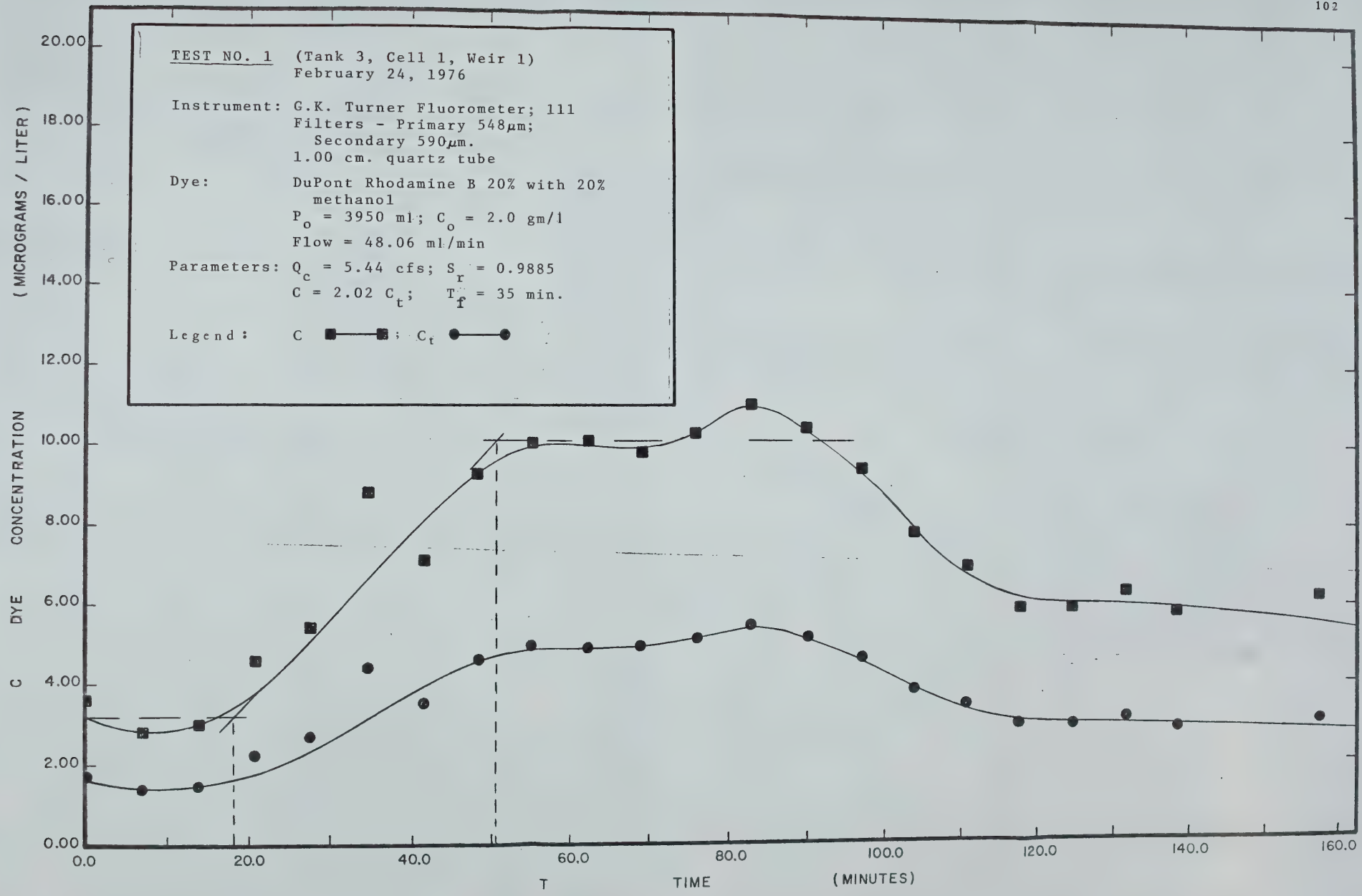

FIG. 4.01 A TIME – CONCENTRATION CURVES

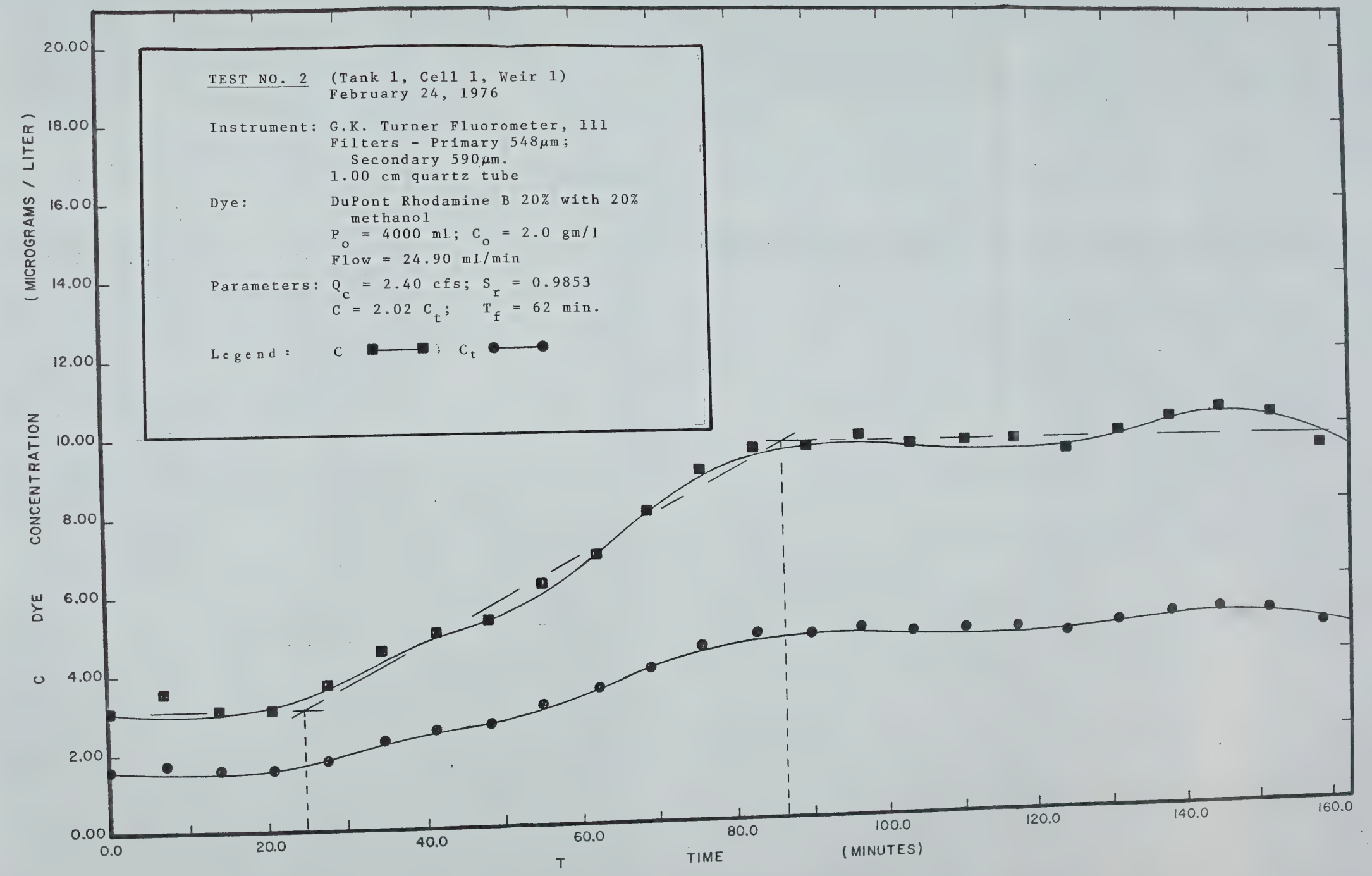

FIG. 4.02 A TIME – CONCENTRATION CURVES

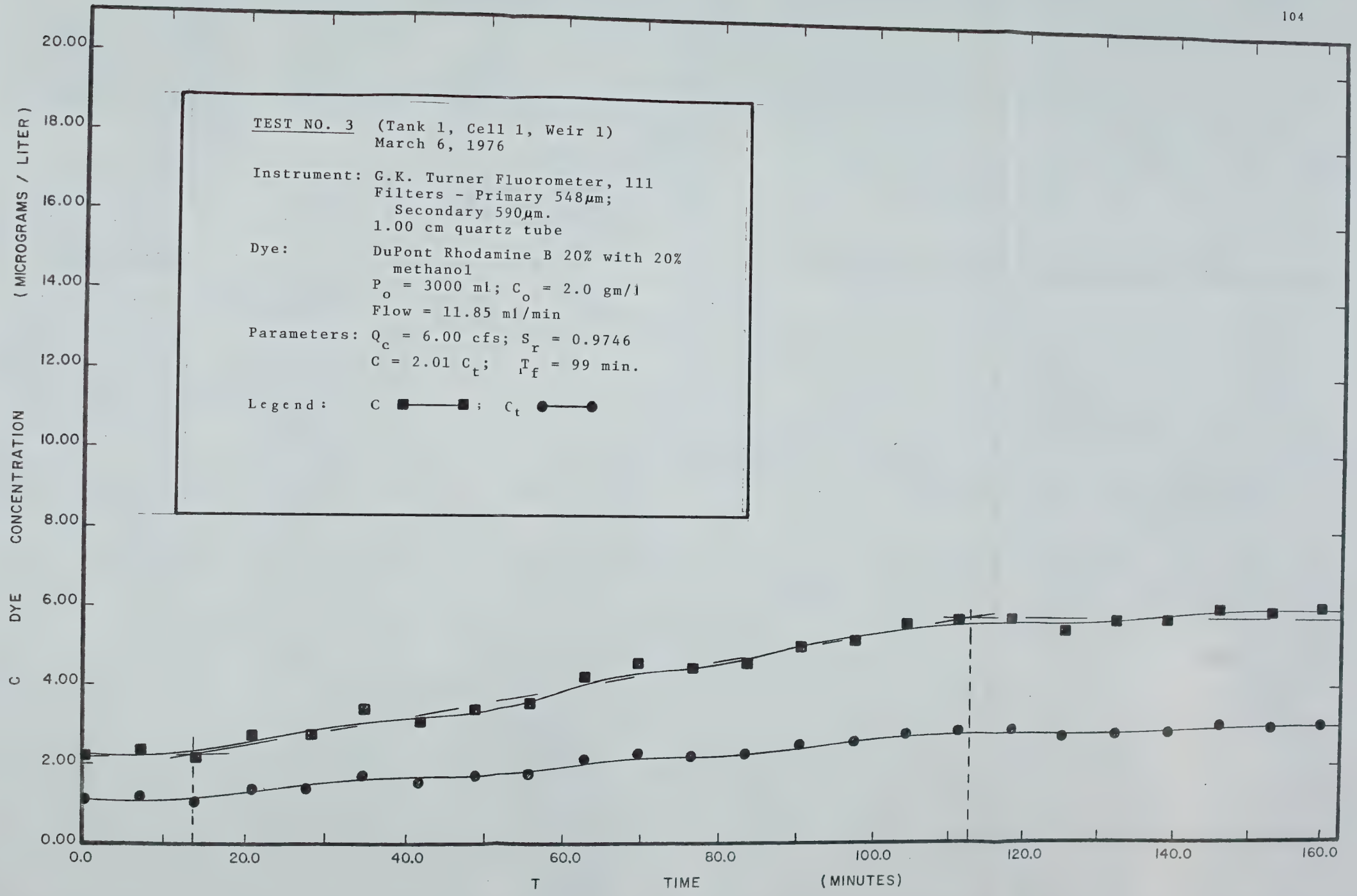

FIG. 4.03 A TIME – CONCENTRATION CURVES

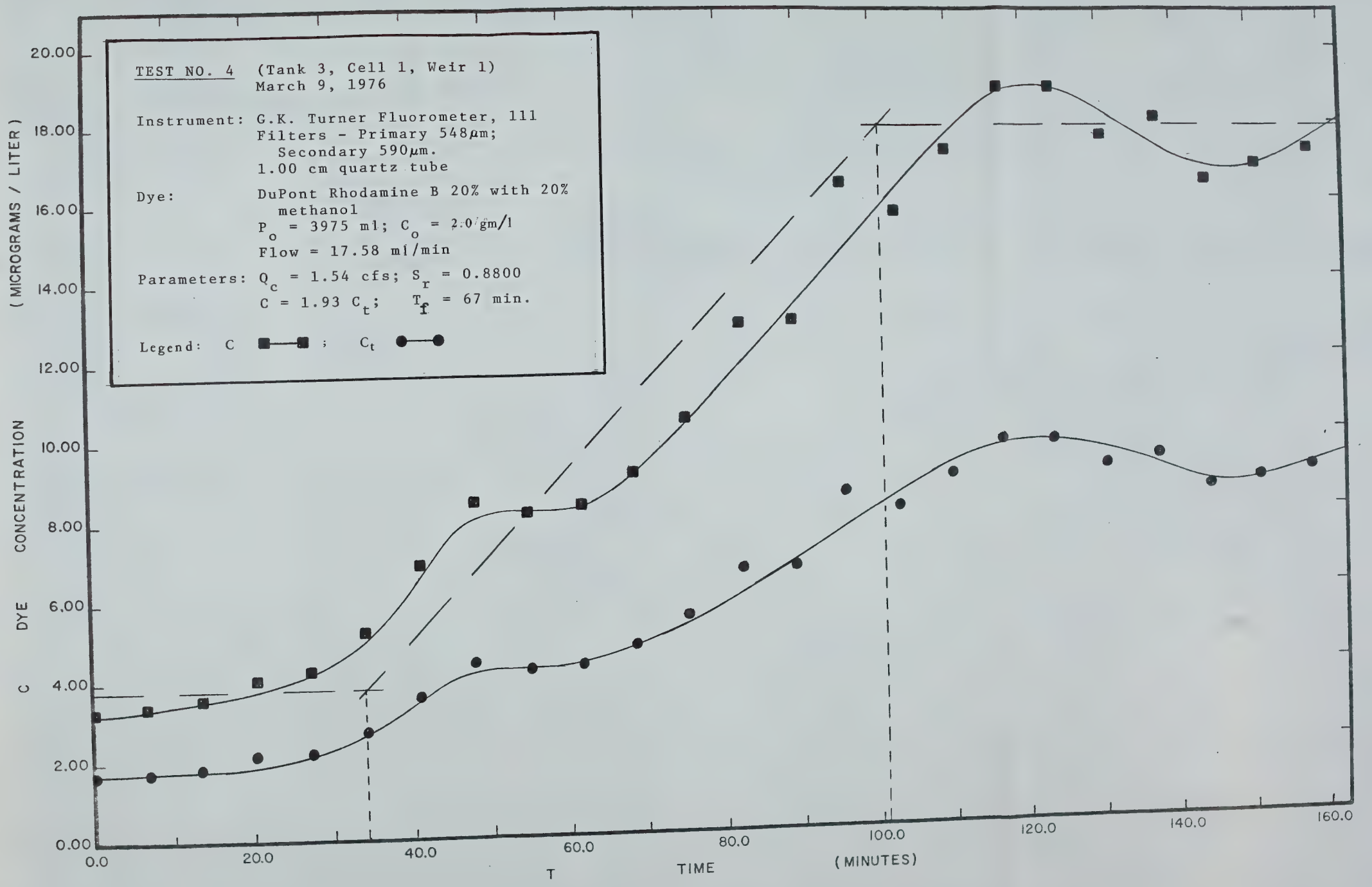

FIG. 4.04 A TIME – CONCENTRATION CURVES

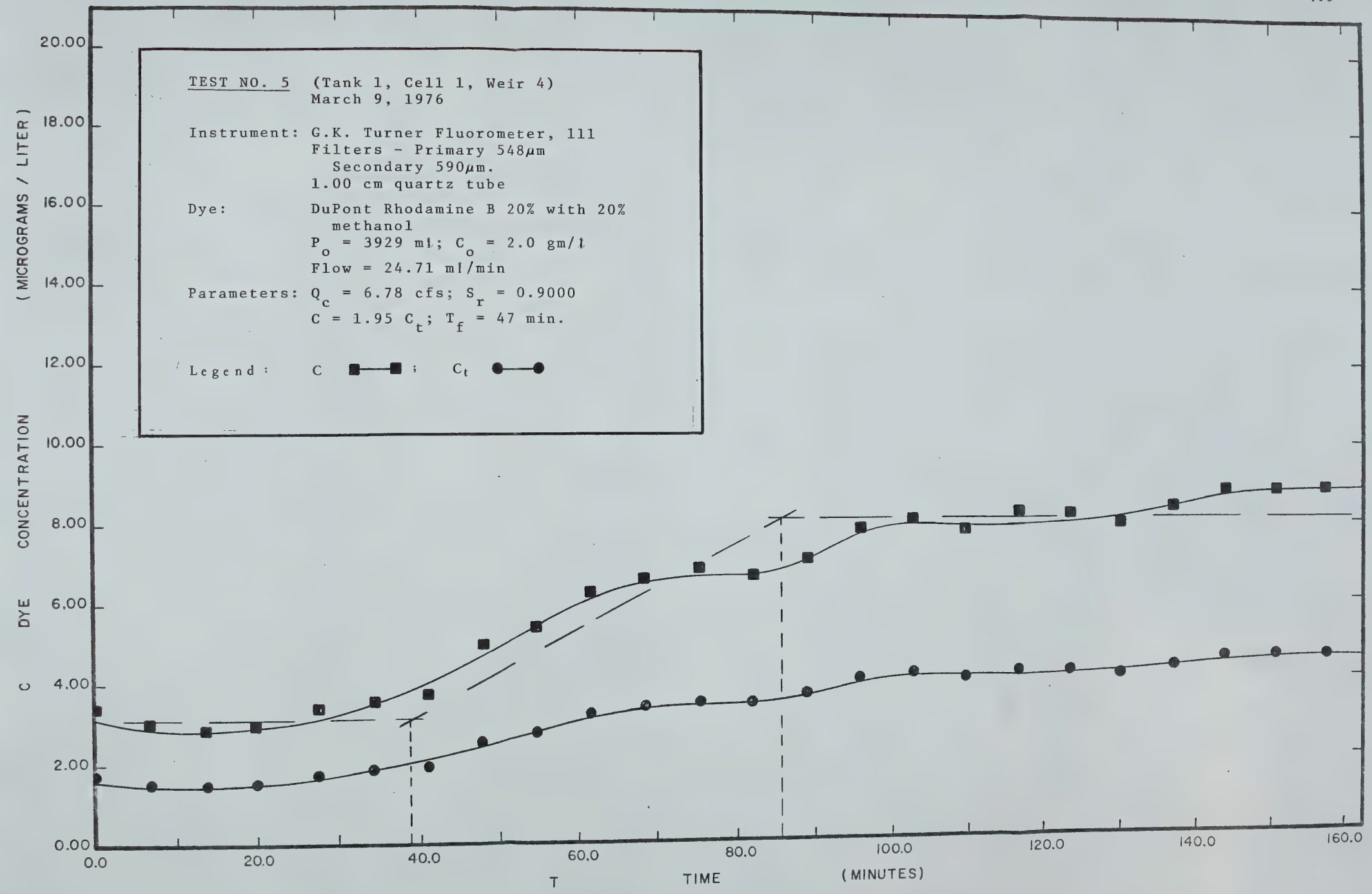

FIG. 4.05 A TIME – CONCENTRATION CURVES

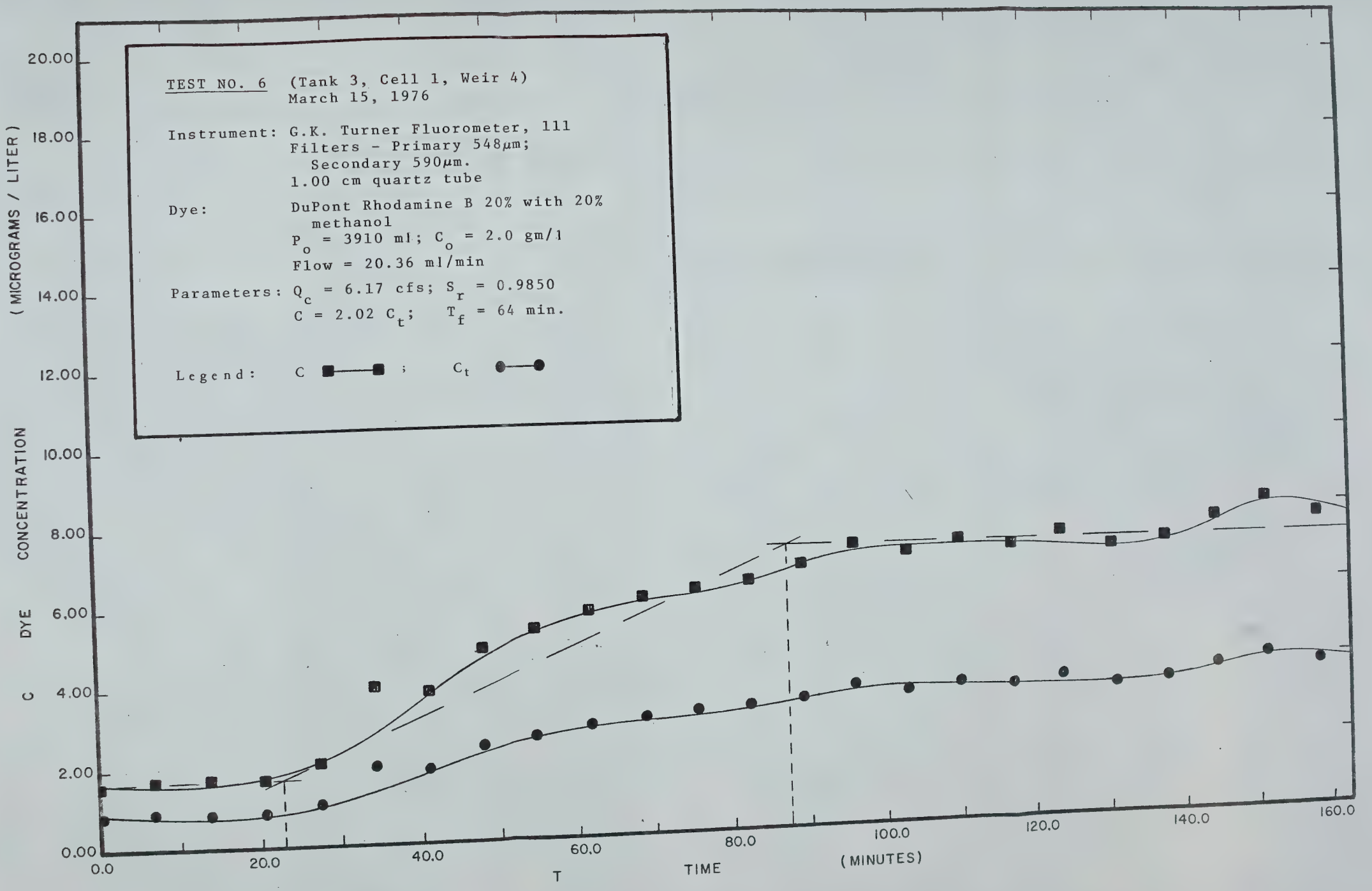

FIG. 4.06 A TIME - CONCENTRATION CURVES

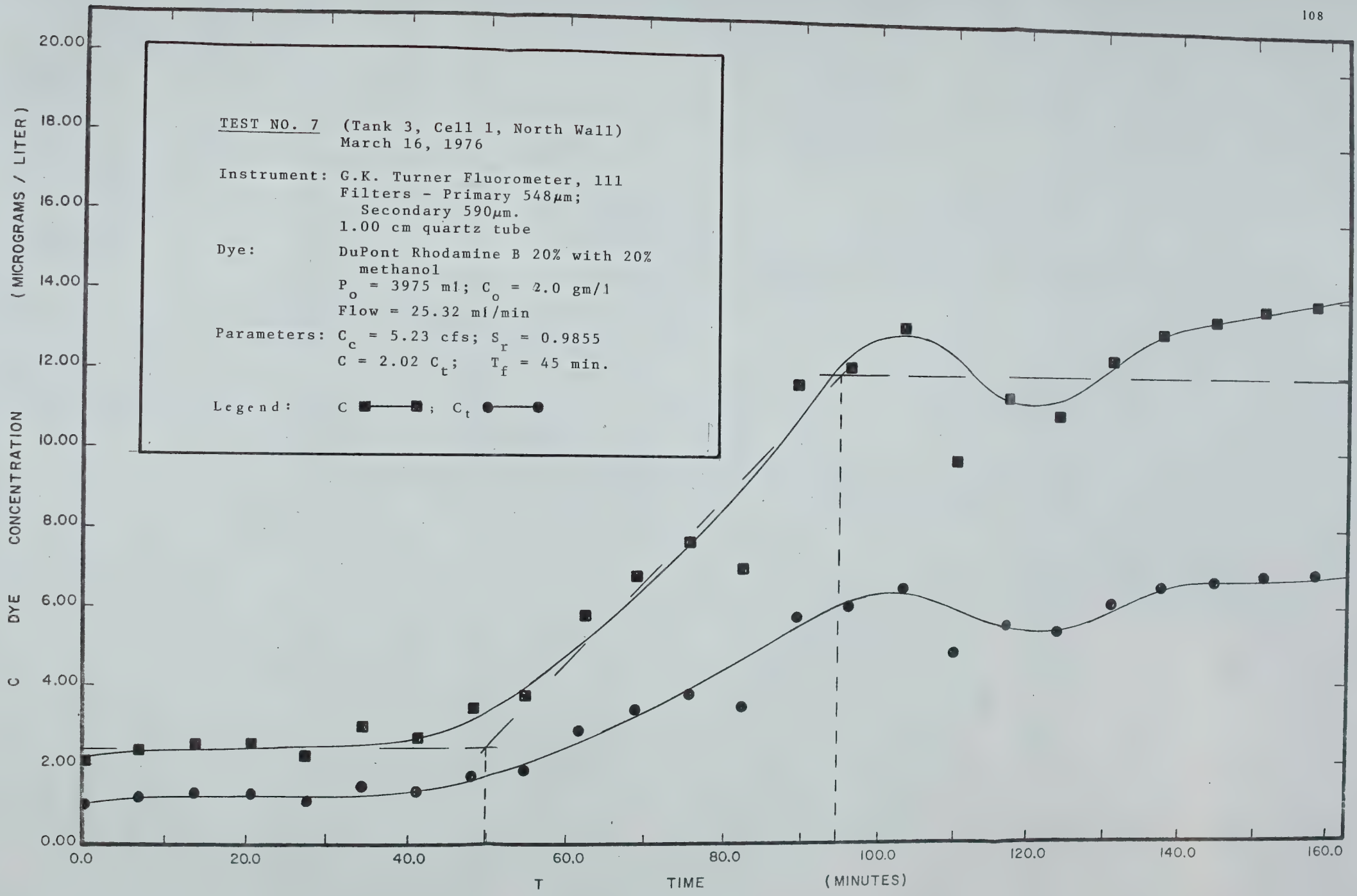

FIG. 4.07 A TIME – CONCENTRATION CURVES

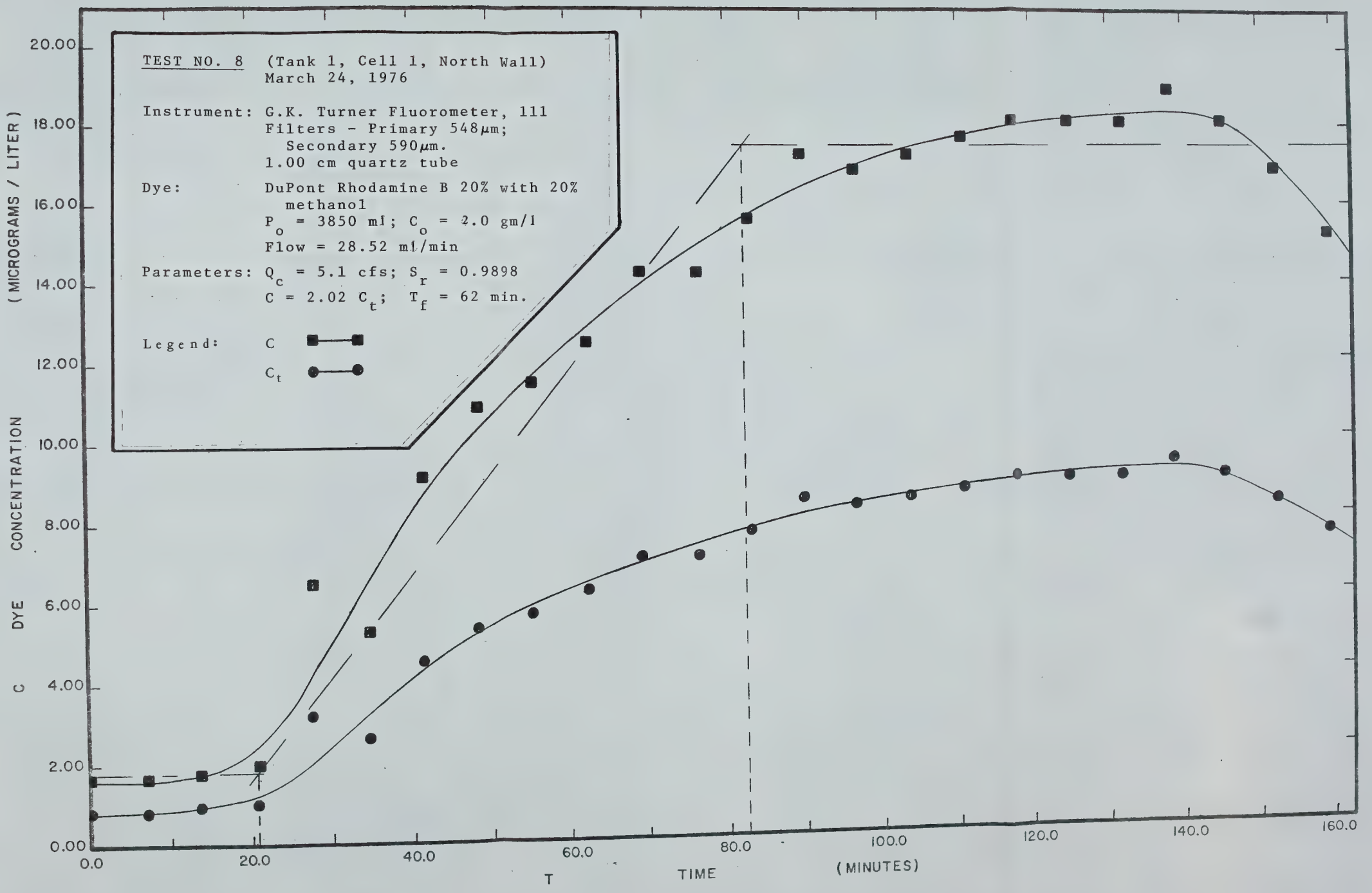

FIG. 4.08 A TIME – CONCENTRATION CURVES

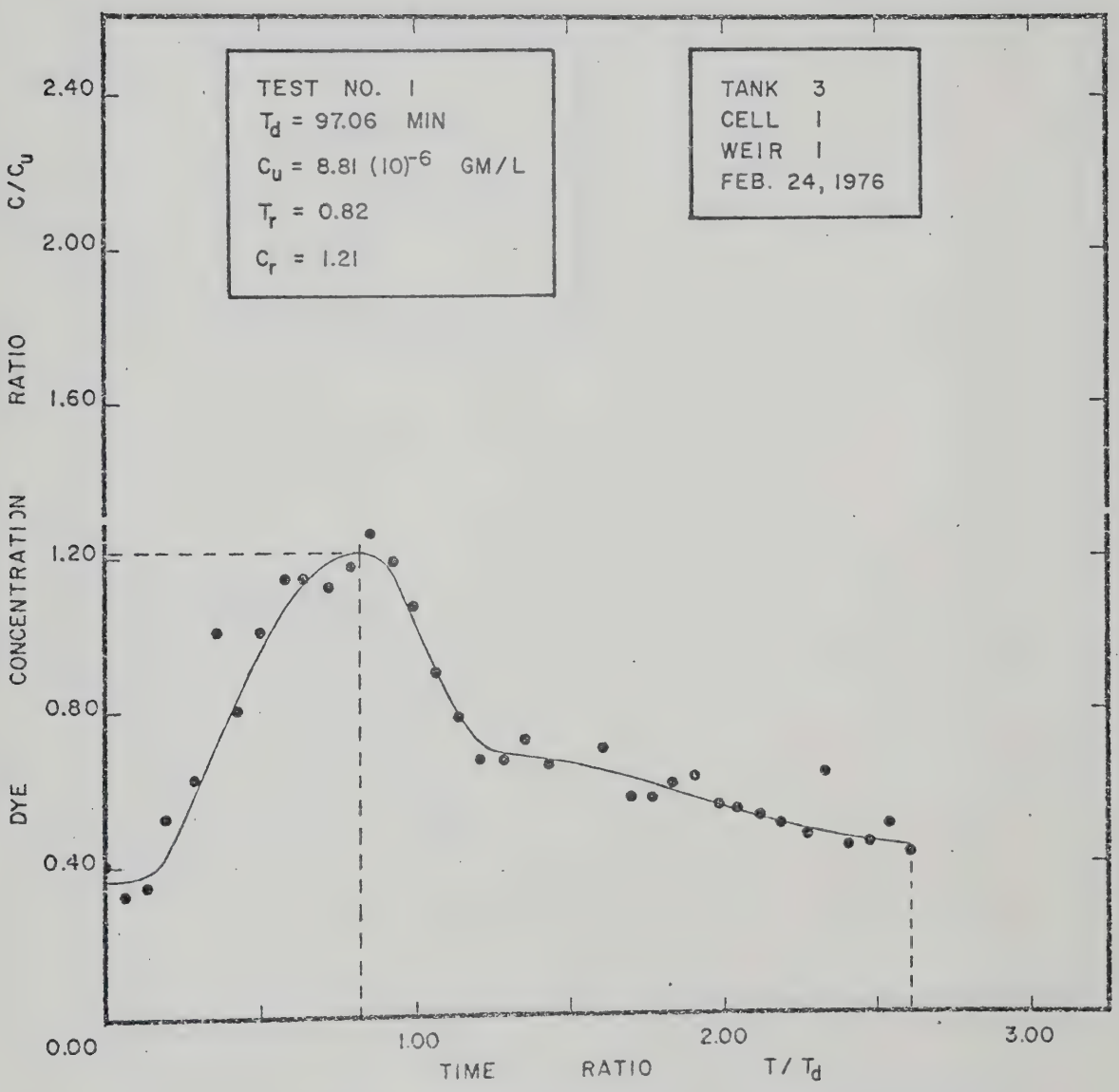

FIG. 5.01A DIMENSIONLESS ANALYSIS OF TIME — CONCENTRATION CURVES

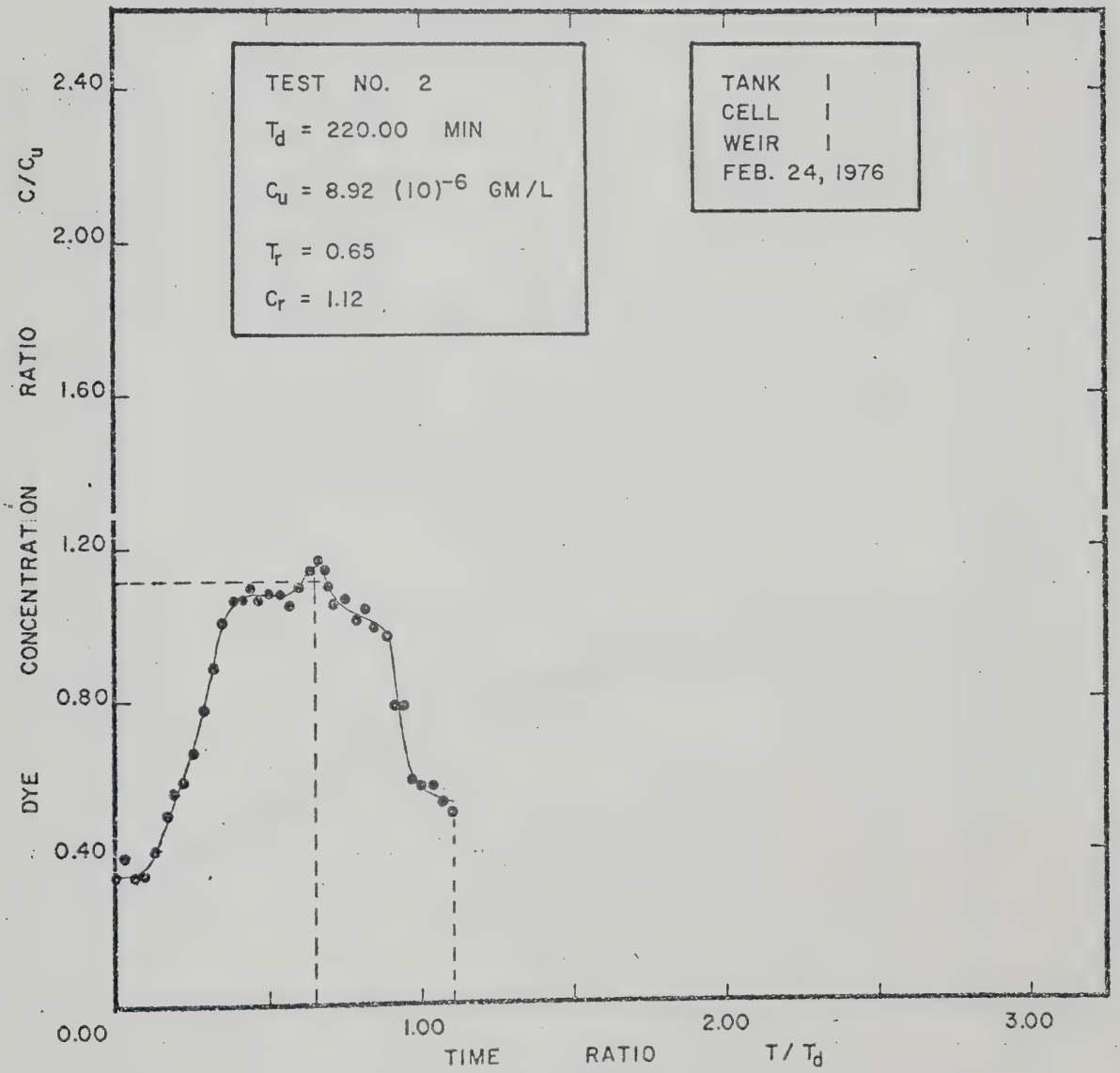

FIG. 5.02 A DIMENSIONLESS ANALYSIS OF TIME — CONCENTRATION CURVES

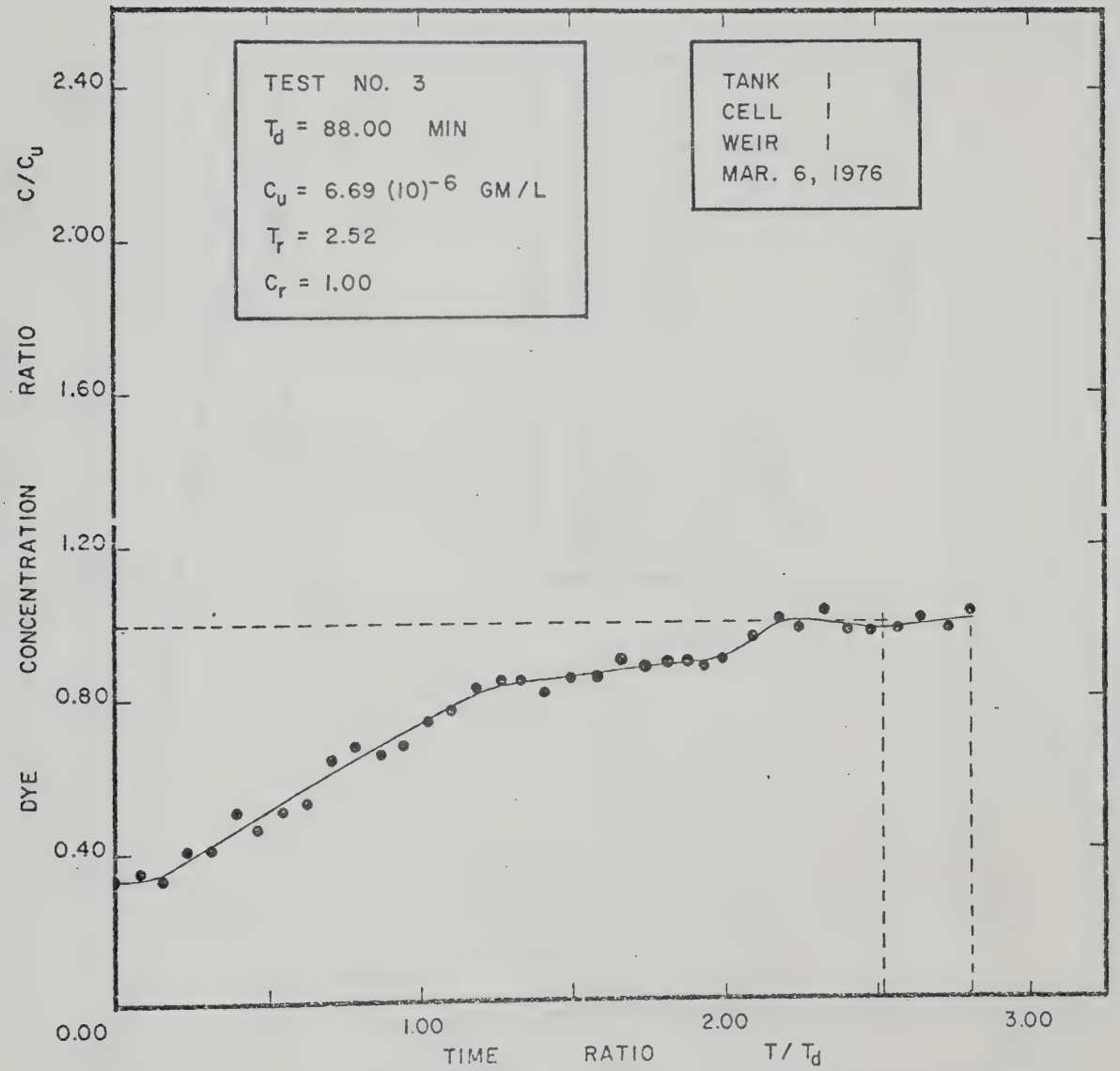

FIG. 5.03 A DIMENSIONLESS ANALYSIS OF TIME — CONCENTRATION CURVES

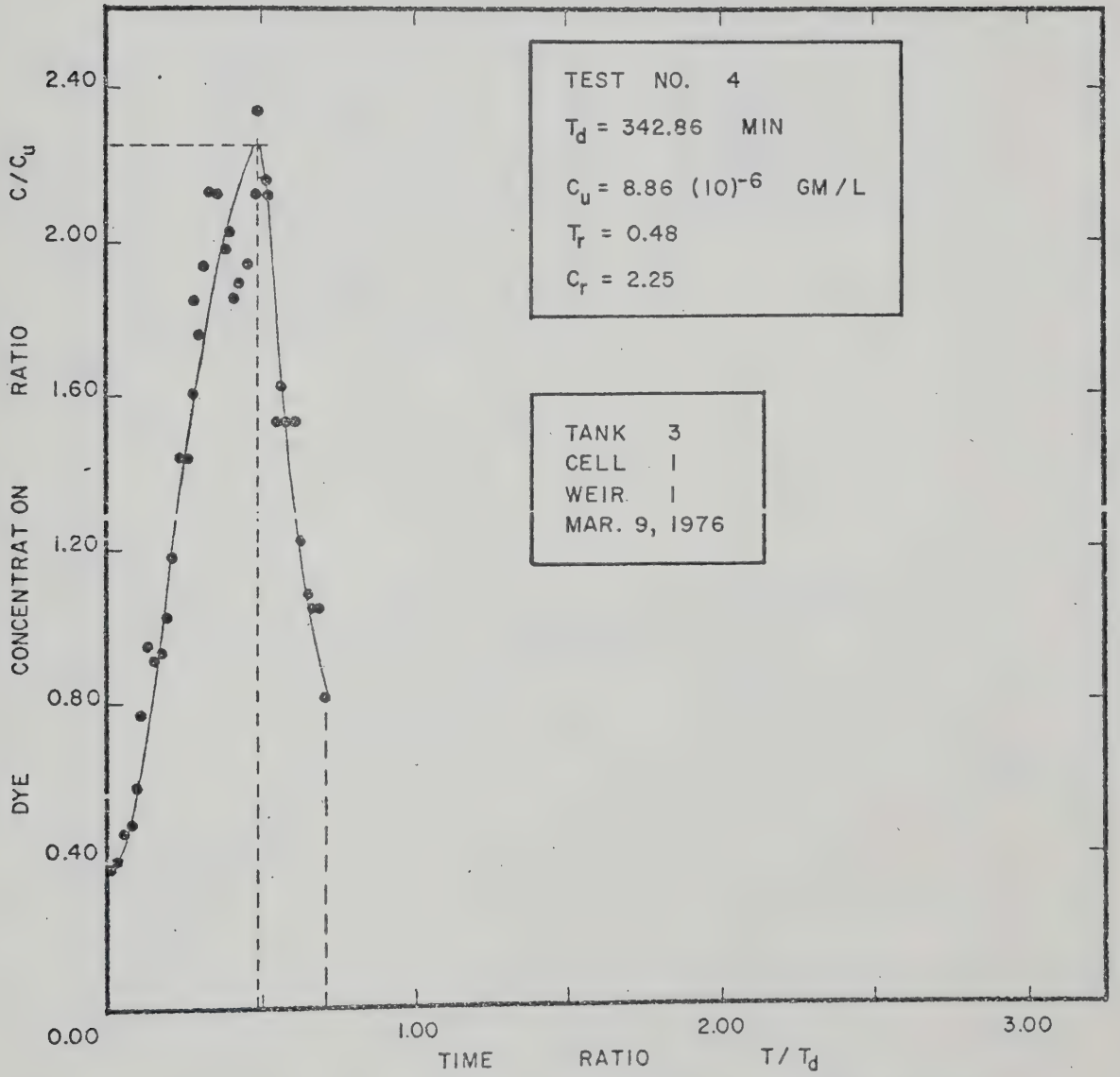

FIG. 5.04 A DIMENSIONLESS ANALYSIS OF TIME — CONCENTRATION CURVES

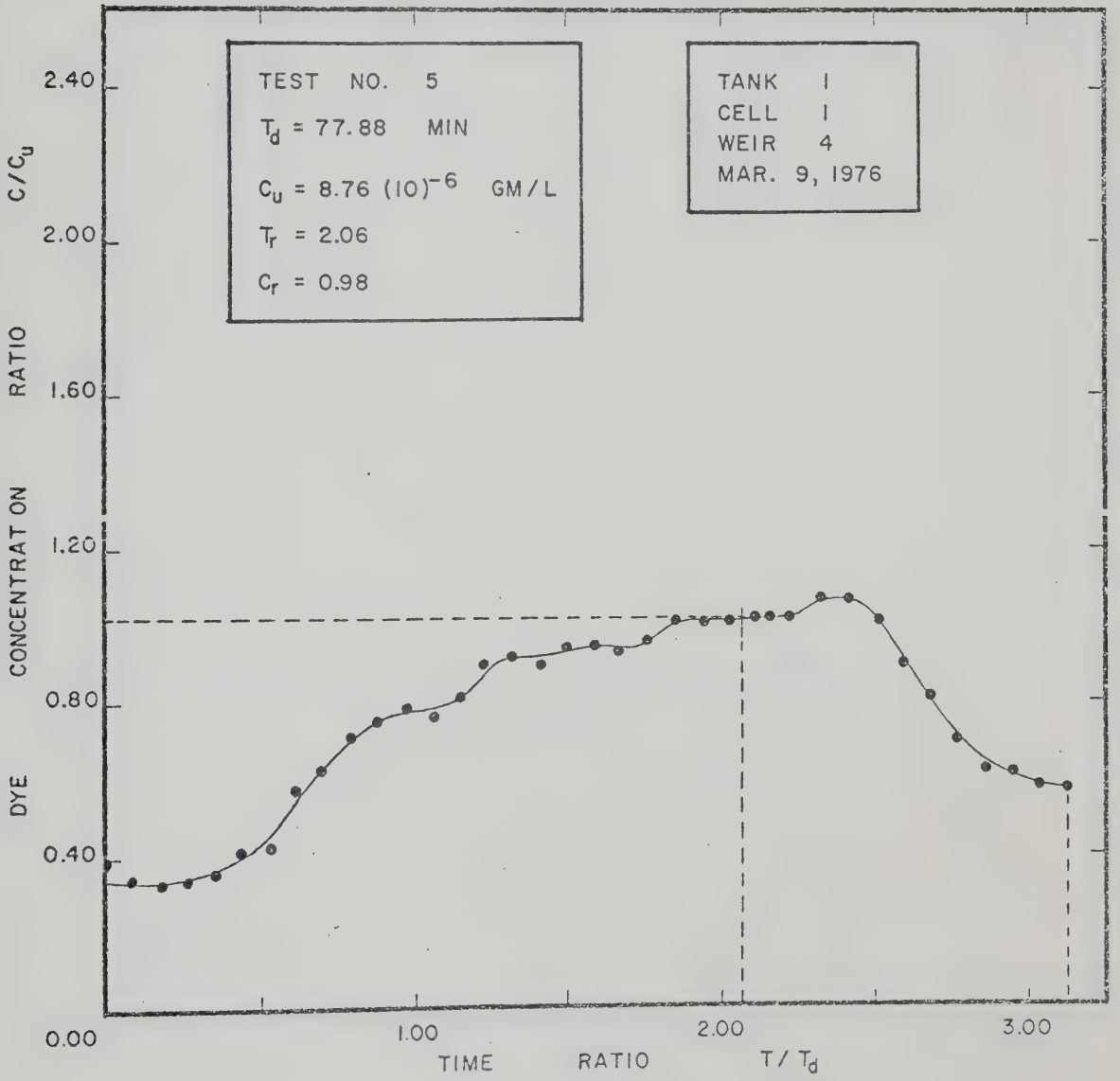

FIG. 5.05A DIMENSIONLESS ANALYSIS OF TIME — CONCENTRATION CURVES

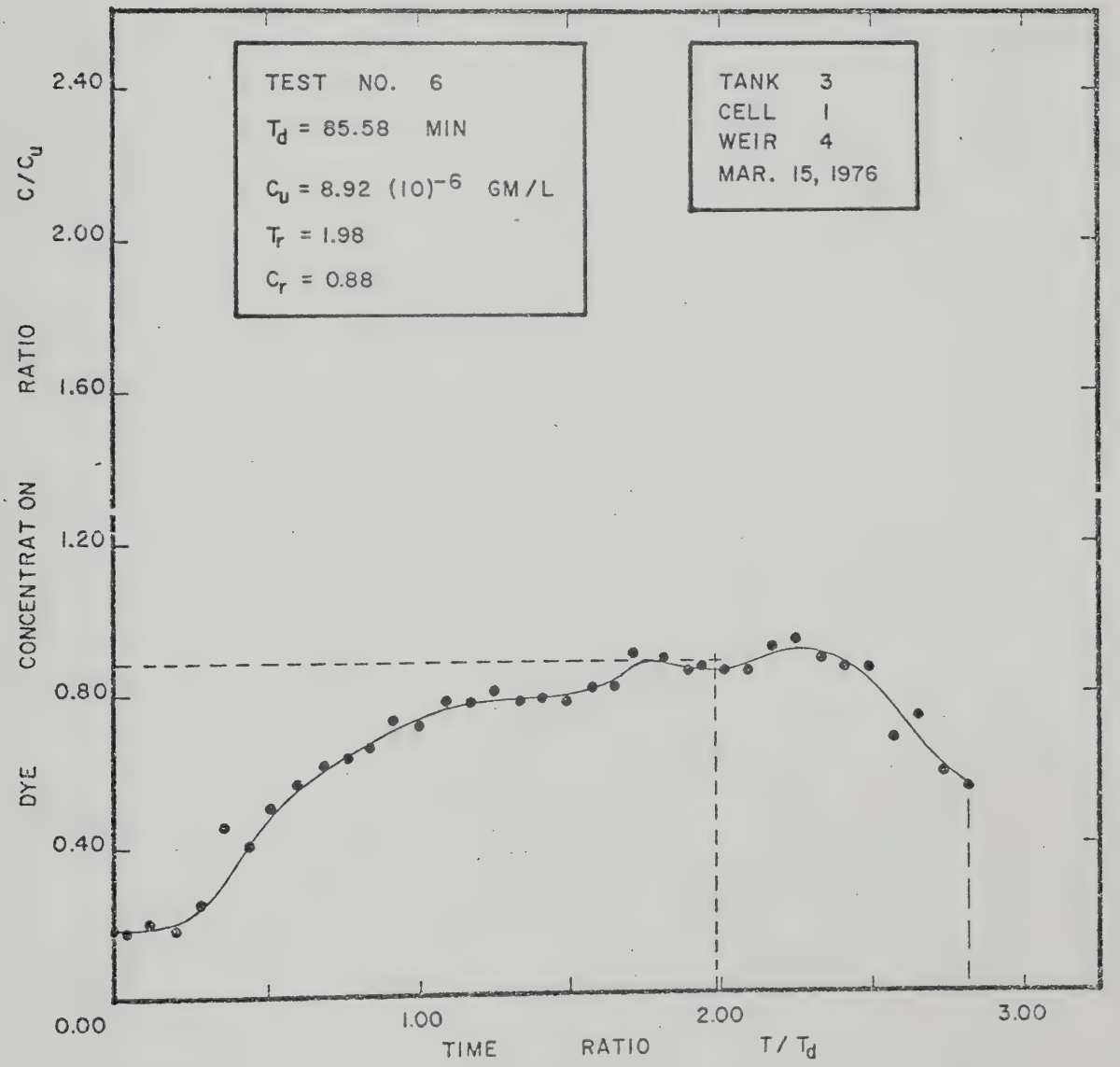

FIG. 5.06 A DIMENSIONLESS ANALYSIS OF TIME — CONCENTRATION CURVES

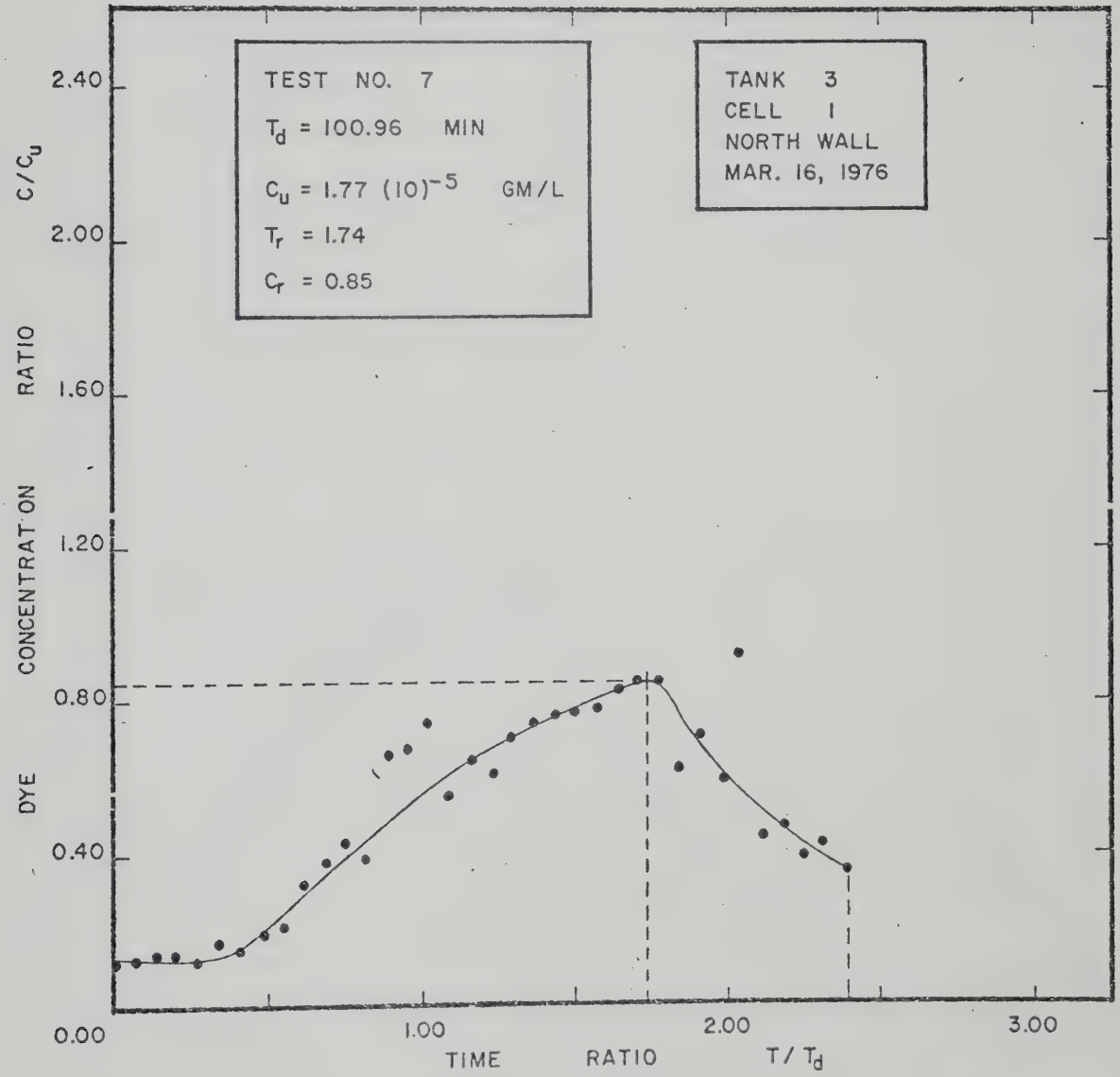

FIG. 5.07A DIMENSIONLESS ANALYSIS OF TIME — CONCENTRATION CURVES

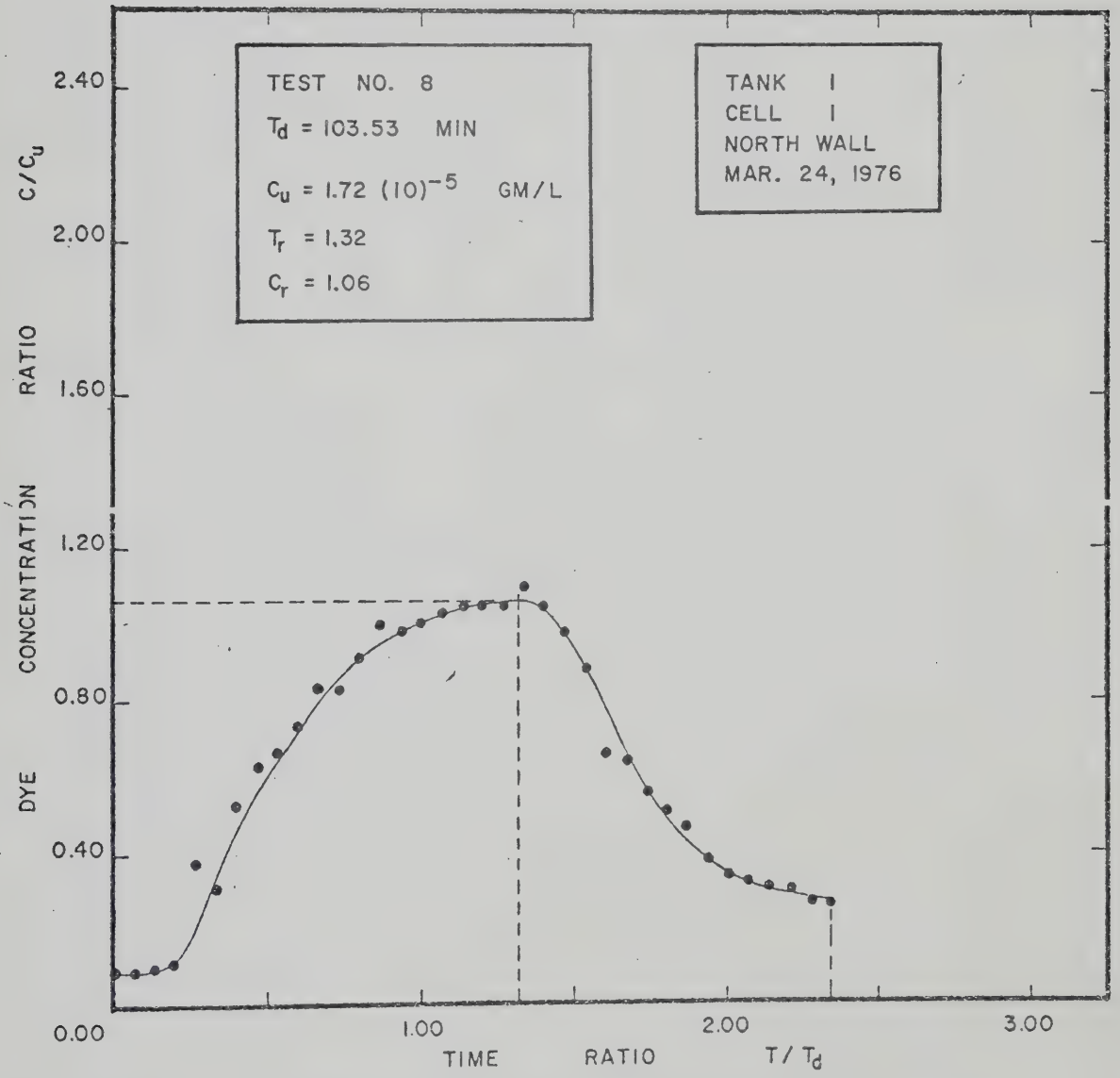

FIG. 5.08 A DIMENSIONLESS ANALYSIS OF TIME — CONCENTRATION CURVES